WCAP-16996-P, "Realistic LOCA Evaluation Methodology Applied to the Full Spectrum of Break Sizes (FULL SPECTRUM LOCA Methodology)"
Requests for Additional Information – (Non-Proprietary)
RAIs 59 -71

November 2013

Westinghouse Electric Company LLC
1000 Westinghouse Drive
Cranberry Township, PA 16066

1. Introduction and Problem Statement

Requests for Additional Information (RAIs) 59 through 71 are focused on the WCOBRA/TRAC-TF2 interfacial drag models, regarding model basis as well as their validation test and Pressurized Water Reactor (PWR) plant simulations. Responses to these RAIs are provided in this letter. As an extension to Westinghouse's current approved methodology (Reference 1-1) for Large-Break loss-of-coolant accident (LBLOCA) analysis, WCOBRA/TRAC-TF2 is designed to be capable of predicting the LOCA event covering the full spectrum of break sizes. For small-break LOCA (SBLOCA), the interfacial drag models in the code directly impact the core two-phase mixture level and void fraction distribution, which are critical to predicting the fuel rod heat up. As such, the responses to the questions included in this set of RAIs focus on discussing the adequacy of the WCOBRA/TRAC-TF2 interfacial drag models and their key validation tests in the context of SBLOCA analysis, in direct association with the several key issues expressed in theses RAIs.

The first issue is the nodalization sensitivity of the Oak Ridge National Laboratory (ORNL) Thermal-Hydraulic Test Facility (THTF) level swell and boil-off test validations and the PWR plant simulations, and the second is the interfacial drag model accounting for the effect of significant vapor generation at the wall in the small and small to large bubble flow regime. These two issues are discussed in Sections 2 and 3 that follow, respectively. The answers to the individual questions besides those involved in the aforementioned issues in these RAIs are found in Section 4 of this response. Section 5 of this letter includes an updated Section 5.4 of the Topical report (Reference 1-2). This updated topical section is provided as part of the response to RAI 66 (1) to resolve inconsistencies between the interfacial drag factor correlations as-written and the general form in technical publications, and inconsistencies between the topical description and the WCOBRA/TRAC-TF2 source code. The revised description of vessel component interfacial drag factors in topical report Section 5.4 as enclosed in Section 5 of this letter will be incorporated in Reference 1-2 when the topical report is updated.

The vessel component interfacial drag models in WCOBRA/TRAC-TF2 describe the momentum interaction of the three fields of vapor, continuous and dispersed liquid and are flow regime dependent. Section 4.0 of Reference 1-2 discusses the flow regimes and associated interfacial area, while the flow regime dependent interfacial drag models are described in Section 5.0 of Reference 1-2.

Reference 1-2 is interchangeably referred to as 'the Topical' in the discussion that follows.

Reference(s)

1-1. WCAP-12945-P-A, "Code Qualification Document for Best Estimate LOCA Analysis," March 1998.

1-2. WCAP-16996-P, "Realistic LOCA Evaluation Methodology Applied to the Full Spectrum of Break Sizes (FULL SPECTRUM LOCA Methodology)," November 2010.

2. Nodalization and Timestep Studies

A number of nodalization and maximum timestep size sensitivity studies were executed in order to show that the selected core nodalization and timestep size produce reasonable code convergence.

Oak Ridge National Laboratory Core Axial Noding Studies

Core axial noding sensitivity studies were run with ORNL Tests I, L, AA, and DD. The number of nodes in the core was doubled such that the hydraulic node length was reduced from about 12 inches to about 6 inches. The resulting core node sizes cover the range typically used for PWR analysis.

The results of these ORNL axial noding studies are presented in Figures 2-1 through 2-4. The void distributions presented are for channel 2, which is the interior core channel. Refer to Section 13.4.2 of WCAP-16996-P (Reference 2-1) for additional information regarding the ORNL noding.

The base cases are the red, solid lines and the sensitivity cases with increased core noding are the dashed, green lines. It is observed that the resulting void fraction profiles with the additional core nodes are comparable to the base case results; indicating that reasonable convergence is obtained relative to the core axial noding. Since the code results are comparable for this noding study, and the 6-inch to 12-inch nodes cover the typical PWR range (refer to Table 26.1-1 in WCAP-16996-P (Reference 2-1) for typical PWR core node lengths), it is judged that additional noding studies with finer core noding are not required. Furthermore, the inclusion of level sharpening logic (as described in the response to RAI-17 (Reference 2-2)) allows for resolution of the two-phase level beyond the hydraulic cell mesh at the rod heat-transfer node mesh. The maximum heat transfer node size for the fuel rods is 3-inches. The YDRAG range utilized in the uncertainty analysis is then biased low to produce a conservative prediction of the level swell for the uncertainty analysis, as described in the response to RAIs-72, 73 and 74 per LTR-NRC-13-41 (Reference 2-3).

Beaver Valley Unit 1 (DLW) PWR Core Axial Noding Study

A core axial noding sensitivity study was also run with the Beaver Valley PWR input deck. The base case was taken as one of the cases from Study C in the response to RAI-9, transmitted to the Nuclear Regulatory Commission (NRC) in LTR-NRC-13-45 (Reference 2-4). The number of hydraulic nodes used to model the active fuel region was increased, using two nodes for each original node (except for the top two nodes which were already less than eight-inches in the base case). The result is 26 hydraulic nodes in the active fuel region for the sensitivity study compared to 14 nodes in the case base.

Figures 2-5 through 2-9 present the lower plenum pressure, lower plenum liquid temperature, cladding temperature at NSAPLOT node 65, and cladding temperature at NSAPLOT node 75, and core axial void fraction profile near the Peak Cladding Temperature (PCT) time for the Beaver Valley PWR axial noding sensitivity, respectively. The base cases are the red, solid lines and the sensitivity cases with increased core noding are the dashed, green lines. These plots show little difference through the duration of the transient. The effect on the calculated cladding temperature is minimal (Figures 2-7 and 2-8); there is just a small difference in transient timing observed as the base case peaks higher at one elevation while the sensitivity case peaks higher at the other elevation. The timing difference is also observed in the core axial void fraction distribution (Figure 2-9). As such, it is concluded that solution is reasonably converged with the base case node size.

ORNL Maximum Timestep Size Studies

Maximum timestep size sensitivity studies were run with ORNL Tests I and CC. The maximum timestep size was reduced by an order of magnitude from 0.005 s to 0.0005 s. The resulting timestep sizes cover the range typically used for PWR analysis.

The results of these ORNL maximum timestep size studies are presented in Figures 2-10 and 2-11. The base cases are the red, solid lines and the sensitivity cases with decreased maximum timestep size are the dashed, green lines. It is observed that the resulting void fraction profiles with the reduced maximum timestep size are nearly identical to the base case results, indicating that the code is well converged with the base case timestep size.

Conclusion

The ORNL and PWR nodalization and maximum timestep size sensitivity studies executed indicate that the selected core nodalization and timestep size produce reasonable code convergence. Additional studies with 3-inch core nodes are judged unnecessary since the convergence was not sensitive to the noding studies already executed, and the PWR noding is covered by the noding studies already executed.

Reference(s)

2-1. WCAP-16996-P, "Realistic LOCA Evaluation Methodology Applied to the Full Spectrum of Break Sizes (FULL SPECTRUM LOCA Methodology)," November 2010.

2-2. LTR-NRC-13-37, "Submittal of Westinghouse Responses to 'WCAP-16996-P, 'Realistic LOCA Evaluation Methodology Applied to the Full Spectrum of Break Sizes (FULL

SPECTRUM LOCA Methodology)' Request for Additional Information' (Proprietary/Non-Proprietary), Project 700, TAC No. ME5244," June 5, 2013.

2-3. LTR-NRC-13-41, "Submittal of Westinghouse Responses to 'WCAP-16996-P, 'Realistic LOCA Evaluation Methodology Applied to the Full Spectrum of Break Sizes (FULL SPECTRUM LOCA Methodology)' Request for Additional Information – RAIs 72, 73, 74 and 76' (Proprietary/Non-Proprietary), Project 700, TAC No. ME5244," June 21, 2013.

2-4. LTR-NRC-13-45, "Submittal of Westinghouse Responses to 'WCAP-16996-P, 'Realistic LOCA Evaluation Methodology Applied to the Full Spectrum of Break Sizes (FULL SPECTRUM LOCA Methodology)' Request for Additional Information – RAIs 9 and 12' (Proprietary/Non-Proprietary), Project 700, TAC No. ME5244," June 26, 2013.

[ ] a,c

Figure 2-1 – Void Fraction Profile for ORNL Test 3.09.10l Axial Noding Sensitivity

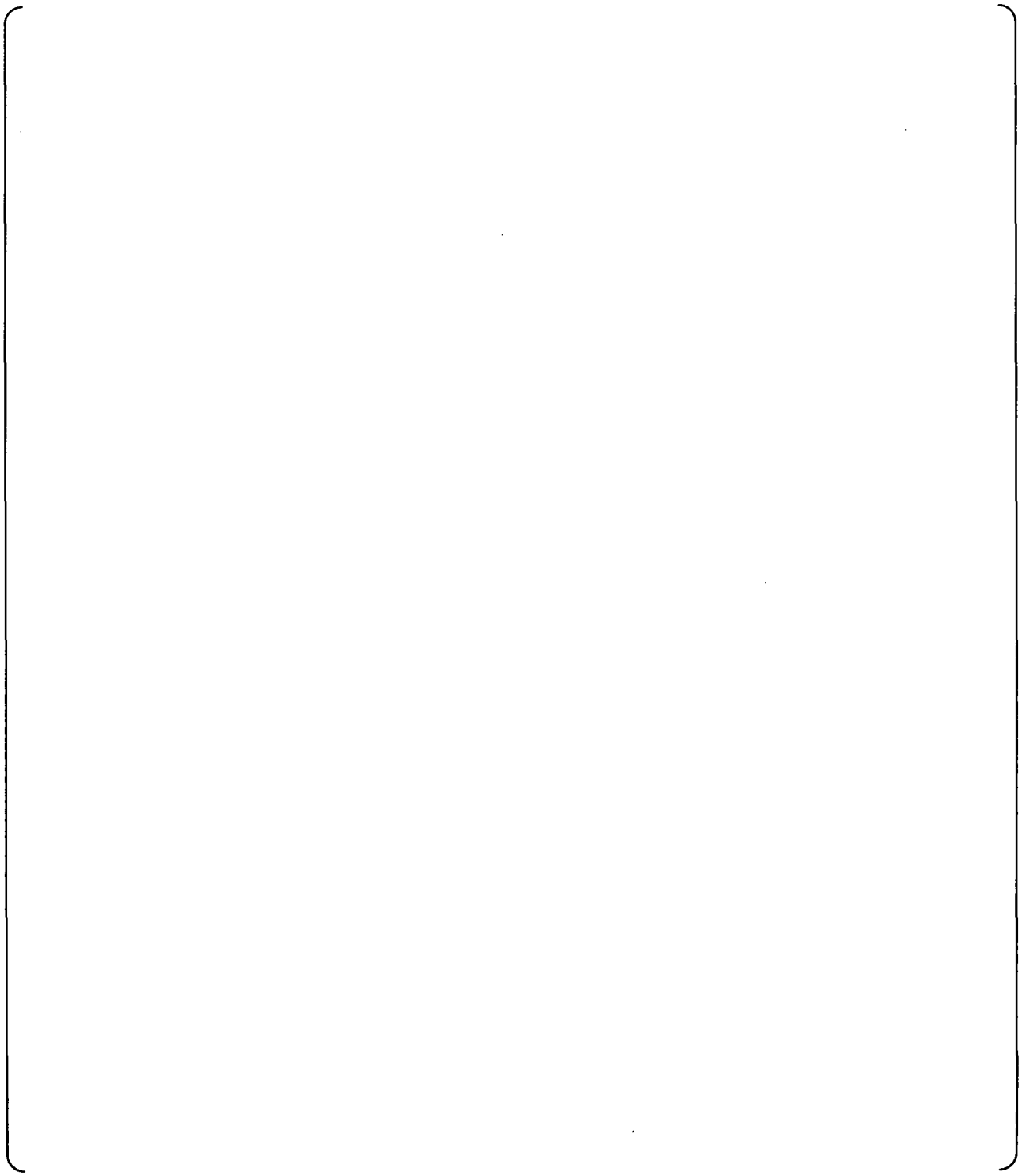

a,c

Figure 2-2 – Void Fraction Profile for ORNL Test 3.09.10L Axial Noding Sensitivity

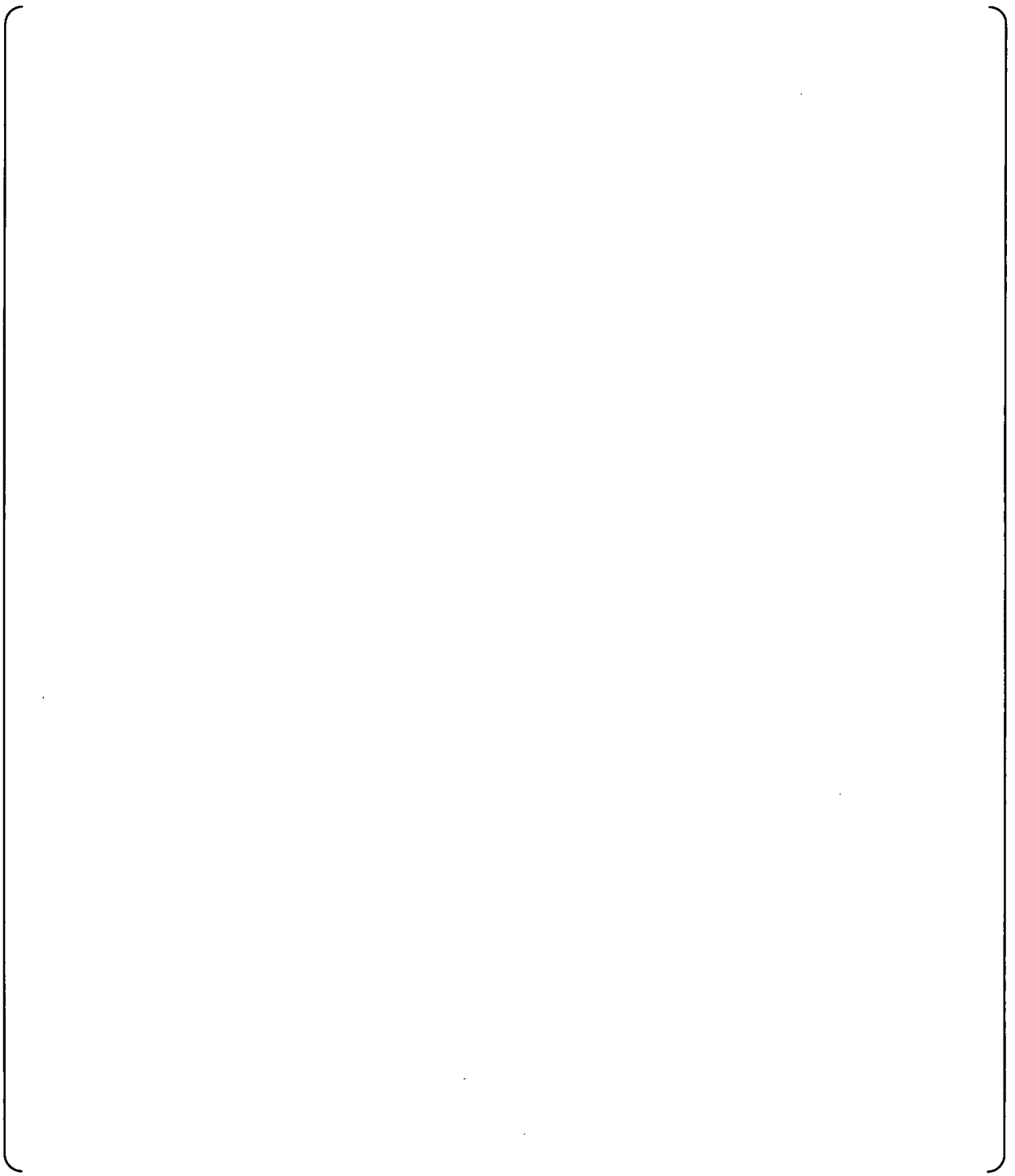

a,c

Figure 2-3 – Void Fraction Profile for ORNL Test 3.09.10AA Axial Noding Sensitivity

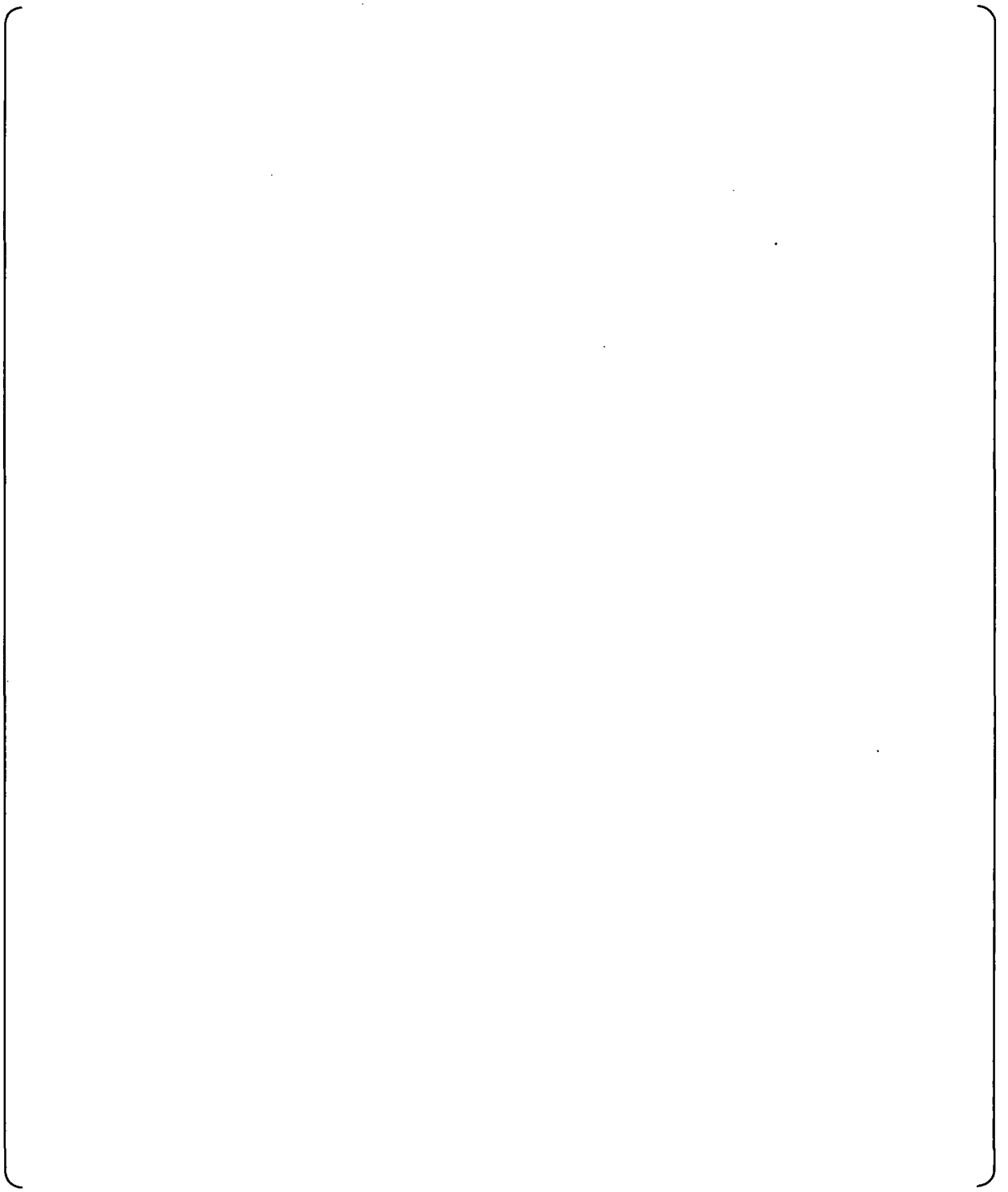

a,c

Figure 2-4 – Void Fraction Profile for ORNL Test 3.09.10DD Axial Noding Sensitivity

[ ] a,c

Figure 2-5 – Lower Plenum Pressure for the Beaver Valley PWR Axial Noding Study

[ ] a,c

Figure 2-6 – Lower Plenum Liquid Temperature for the Beaver Valley PWR Axial Noding Study

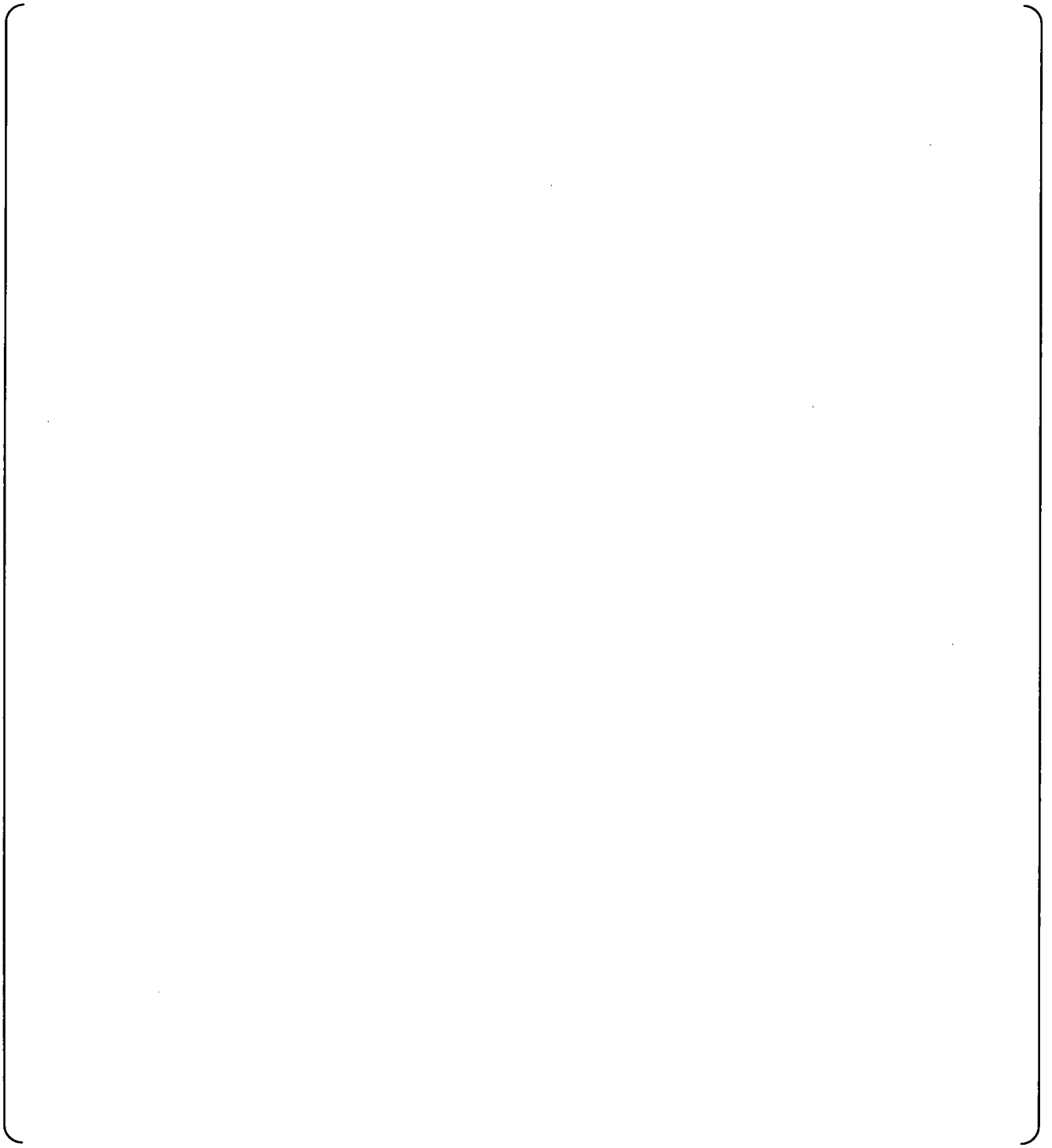

a,c

Figure 2-7 – NSAPLOT Node 65 Cladding Temperature for the Beaver Valley PWR Axial Noding Study

a,c

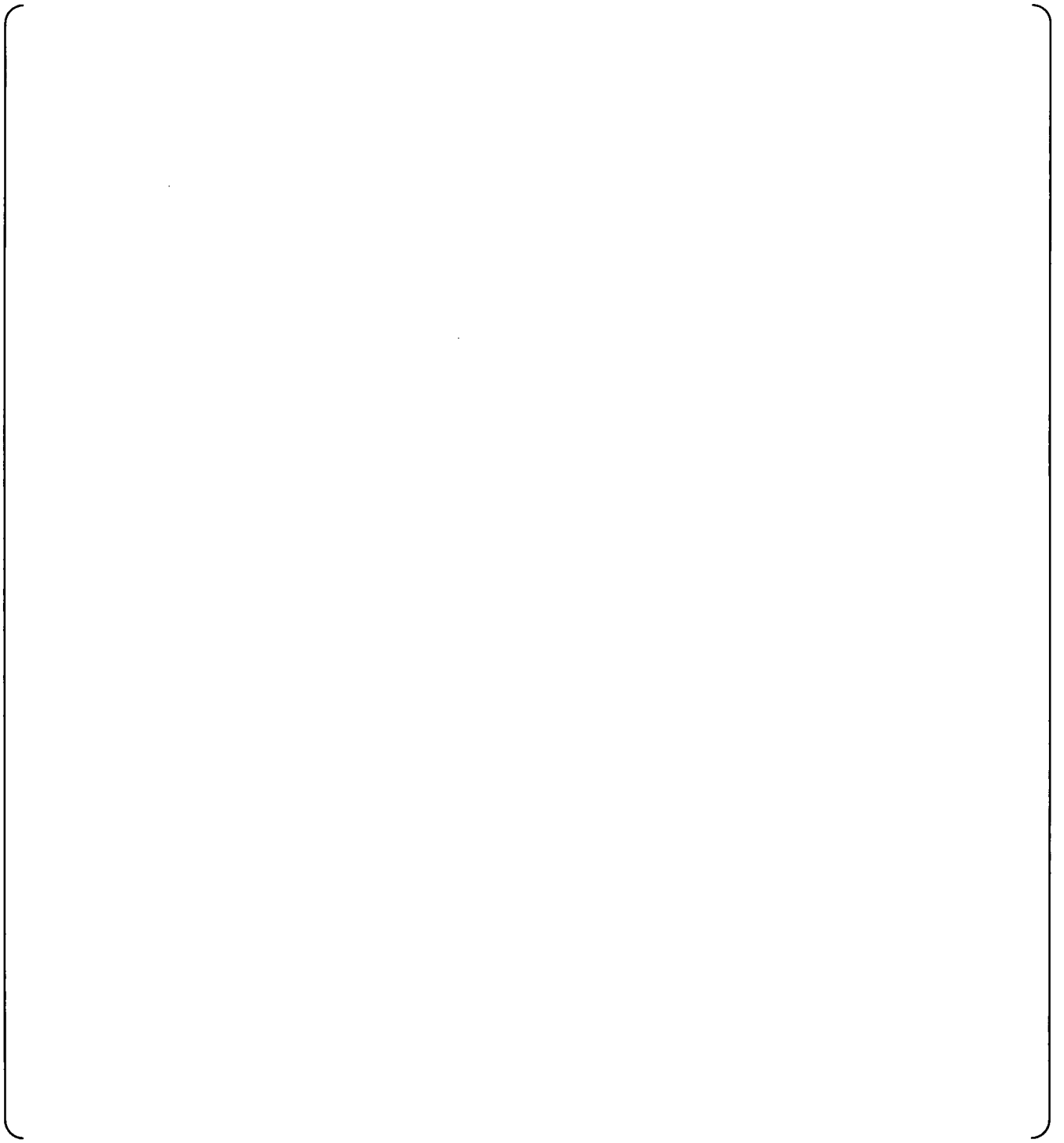

Figure 2-8 – NSAPLOT Node 75 Cladding Temperature for the Beaver Valley PWR Axial Noding Study

a,c

Figure 2-9 – Axial Void Fraction Profile in the Hot Channel Near the PCT Time for the Beaver Valley PWR Axial Noding Study

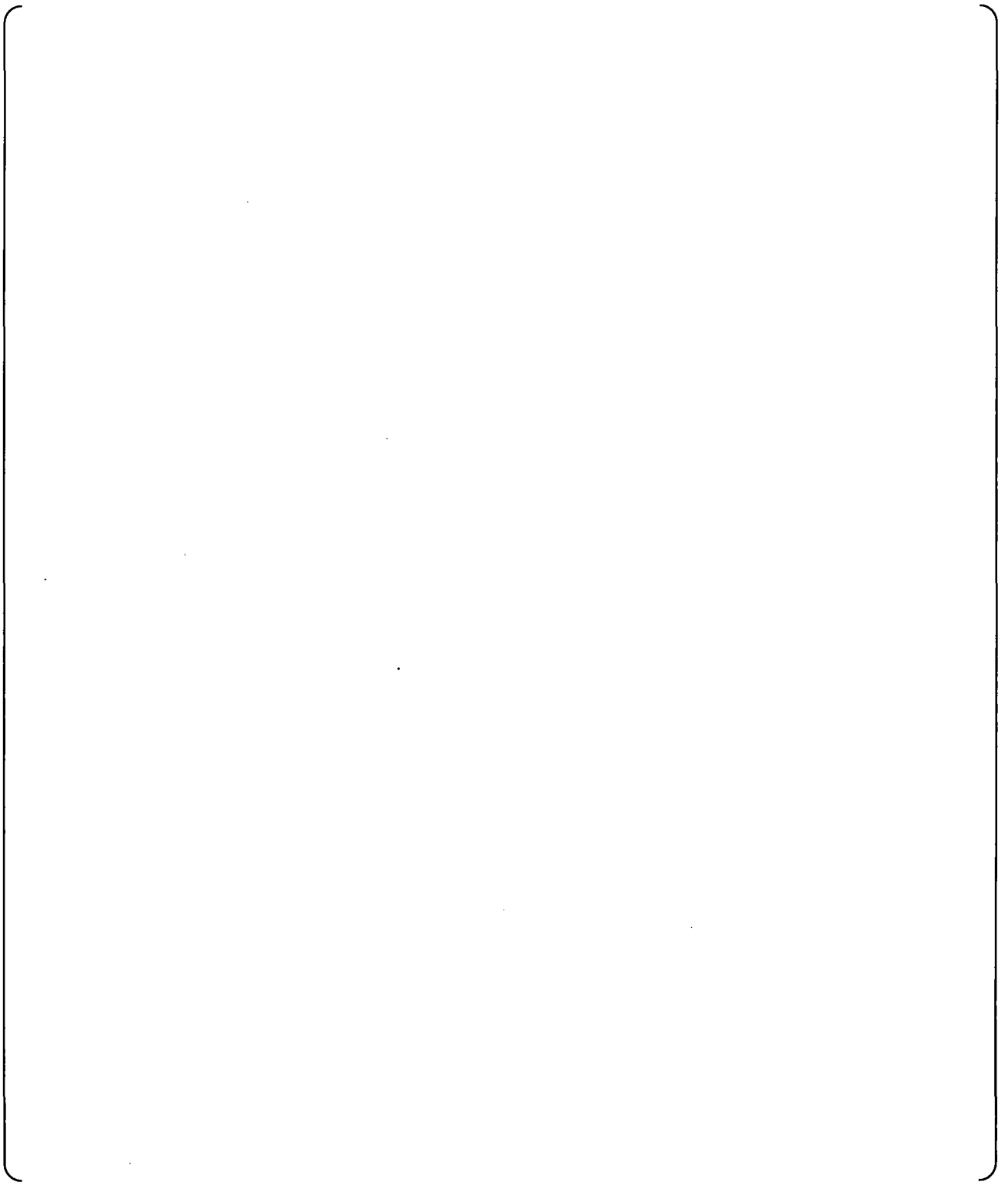

a,c

Figure 2-10 – Void Fraction Profile for ORNL Test 3.09.10l Timestep Size Sensitivity

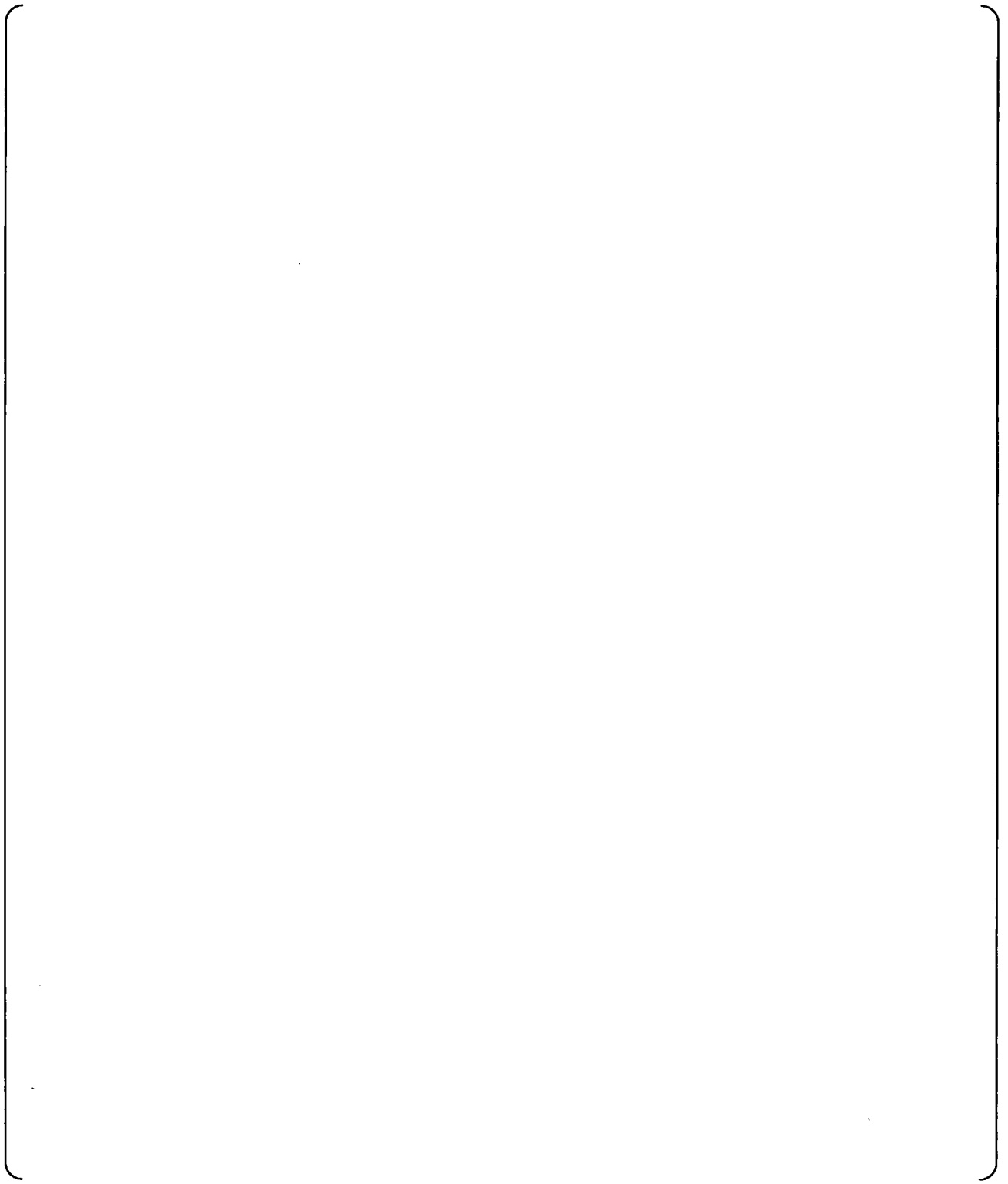

a,c

Figure 2-11 – Void Fraction Profile for ORNL Test 3.09.10CC Timestep Size Sensitivity

a,c

Figure 2-12 – Comparison of Predicted Void Profiles for FDRAG Sensitivity Study, ORNL – THTF Test 3.09.10CC

3. Hot Wall Ramp

By 'Hot wall ramp', it means a WCOBRA/TRAC-TF2 interfacial drag model to account for the vapor generation by wall heat transfer in Small Bubble flow regime. It is based on the premise that if boiling occurs at a solid boundary in a channel, the rate at which the vapor can be carried away from the wall is limited by the ability of the bubbles in the channel to perform this function. If more vapor is generated than can be carried away, vapor will begin to accumulate at the wall and the vapor/liquid interfacial geometry will take on the appearance of an inverted annular/slug regime. In consequence, the interfacial shear between the vapor and the bulk liquid is modeled ramping between the shear determined by the bubbly and inverted annular flow shear models.

In Small to Large Bubble flow regime, WCOBRA/TRAC-TF2 assumes large bubbles always co-exists with small bubbles, and the hot wall ramp algorithm is implemented for both Small Bubble and Small to Large Bubble flow regimes, as described in Sections 5.4.1 and 5.4.2 of Reference 3-1. However, effect is expected to diminish as the void fraction increases in this flow regime and results in more vapor flow area for vapor to be carried away from the boiling, as seen from Equation (5-69) of the Topical.

Further, for the Churn Turbulent flow regime, the interfacial drag force could potentially involve hot wall ramp effect since it is calculated by interpolating between the drag forces of the Small to Large Bubble and Film Mist flow regimes. Due to the associated high void fraction range in this regime, the chance to activate the hot wall ramp model is expected to be very small.

As a result of the detailed review of the hot wall ramp model on both the model description in the Topical (Reference 3-1) and how the model is coded in WCOBRA/TRAC-TF2, instances of inconsistency were identified between the coding and the topical report model descriptions, as well as between the design intent of the model and the coding. As a result, both the topical report and coded model need to be revised and they are detailed as follows.

- Based on the code review, Equation (5-67b) in the Topical will be revised to be consistent with WCOBRA/TRAC-TF2 coding as:

  [ ]^{a,c} (5-67b)

  where $K_{iX,v\ell,SB}$ is defined by (5-67a) in the Topical and revised to be consistent with the WCOBRA/TRAC-TF2 coding as:

  [ ]^{a,c} (5-67a)

  The term [ ]^{a,c} is included for Small Bubble regime to reduce the interfacial drag if relative velocity is high. This is to ensure that the drag coefficient remains reasonable for numerical stability reasons.

- It was found that U_Γ as defined by Equation (5-69) is not consistent with the physical meaning of wall heat transfer terms of $Q_{w\ell}$ and Q_b, Equation (5-69) needs to be corrected as:

  [ ]^{a,c} (5-69)

  where A_x is the cell momentum area in the axial direction and $Q_{w\ell}$ and Q_b are the heat flow from wall to liquid and the subcooled boiling heat flow, respectively (Section 7.2), which represent the 'implicit' and 'explicit' portions of the boiling heat transfer to account for the vapor generation in the saturated and subcooled boiling applications.

  The Γ_v term in Equation (5-69) of the Topical report is also removed as shown above after careful review of the model in the context of its applicable transient conditions. As pointed out in RAI 67 (4), the [

  ]^{a,c}.

The interfacial drag models of the cold wall flow regimes play key roles in determining the level swell and rod heat up in SBLOCA applications; however their impacts to a LBLOCA transient are expected to be small. As part of the cold wall regime interfacial models, the hot wall ramping model is not validated directly by itself, instead the WCOBRA/TRAC-TF2 interfacial drag correlations including the hot wall ramping algorithm are validated through key SBLOCA tests, such as ORNL-THTF small break tests and G-1 and G2 core uncover tests (Section 13 of Reference 3-1). In order to assess the impact of the hot wall ramping model to the SBLOCA transients, the sensitivities of the validation results of selected ORNL-THTF small break tests and a sample PWR SBLOCA run are evaluated using interfacial drag models with and without implementing the hot wall ramping algorithm. These evaluation results are presented in Figures 3-1.1 through 3-1.12 for ORNL small break tests, and Figure 3-1.13 for Beaver Valley 2.6 inch small break run PCT. Please note that these sensitivity studies are performed without implementing the hot wall ramping model modifications discussed in this subsection.

The following conclusions are drawn through these sensitivity runs of the hot wall ramping model:

- [

  ]^{a,c}

[

•

]^{a,c}

Reference(s)

3-1. WCAP-16996-P, "Realistic LOCA Evaluation Methodology Applied to the Full Spectrum of Break Sizes (FULL SPECTRUM LOCA Methodology)," November 2010.

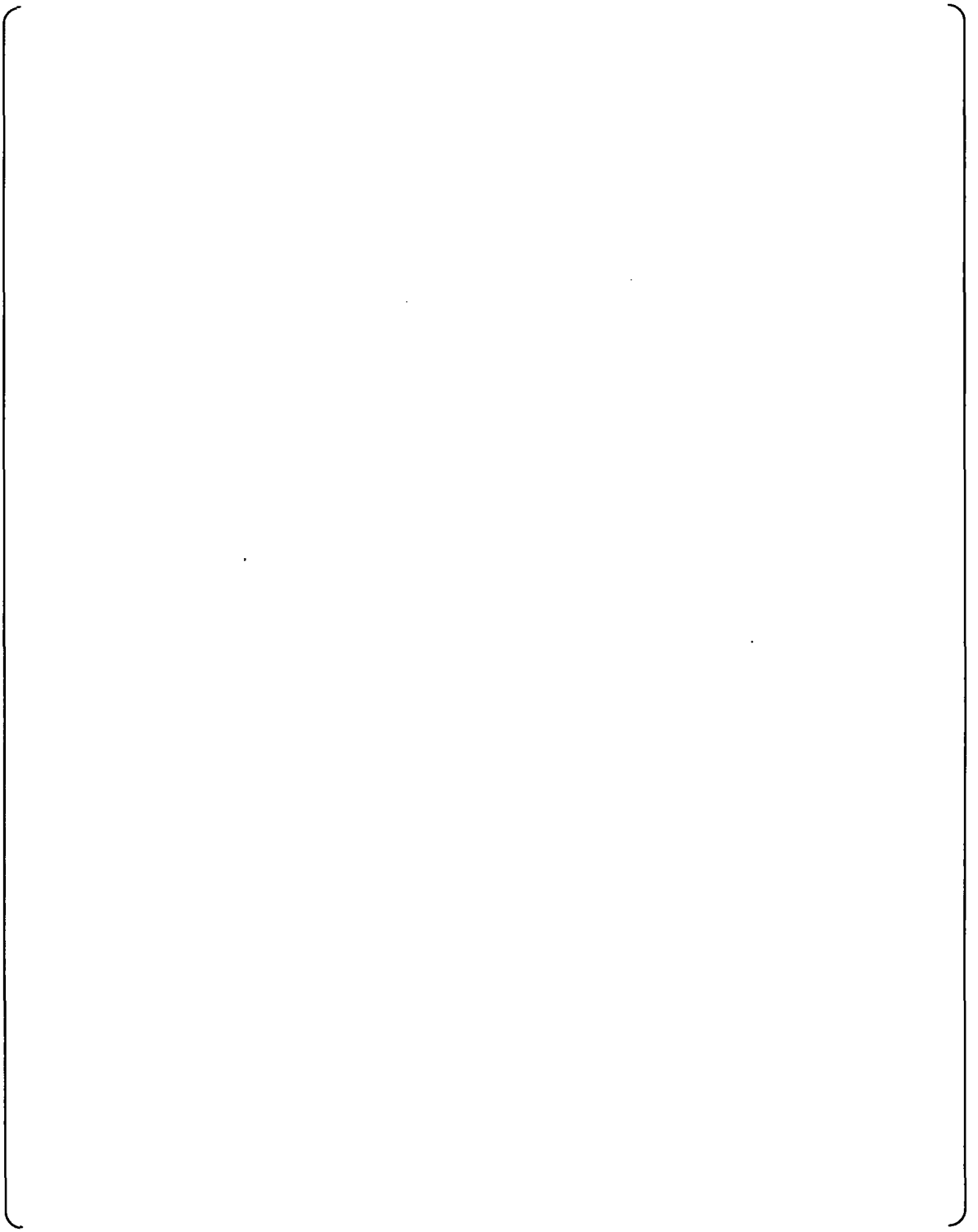

a,c

Figure 3-1.1 Hot Wall Ramping Model Sensitivity of ORNL (Case i)

(Solid: No Hot Wall Ramping; Dashed: With Hot Wall Ramping)

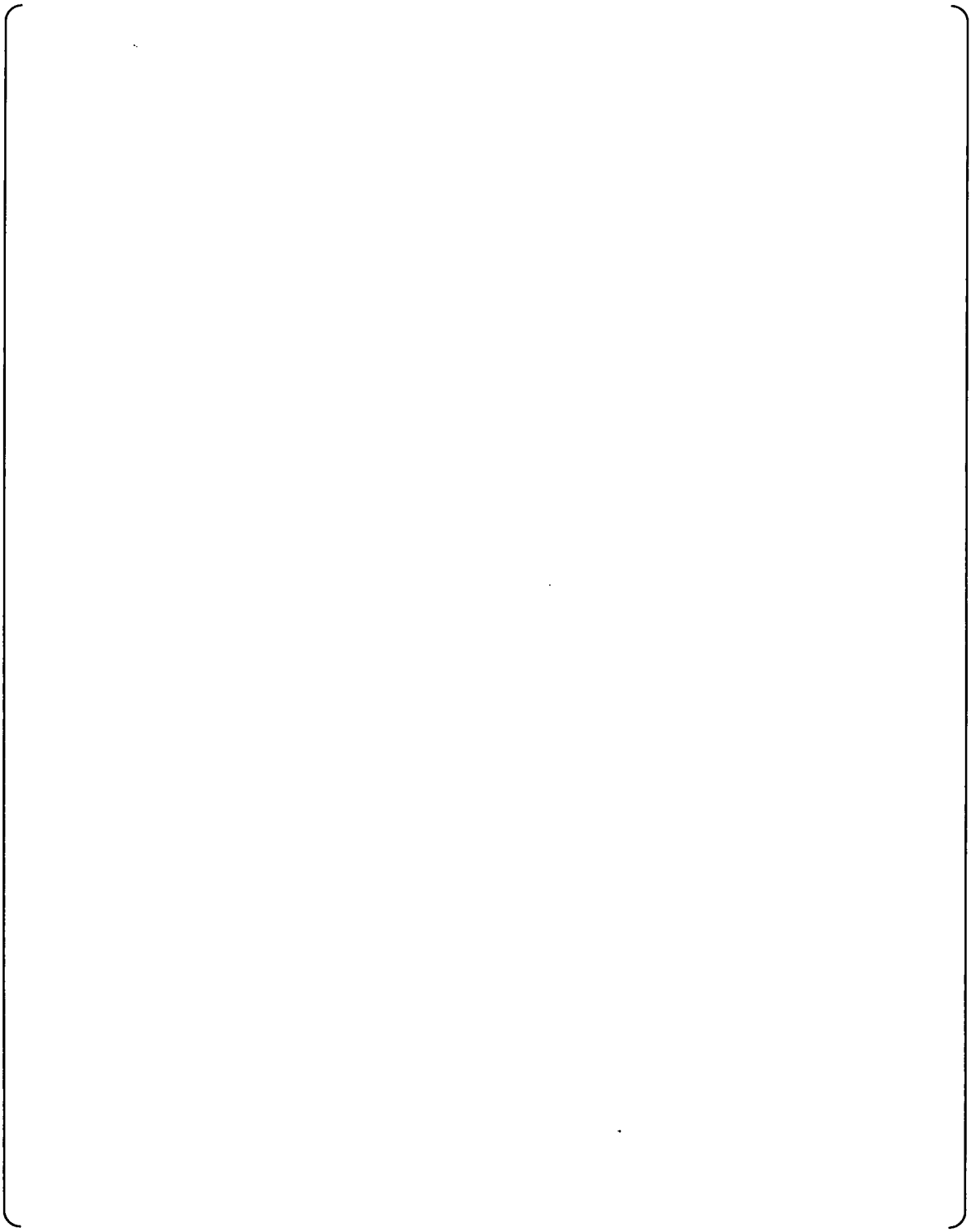

a,c

Figure 3-1.2 Hot Wall Ramping Model Sensitivity of ORNL (Case j)

(Solid: No Hot Wall Ramping; Dashed: With Hot Wall Ramping)

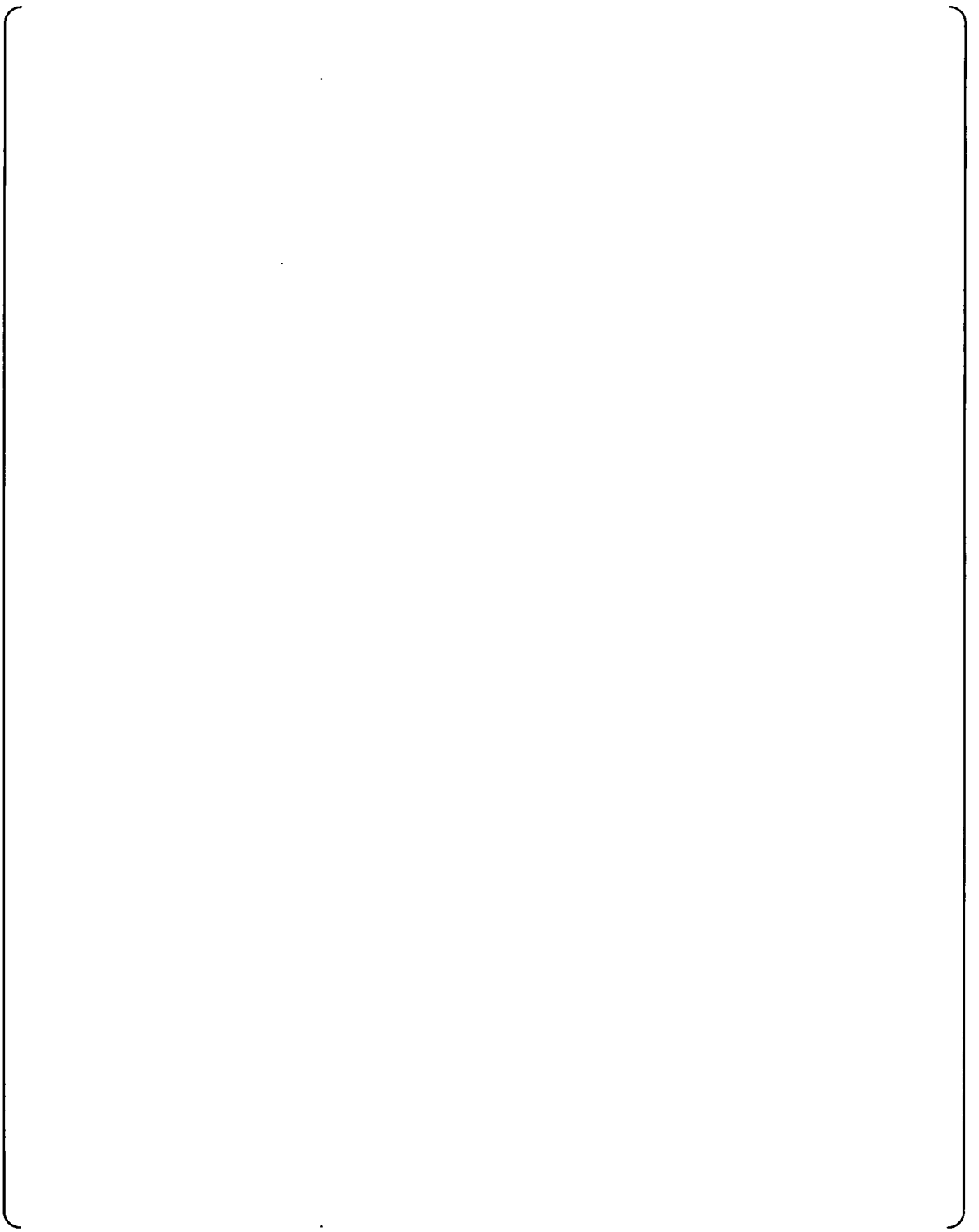

a,c

Figure 3-1.3 Hot Wall Ramping Model Sensitivity of ORNL (Case k)

(Solid: No Hot Wall Ramping; Dashed: With Hot Wall Ramping)

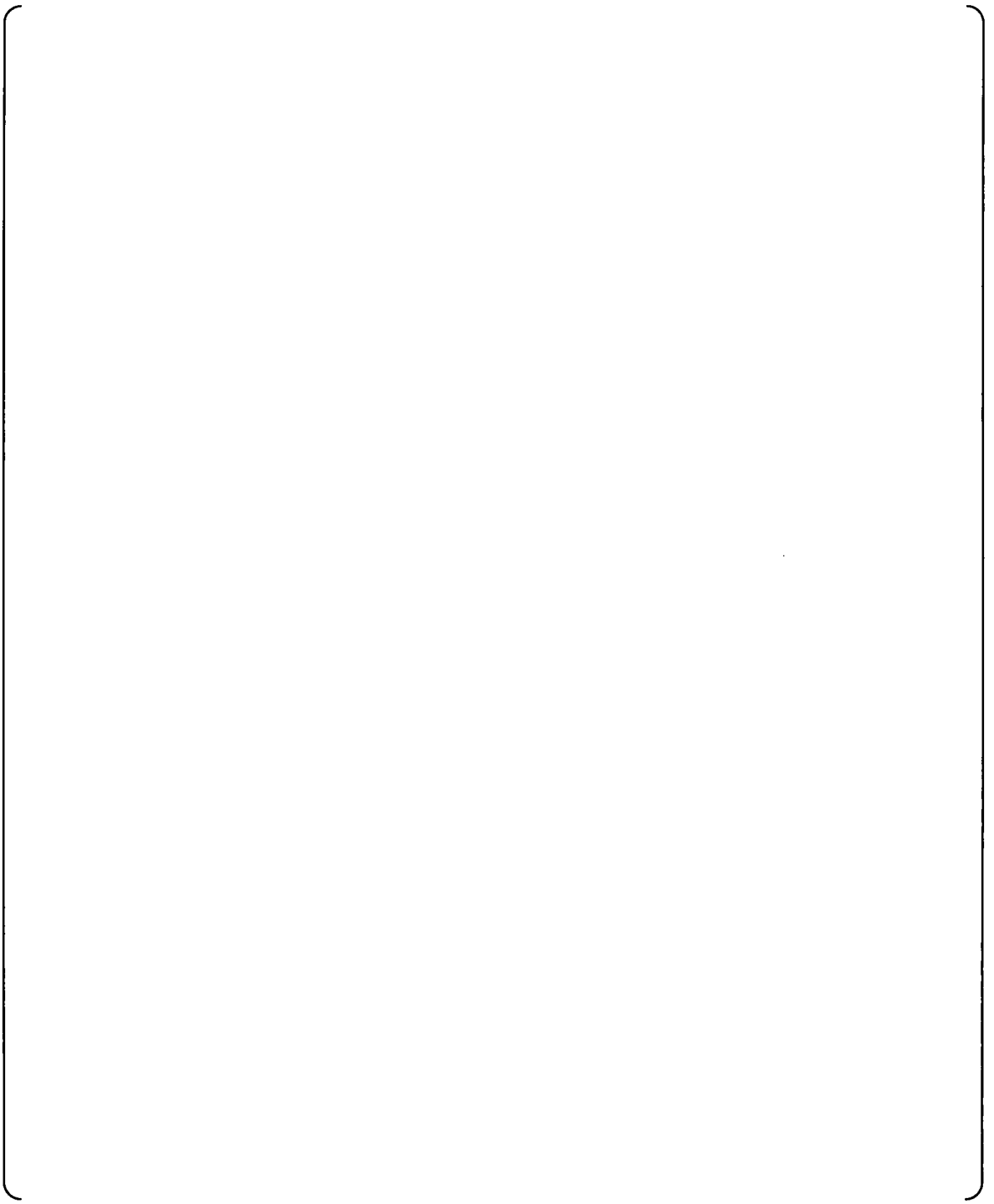

a,c

Figure 3-1.4 Hot Wall Ramping Model Sensitivity of ORNL (Case I)

(Solid: No Hot Wall Ramping; Dashed: With Hot Wall Ramping)

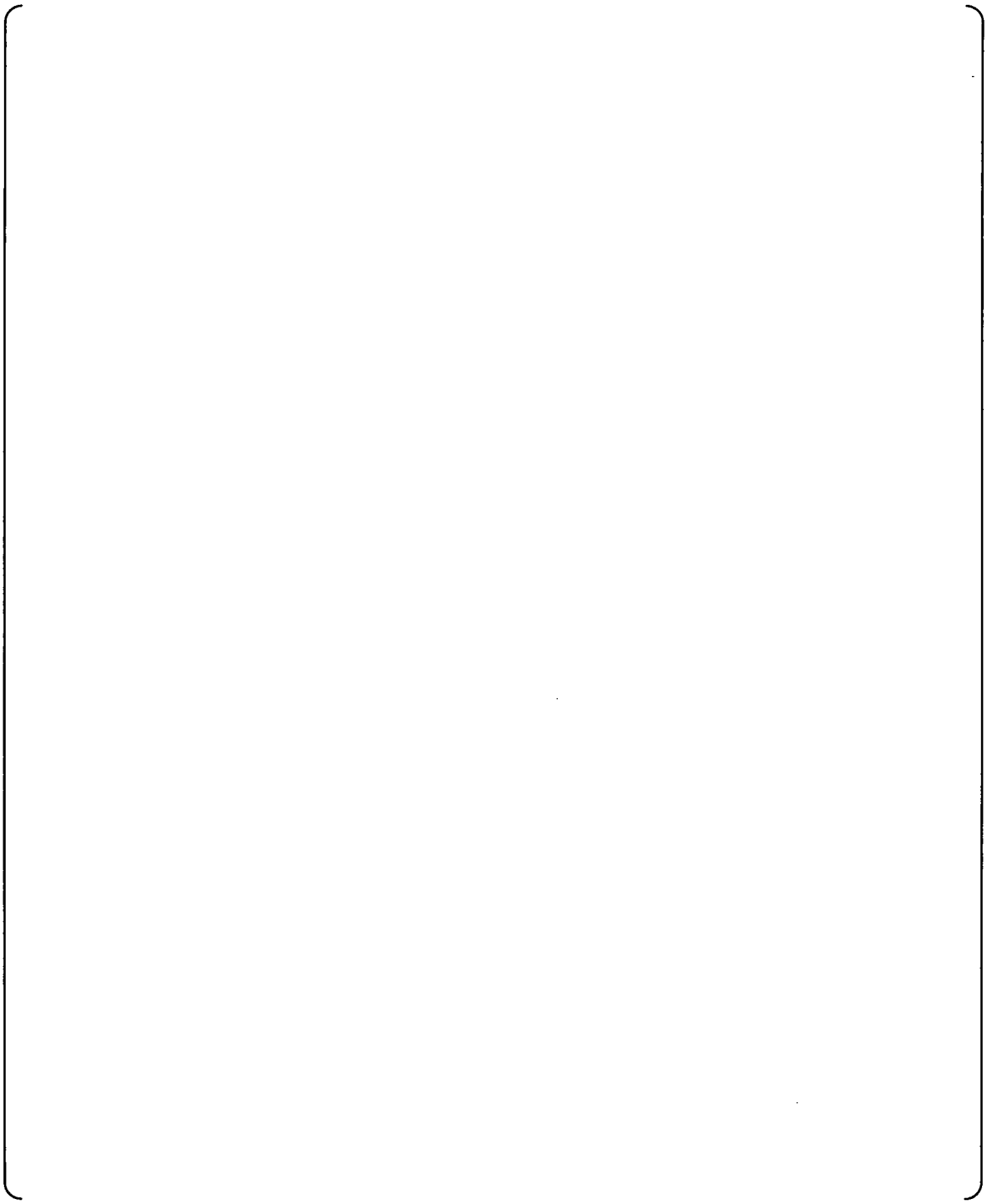

a,c

Figure 3-1.5 Hot Wall Ramping Model Sensitivity of ORNL (Case m)

(Solid: No Hot Wall Ramping; Dashed: With Hot Wall Ramping)

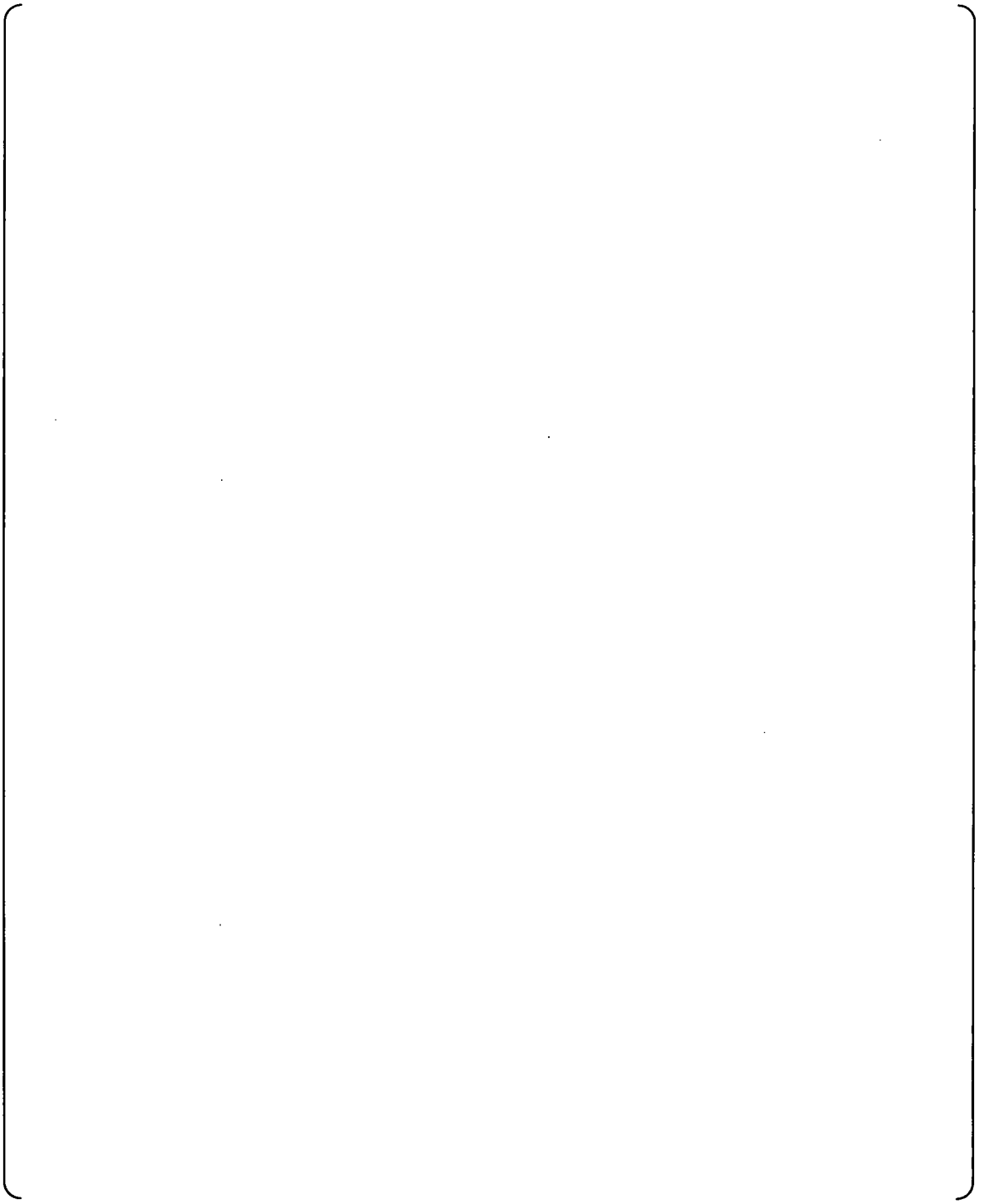

a,c

Figure 3-1.6 Hot Wall Ramping Model Sensitivity of ORNL (Case n)

(Solid: No Hot Wall Ramping; Dashed: With Hot Wall Ramping)

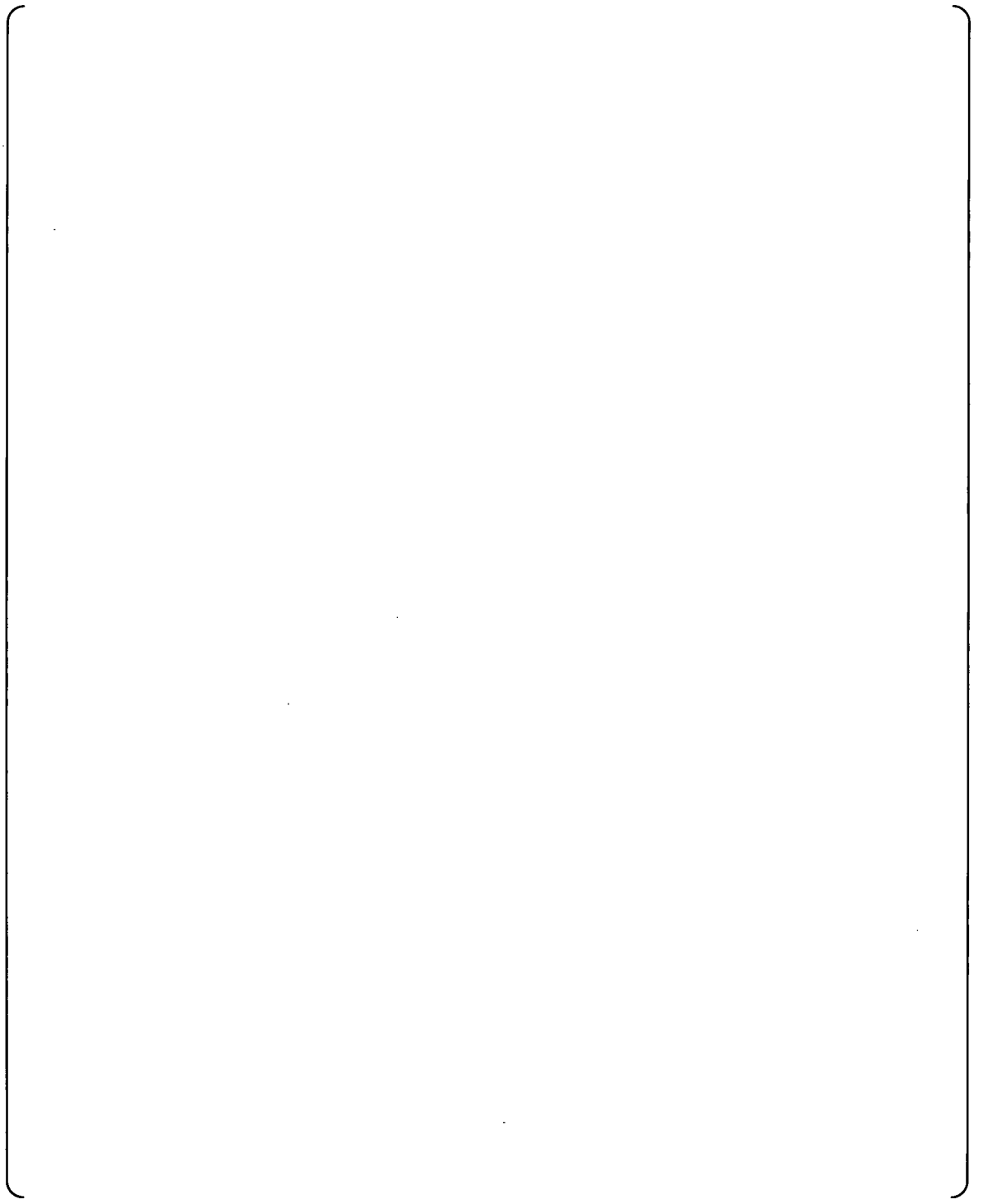

a,c

Figure 3-1.7 Hot Wall Ramping Model Sensitivity of ORNL (Case aa)

(Solid: No Hot Wall Ramping; Dashed: With Hot Wall Ramping)

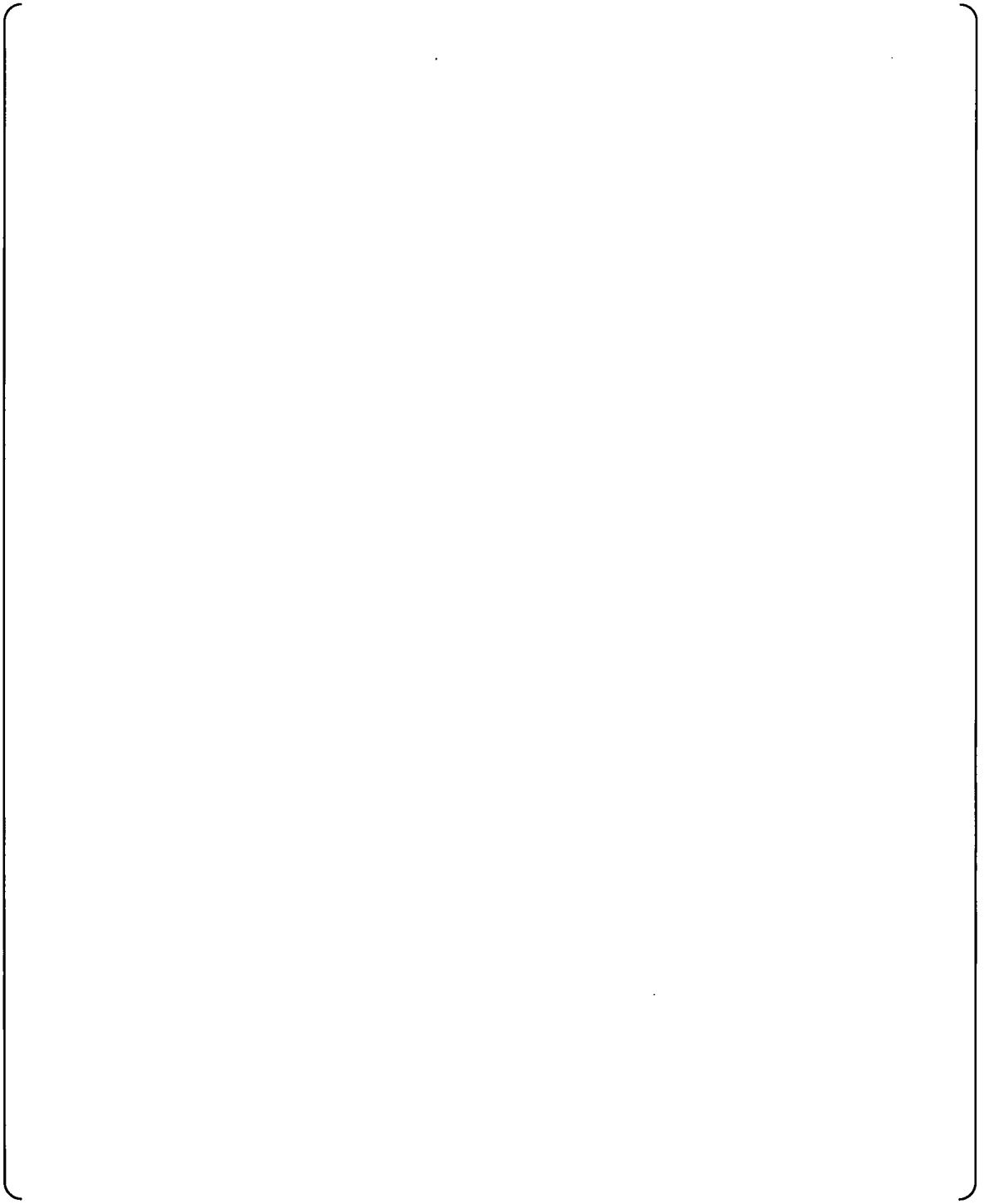

a,c

Figure 3-1.8 Hot Wall Ramping Model Sensitivity of ORNL (Case bb)

(Solid: No Hot Wall Ramping; Dashed: With Hot Wall Ramping)

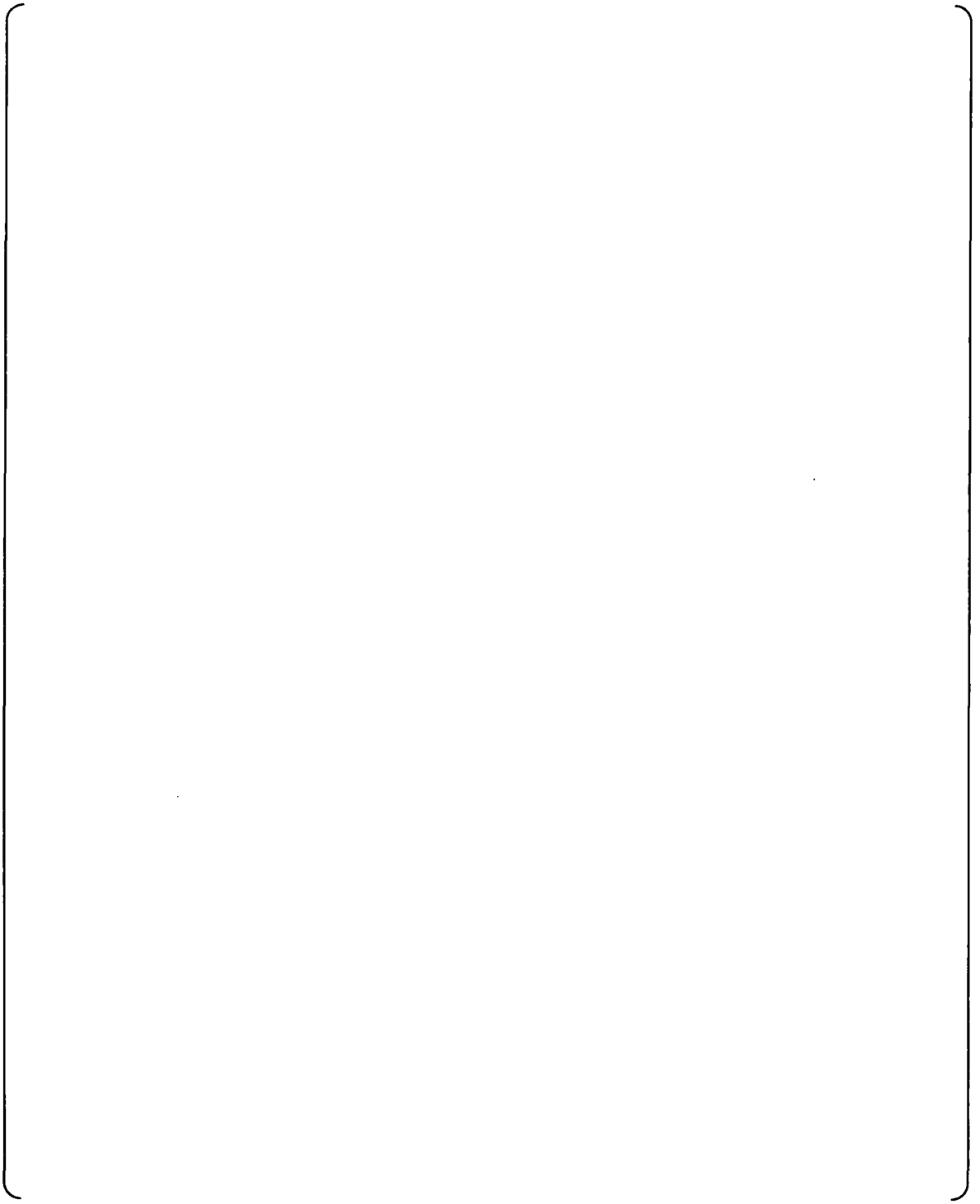

a,c

Figure 3-1.9 Hot Wall Ramping Model Sensitivity of ORNL (Case cc)

(Solid: No Hot Wall Ramping; Dashed: With Hot Wall Ramping)

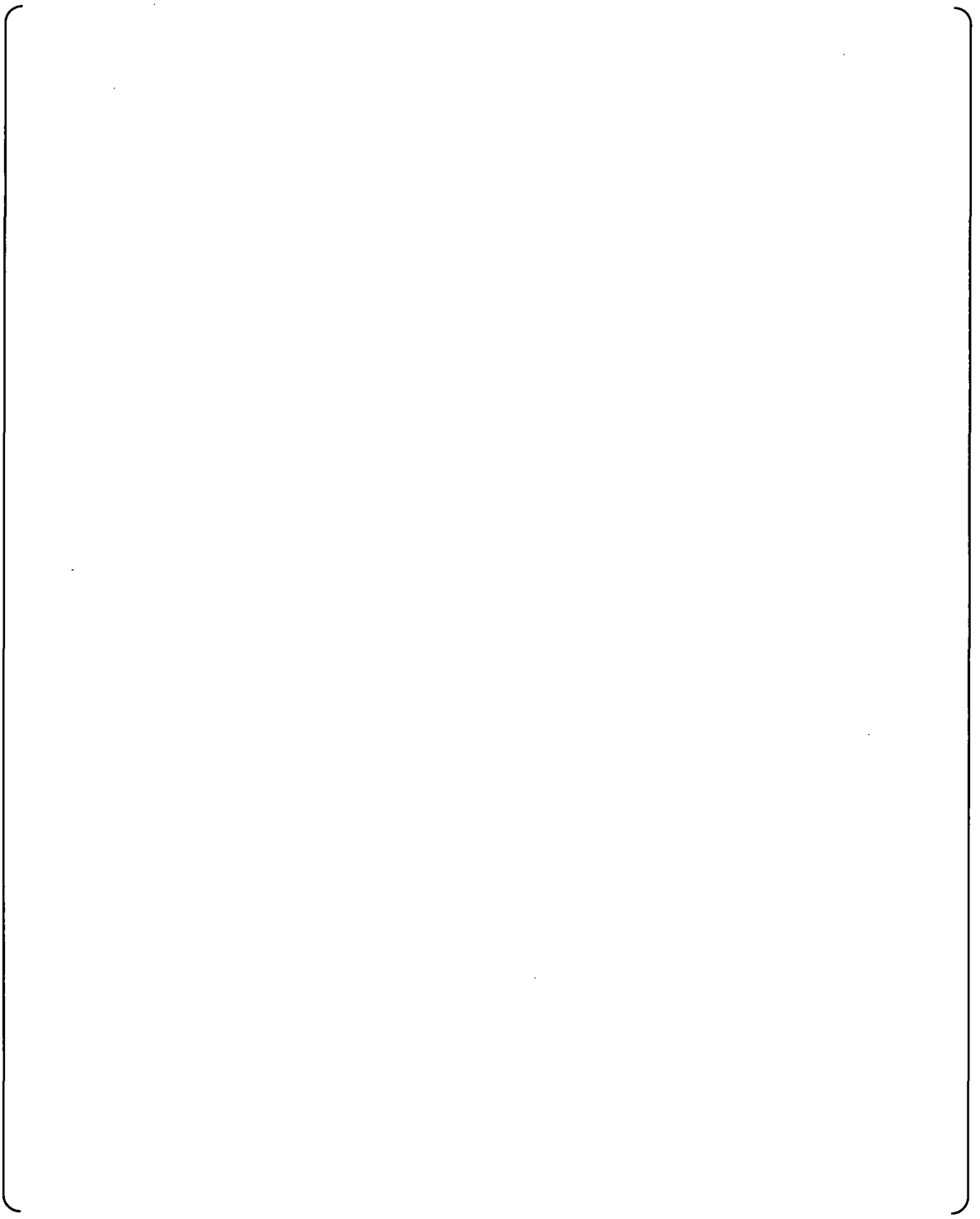

a,c

Figure 3-1.10 Hot Wall Ramping Model Sensitivity of ORNL (Case dd)

(Solid: No Hot Wall Ramping; Dashed: With Hot Wall Ramping)

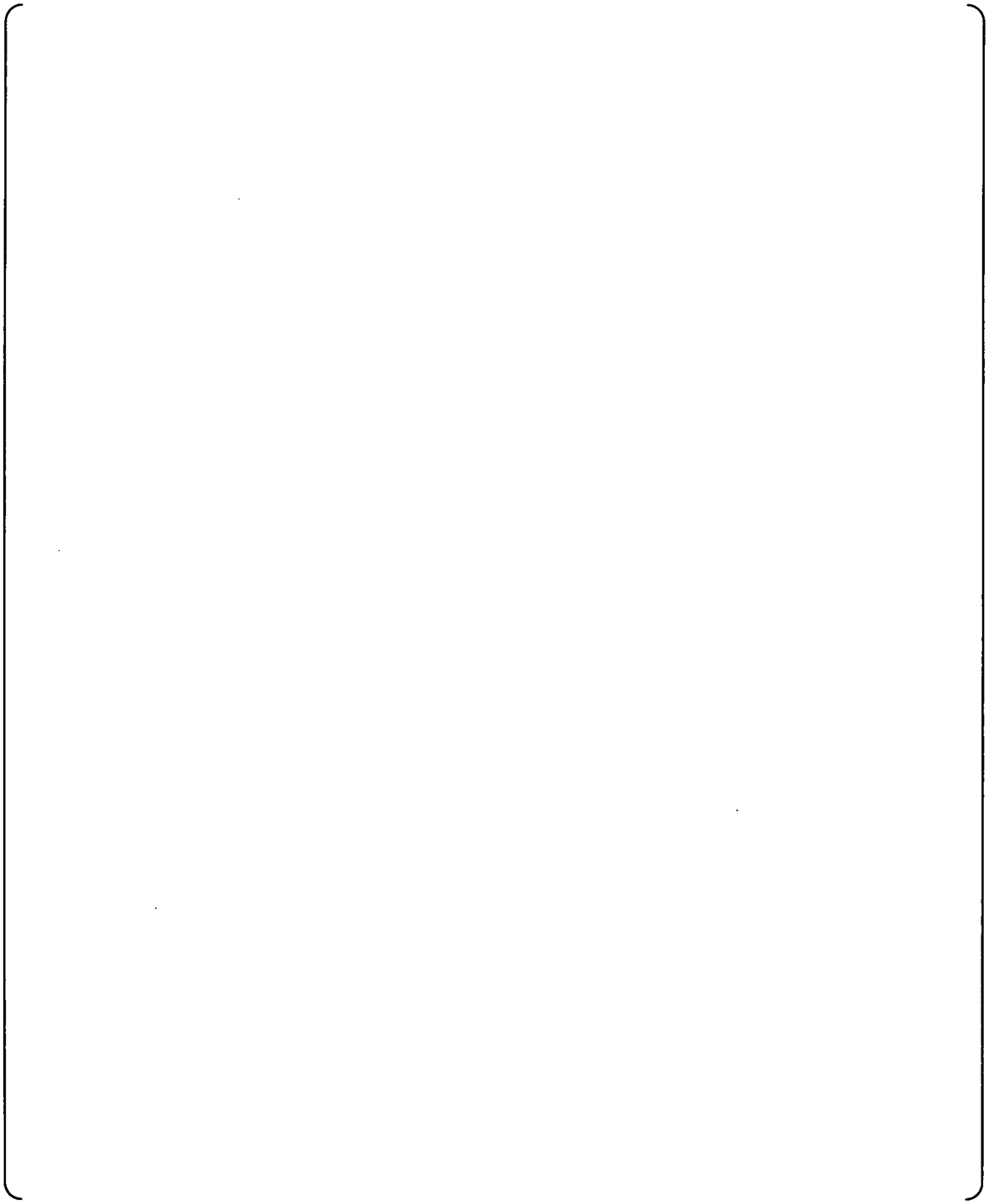

a,c

Figure 3-1.11 Hot Wall Ramping Model Sensitivity of ORNL (Case ee)

(Solid: No Hot Wall Ramping; Dashed: With Hot Wall Ramping)

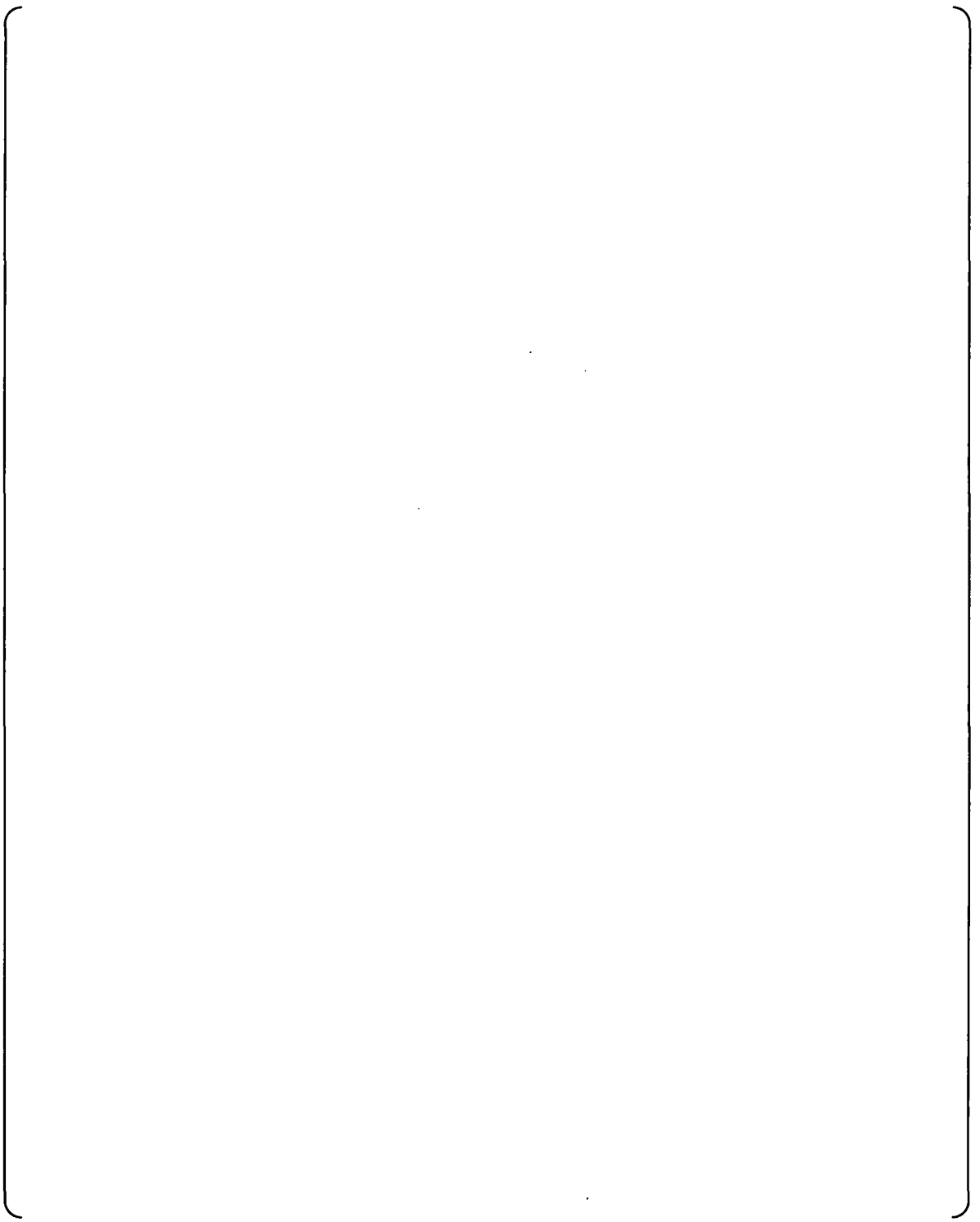

a,c

Figure 3-1.12 Hot Wall Ramping Model Sensitivity of ORNL (Case ff)

(Solid: No Hot Wall Ramping; Dashed: With Hot Wall Ramping)

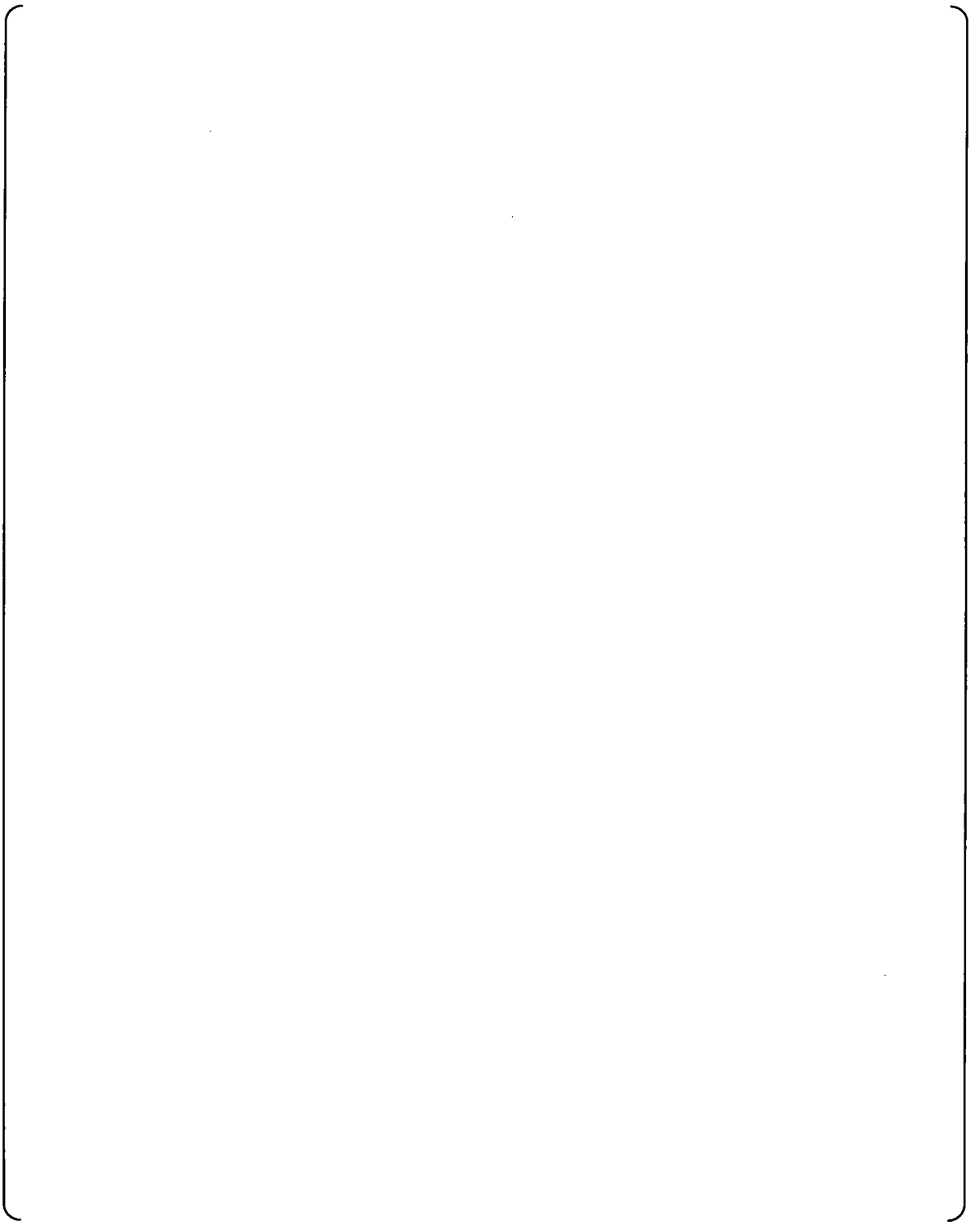

a,c

Figure 3-1.13 Hot Wall Ramping Model Sensitivity of DLW SB

(Solid: No Hot Wall Ramping; Dashed: With Hot Wall Ramping)

4. RAI Questions and Responses

4.1 RAI 59

Question #59: WCOBRA/TRAC-TF2 Flow Maps for Vessel and One-Dimensional Components

WCAP-16996-P/WCAP-16996-NP, Volumes I, II, and III, Revision 0, Subsection 4.2.2, "Small Bubble Regime," explains that the SB regime is applied when the two-phase flow void fraction is less than 20 percent. As such, it models what is generally referred to as "bubbly flow" in the two-phase flow literature. In this regime, the vapor phase is assumed to exist as uniform spherical bubbles dispersed in a continuous liquid phase. The bubble radius is determined by Equation (4-15) using a critical Weber number of 10 and applying the vector sum of the maximum lateral relative velocity and the axial relative velocity for the cell. According to Equation 4-16, the bubble diameter is limited to the cell hydraulic diameter or [ ]^{a,c} whichever is smaller.

According to WCAP-16996-P/WCAP-16996-NP, Volumes I, II, and III, Revision 0, Subsection 4.2.3, "Small to Large Bubble Regime," this regime is applied for void fractions greater than or equal to 20 percent and less than or equal to 50 percent. In the SLB regime, the vapor phase is modeled by a SB field accounting for 20 percent void fraction with the remaining vapor content being attributed to one or more large bubbles. The large bubble radius is determined by Equation (4-24) and it cannot be larger than the cell hydraulic diameter or [ ]^{a,c} according to Equation (4-23).

WCAP-16996-P/WCAP-16996-NP, Volumes I, II, and III, Revision 0, Subsection 4.2.4, "Churn-Turbulent Flow Regime," explains that this regime is used when the void fraction is above 50 percent and remains below a certain critical void fraction at which a stable liquid film at the wall is formed. It is explained that this critical void fraction, determined by the flow channel size and the vapor velocity, is limited to a minimum void fraction of 80 percent as below this value waves are expected to bridge across the flow channel and cause a transition to CT flow. The CT regime as modeled as a combination of the Large Bubble and the FD regimes.

According to WCAP-16996-P/WCAP-16996-NP, Volumes I, II, and III, Revision 0, Subsection 4.2.5, "Film/Drop Flow Regime," this regime exists above a certain critical void fraction criterion. The liquid phase is present as a wall film and possibly droplets that can be entrained by the steam flow. The droplet diameter is determined by Equation (4-48) using the entrained liquid fraction and it is limited to [ ]^{a,c} Table 1 below presents major correlations used in the implementation of the "Cold Wall" flow regime map in WCOBRA/TRAC-TF2.

(1) Please demonstrate the applicability of the value used for the critical Webber number in Equation (4-15) to predict the diameter of the small bubble, D^*_b. Provide the units for the SB radius as defined by this equation. Define the range of applicability of this expression with regard to hydraulic diameter, pressure, phase mass flow rates, and void fraction, along with supporting test data. Explain how the vector sum of relative velocities between the vapor

and continuous liquid phases, $\underline{U}_{vl}$, used in Equation (4-15), is calculated, and describe any limitations with regard to slip (velocity ratio). Please explain if Equations (4-15) and (5-60) define the same physical parameter.

(2) Equation (4-24) defines the large bubble diameter, D^*_{LB}, as being proportionate to the volume of the hydraulic computational cell, $\Delta V=A_x \Delta X$:

$D^*_{LB} \sim (A_x \Delta X)^{1/3}$.

Please explain the appropriateness of defining a physical parameter that is introduced to describe a phenomenon of relevance for the core two-phase level swell modeling by making this diameter dependent upon the fluid volume in a computational mesh cell. Nodalization can vary and so will the predicted value of the relevant physical parameter describing the phenomenon of interest. Such an approach can introduce uncertainties and nonphysical behavior in code predictions through artificial distortions of physical models used in the prediction of safety relevant thermal-hydraulic process. Please estimate the bounding effect on core level-swell prediction results. Define the range of applicability of this expression with regard to hydraulic diameter, pressure, phase mass flow rates, void fraction, and slip along with supporting test data.

Table 1: Major Correlations in the WCOBRA/TRAC-TF2 "Cold Wall" Flow Regime Map

Flow Regime	Void Fraction, α (%)	Bubble/Droplet Diameter or Film Thickness	Size Limitations	Flow Structure
Small Bubble	$0 < \alpha \leq 20$	Small bubble diameter, Equation (4-15): $D^*_b=We_{crit}\sigma g_c/(\rho_l \underline{U}^2_{vl})+0.00002$ $\underline{U}_{vl}$ – vector sum of relative velocities between vapor and continuous liquid $We_{crit}=10$	[ ]^{a,c}	Small bubble only
Small-to-Large Bubble	$20 < \alpha \leq 50$	Large bubble diameter, Equation (4-24): $D^*_{LB}=[3/(4\pi)(\alpha_v-V_{SB}/\Delta V)\Delta V]^{1/3}$ $\Delta V=A_x/\Delta X$ – cell volume V_{SB} – volume of small bubbles	[ ]^{a,c}	Small and large bubbles
Churn-Turbulent	$50 < \alpha \leq \alpha_{crit}$	Entrained droplet diameter, Equation (4-48): [ ]^{a,c}	[ ]^{a,c}	
Film/Drop	$\alpha_{crit} < \alpha \leq 100$	Critical layer thickness and void, Equation (4-39): $\delta_{crit}=C_l\sigma/(\rho_v\lvert\underline{U}_{vl}\rvert^2)$ $\underline{U}_{vl}$ – relative velocity between continuous liquid and vapor $\alpha_{crit}=1-4\delta_{crit}/D_h-\alpha_e$ $C_l=0.5$	$\alpha_{crit,\,min}=80\%$	Liquid film and entrained drops, if any

(3) According to Equation (4-16), the bubble diameter in the SB regime is limited to [ ]^{a,c} or to the hydraulic diameter. A typical fuel assembly has a hydraulic diameter of 0.045 ft (0.53 in or $13.6x10^{-3}$ m). Based on Equation (4-23), the large bubble diameter in the SLB or CT flow regimes cannot be larger than the cell hydraulic diameter or [ ]^{a,c} whichever is smaller. Accordingly, for a two-phase flow in a fuel bundle, the SB diameter would be limited to [ ]^{a,c} and the large bubble diameter would be limited [

]^{a,c} Please explain the appropriateness and applicability of the applied limits for the diameters of the small and large bubbles. Please explain the technical basis for the [ ]^{a,c} limit for the large bubble diameter limit and its impact on two-phase level swell calculations.

(4) Equation (4-41) defines the critical film thickness used in the CT flow regime modeling. Please define the range of applicability of this expression with regard to hydraulic diameter, pressure, and phase mass flow rates along with supporting test data. Explain how the relative velocity between the continuous liquid and the vapor phase, $\underline{U}_{vl}$, used in Equation (4-41), is calculated. Explain how the entrained liquid fraction, α_e, appearing in Equation (4-41) and Equation (5-80), is calculated. Please clarify why the critical void fractions, as defined in Equation (5-93) in WCAP-16996-P/WCAP-16996-NP, Volumes I, II, and III, Revision 0, Subsection 5.4.4, "Film/Drop Flow Regime," and in Equation (5-127) in Subsection 5.6.2, "Entrainment in Film Flow," do not take into account the entrained liquid fraction, α_e. Please address the threshold conditions for liquid entrainment and define the range of applicability of the correlations used to predict the entrained liquid fraction, α_e, with regard to hydraulic diameter, pressure, and phase mass flow rates, and void fraction along with supporting test data. In addition, please explain the way in which WCOBRA/TRAC-TF2 predicts the diameter of the entrained droplets, the number of droplets and the drop interfacial area density. Given these droplet diameters and associated interfacial areas, describe how this formulation is used in or related to the computation of interfacial heat transfer between the steam and liquid phases. Please explain if this model predicts entrained droplets leaving the two-phase surface and entering the steam region during periods of predicted core uncovery for small breaks in the order of 0.02 to 0.01 ft^2.

(5) WCAP-16996-P/WCAP-16996-NP, Volumes I, II, and III, Revision 0, Subsection 5.4.3, "Churn-Turbulent Flow Regime Interfacial Drag," explains that "The churn-turbulent regime is assumed to be a combination of the large bubble regime and the film/drop regime." Please explain how the CT flow is modeled in WCOBRA/TRAC-TF2 as a combination of LB and FD regimes. In particular, please explain the assumed forms of presence for each phase, e.g., small bubbles, large bubbles, droplets, slugs, continuous form.

(6) Please provide a table that describes constitutive correlations used for flow regime identification by the "Cold Wall" and "Hot Wall" flow maps for a vessel component and the flow regime map for the one-dimensional components in WCOBRA/TRAC-TF2. For each

individual correlation, please provide information that describes the source reference, applicability range for defining parameters, extrapolations, and limitations outside of applicability ranges as appropriate, and the supporting technical basis including applicable test data and references to validation analyses. Include the flow regime indicator and number for each individual flow regime as Table 4.2-1 appears incomplete. In addition, please describe major differences in the modeling of corresponding flow regimes for the vessel and one-dimensional components.

Response:

Part (1)

In bubbly flow dynamics, an important dimensionless group to determine the stability of a single bubble is the Weber (We) number. The Weber number represents the ratio of inertia to surface tension. The inertia force tends to deform and break bubble while the surface tension tends to stabilize the bubble surface. The Weber number for bubbles is usually defined using liquid density, bubbly diameter, surface tension, and relative velocity or turbulent velocity. Eq. 4-15 of the topical report predicts the diameter of small bubbles by assuming a critical Weber number, which is an empirical value. The technical basis of adopting a critical Weber number to evaluate the interfacial drag in a two phase flow has been detailed by Wallis (Reference 4.1-1, Chapter 12) and Ishii (Reference 4.1-2, Chapters 11 and 12). In Chapter 11, Section 1.2.1 of Reference 4.1-2, the critical Weber number for bubble break up due to turbulent impact was determined to be 6.0 experimentally, and the critical Weber number is around 12 for droplet break up as shown in Chapter 12, Section 1.2.1 (Reference 4.1-2). For churn-turbulent flow regime, Section 1.2.2 of Chapter 12 (Reference 4.1-2) reported the critical Weber number is 8 for bubble and 12 for droplet. Eq. 4-15 in the topical report assumes a critical Weber number of [ ]^{a,c} to the values by Ishii (Reference 4.1-2). With knowing the Weber number of [ ]^{a,c}, one could calculate void fraction distribution in a vertical pipe using the small bubble interfacial drag model in the topical report and the force balance between the interfacial drag and buoyancy. Figure 4.1-1 and Figure 4.1-2 compare the calculated void fractions assuming [ ]^{a,c} with the void fraction prediction based on the Zuber-Findlay drift flux model (Reference 4.1-10) at different vapor superficial velocities at low pressure (40 psia) and high pressure (1000 psia), respectively. The void fractions in the small bubble flow regime are [

]^{a,c}

Using a critical Weber number to predict bubble size is common in the thermal hydraulic codes. A review of those thermal hydraulic codes shows the critical Weber number of [ ]^{a,c} is similar to the values selected by other thermal hydraulic codes. For example, TRAC-PF1 (Reference 4.1-3) uses a critical Weber number of 7.5 for bubbly flow, the critical Weber number is 10 in both RELAP5/MOD2 (Reference 4.1-4) and RELAP5/MOD3.3 (Reference 4.1-5), COBRA-TF (Reference 4.1-6) uses a critical Weber number of 10 for bubbly flow, and the same value of 10 is adopted by GOTHIC (Reference 4.1-7). Those thermal hydraulic codes

have been applied to a wide range of applications. Both TRAC-PF1 and RELAP5/MOD3.3 have been applied to small break and large break LOCA analysis of PWR. The COBRA-TF code has been applied to core thermal hydraulic analysis and transient analysis for both BWR and PWR. GOTHIC has been approved for the containment thermal hydraulic analysis. The diversified applications of those thermal hydraulic codes demonstrated the applicability of using the critical Weber number of [ ]^{a,c} to predict the bubble size.

In the FSLOCA™ topical report, sufficient amount of validations against core level swell experiments in Section 13 demonstrate WCOBRA/TRAC-TF2 reasonably predicts the void fraction distribution compared with the test data at various pressure, mass flux and void fractions. Those tests featured prototypical rod bundle and the comparison of the testing conditions with typical PWR conditions has been provided in Table 13.4.1-1 of the topical report.

In the reactor thermal hydraulic codes, the interfacial drag model is a simplified model developed particularly for predicting thermal hydraulic in the reactor with a coarse nodalization. The simplified interfacial drag model and interfacial area model in WCOBRA/TRAC-TF2 together with the Weber number of [ ]^{a,c} produced reasonable void fraction distribution in the assessments documented in the topical report. The proper scaling between the facilities in the assessment and the PWR ensures the WCOBRA/TRAC-TF2 code is used within the parameter range of its assessments during the LOCA evaluations.

It is noted that both Eq. 4-15 and Eq. 5-60 define the same bubble radius using the critical Weber number. The radius in Eq. 4-15 is applied to the calculation of interfacial area, while the radius in Eq. 5-60 is used for the Reynolds number in the interfacial drag calculation. [

]^{a,c}

It is further clarified that, in the vessel component of WCOBRA/TRAC-TF2 code, [

]^{a,c} is used for the calculation of the Reynolds number (Eq. 5-51), Weber number (Eq. 4-15), and the critical film thickness (Eq. 4-41) for the film/drop flow regime and churn turbulent flow regime. The vector sum of relative velocities is defined in Eq. 5-44. Note that vector sum of relative velocity in Eq. 5-44 is denoted with an asterisk. There is no additional limiter applied to the vector sum of relative velocities in Eq. 4-15.

Part (2) and Part (3)

Equation 4-23 sets reasonable upper limits to large bubble radius. The physical implications of three limits are discussed below.

---

[1] *FULL SPECTRUM™ and FSLOCA™ are trademarks in the United States of Westinghouse Electric Company LLC, its subsidiaries and/or its affiliates. These marks may be used and/or registered in other countries throughout the world. All rights reserved. Unauthorized use is strictly prohibited. Other names may be trademarks of their respective owners.*

The upper limit of [ ]^{a,c} ft for the bubble diameter reflects stability limit for the large bubble. Ishii (Reference 4.1-2) states, in a large diameter channel $D_h > 40\sqrt{\sigma/(g\Delta\rho)}$, slug and large cap bubbles cannot be sustained due to the interfacial instability and they disintegrate to smaller cap bubbles. Section F1.1 of the TRAC-M theory manual (Reference 4.1-8) has discussed the slug to cap bubble transition and assumes the critical bubble size is $D_h = 50\sqrt{\sigma/(g\Delta\rho)}$. This critical bubble size is only a weak function of pressure. [

]^{a,c} (Figure 4.1-3, Figure 4.1-4, Figure 4.1-5, and Figure 4.1-6).

The second limit is the hydraulic diameter of the channel. The limit reflects [

]^{a,c}

The third limit r_{LB}^*, assumes one or more large bubbles accounts for the vapor left when the volume of small bubble vapor is subtracted. The derivation of the bubble radius is shown from Eq. 4-24 through Eq. 4-31. The definition r_{LB}^* involves the volume of the hydraulic cell. It is noted that due to the coarse nodalization implemented for the LOCA analysis, r_{LB}^* tends to be large.

Those 3 limits play a different role in the LOCA analysis depending on the geometry to be analyzed. [

]^{a,c}

To reduce the noding sensitivity in the LOCA analysis, a strict noding consistency between the validation tests and the pilot PWR has been established during the development of the FSLOCA evaluation model. The details of noding strategy and consistency of the FSLOCA Evaluation Model (EM) have been documented in Section 26.1 of the FSLOCA topical report. Particularly for the reactor core, the testing facilities in the level swell validation all featured full scale rod bundle and full pressure (the comparison of the testing conditions with typical PWR conditions has been provided in Table 13.4.1-1 of the topical report). [

]^{a,c}

Part (4) and Part (5)

The churn-turbulent flow regime is designed to be a simple transition between bubbly flow and film/drop flow. It is implemented as a linear interpolation of interfacial drag and interfacial heat transfer between two flow regimes. Section 5.4.3 of the topical report provides formulas for the interpolation of interfacial drag and Section 6.2.3 of the topical report provides formulas for the interpolation of interfacial heat transfer. The churn-turbulent regime as a part of the vessel component of WCOBRA/TRAC-TF2 has been validated against ORNL, G-1, G-2 and JAERI Two-Phase Test Facility (TPTF) level swell tests in Section 13 of the topical report, though the flow regime itself is shown to be much less significant for level swell than the bubbly flow regimes. [

]^{a,c}

The upper bound of void fraction in the churn turbulent flow regime in Eq. 4-41 is established using the critical film thickness developed in NUREG/CR-0312 (Reference 4.1-9). [

]^{a,c}

A major concern on the churn turbulent flow regime is the liquid entrainment in the churn turbulent flow regime and its possible impact to the core heat transfer in a small break LOCA. Thus, a study on entrainment and steam cooling above the two phase mixture level in a typical small break LOCA was conducted to address RAI 17. Figures 17-5a through 17-5d (Reference 4.1-11) provided a comparison of the vapor fraction and entrainment fraction profiles at several times before and after the PCT time. [

]^{a,c} It can be concluded that the impact of the entrainment in churn turbulent flow to the core heat transfer is negligible in a SBLOCA evaluation.

Additional remarks for part (4) and part (5)

- As we explained in the response to part (1), the relative velocity in Eq. 4-41 is the vector sum of relative velocities between the vapor and continuous liquid phases.

- The vessel component of WCOBRA/TRAC-TF2 is modeled with a two-fluid three-field model, which utilizes a droplet interfacial area transportation model to predict interfacial area, droplet size and entrainment fraction. The theoretical basis, transportation equations and implementation of interfacial area transportation model have been summarized in the response to RAI 55 (Reference 4.1-12).
- The entrained liquid fraction α_e has been missed from both Eq. 5-93 and Eq. 5-127. However, the actual coding has been inspected to be correct for both equations.

Part (6)

In general, the vessel component and the one-dimensional component have its distinct set of governing equations and constitutive relations as a result that the vessel component is represented by two-fluid three-field model, and the one-dimensional component is represented by two-fluid (two-field) model. The benefit of each model and it's adequacy to the component have been discussed in Section 1 and Section 3 of the topical report. Inside the WCOBRA/TRAC-TF2 code, the vessel component and the one-dimensional component are solved by a different set of FORTRAN modules with the two components only coupled at the 1D/3D junctions. Section 3.6 of the topical report explained the coupling between the one-dimensional component and the vessel component. Due to the same physical laws governing the two phase flow, part of the formulas in the one-dimensional component and the vessel component share the same model, while some correlations are adjusted to address different concerns in the reactor pressure vessel and the reactor coolant system.

The details of flow regime maps, interfacial momentum transfer models, and interfacial heat transfer models, including formulas, technical basis, and scaling discussions, have been provided in Section 4, Section 5 and Section 6, respectively, in the topical report.

Note the churn turbulent flow regime is absent from Table 4.1-1. The current version of the WCOBRA/TRAC-TF2 code does not output the flow regime indicator for the churn turbulent flow regime to users. It is acceptable because of the insignificance of the churn turbulent flow regime in the PWR LOCA simulation.

a,c

Figure 4.1-1 Comparison of WCOBRA/TRAC-TF2 bubbly flow model with the Zuber-Findlay model with C0=1.2. (P=40 psia, pipe ID=1.0 ft)

a,c

Figure 4.1-2 Comparison of WCOBRA/TRAC-TF2 bubbly flow model with the Zuber-Findlay model with C0=1.2. (P=1000 psia, pipe ID=1.0 ft)

a,c

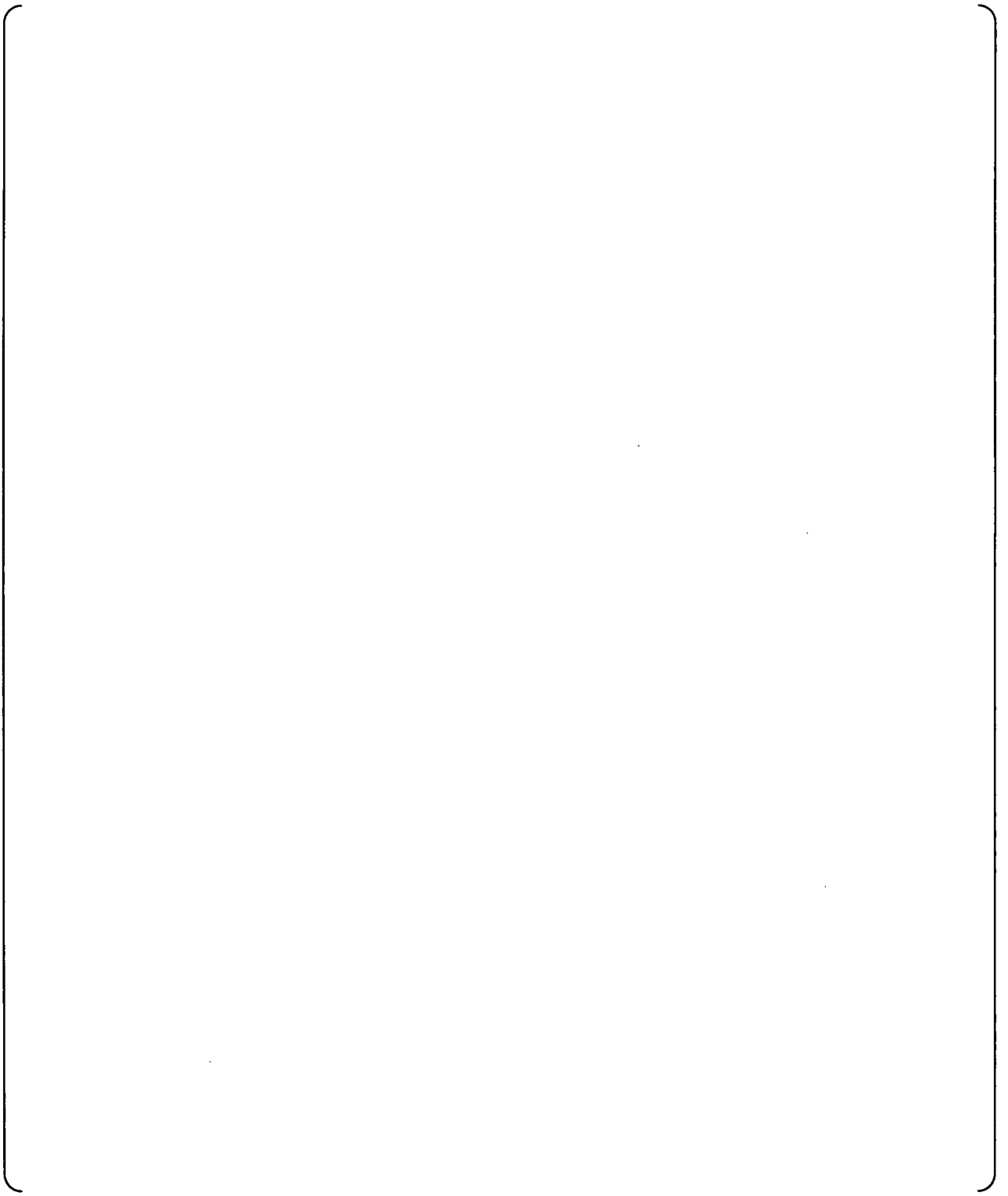

Figure 4.1-3 Comparison of reactor vessel inventories in ROSA SB-CL-18 with different large bubble radius limits.

a,c

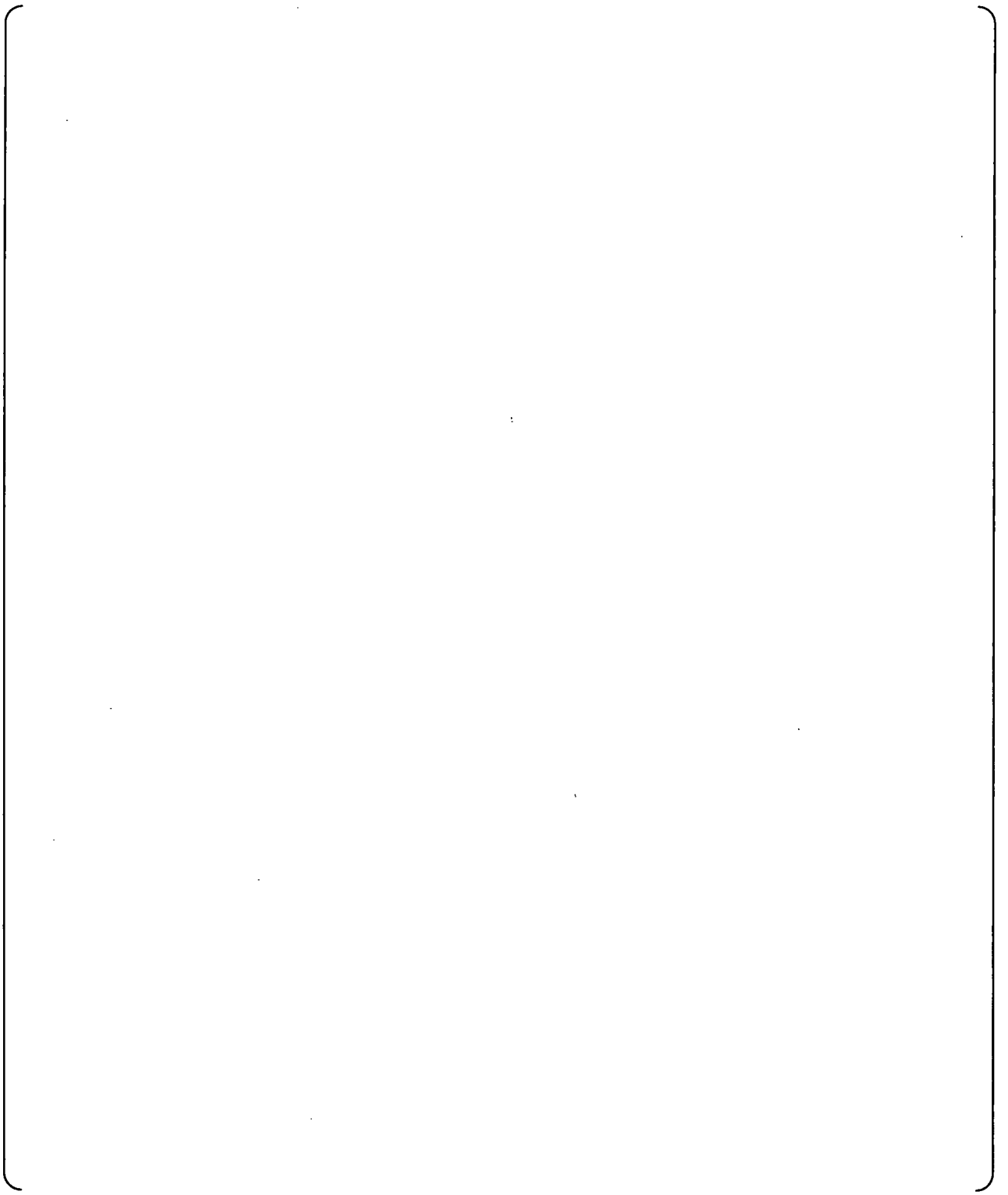

Figure 4.1-4 Comparison of heater rod peak cladding temperatures in ROSA SB-CL-18 with different large bubble radius limits.

a,c

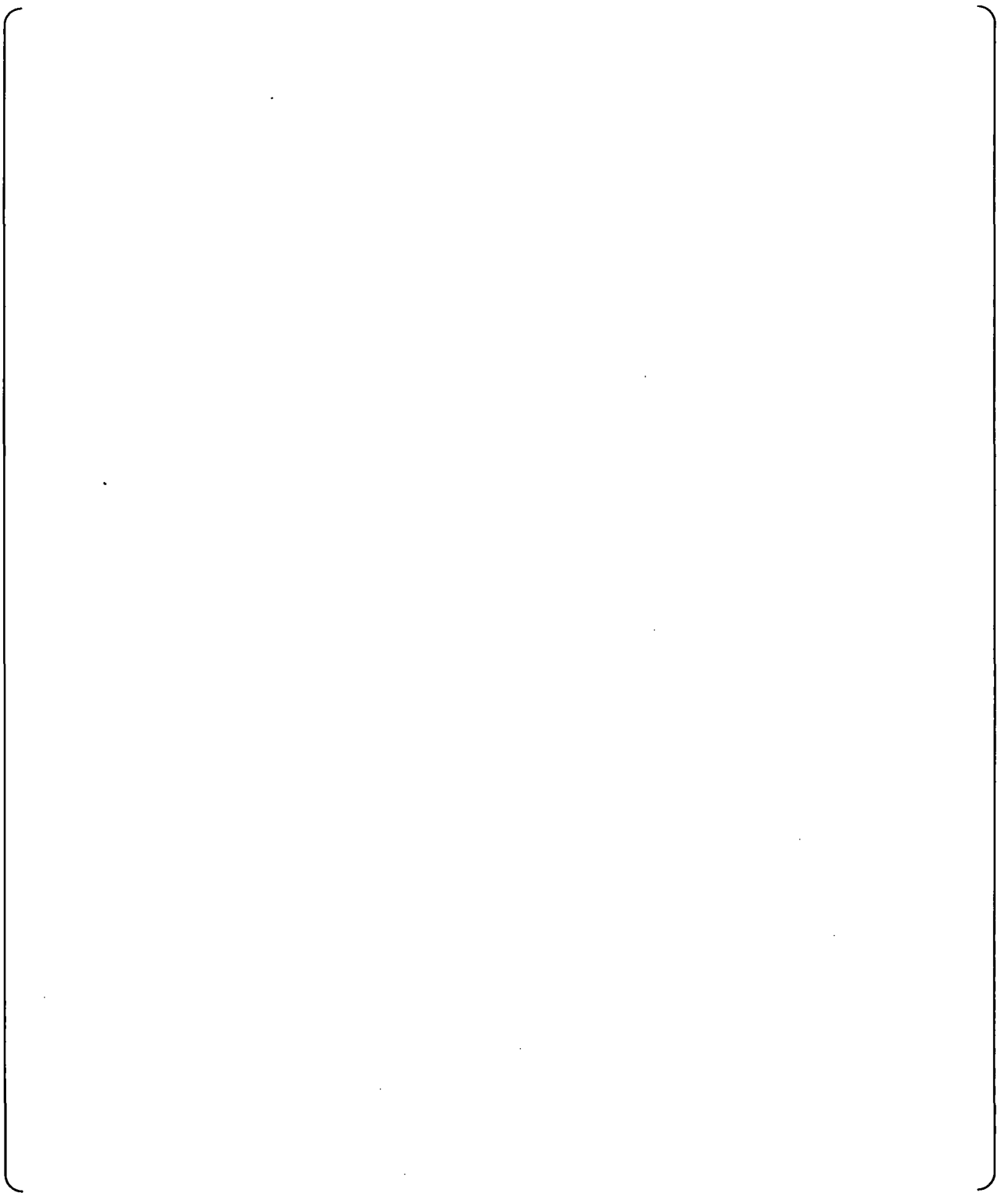

Figure 4.1-5 Comparison of reactor vessel inventories in Beaver Valley Unit 1 2.6 inch SBLOCA with different large bubble radius limits.

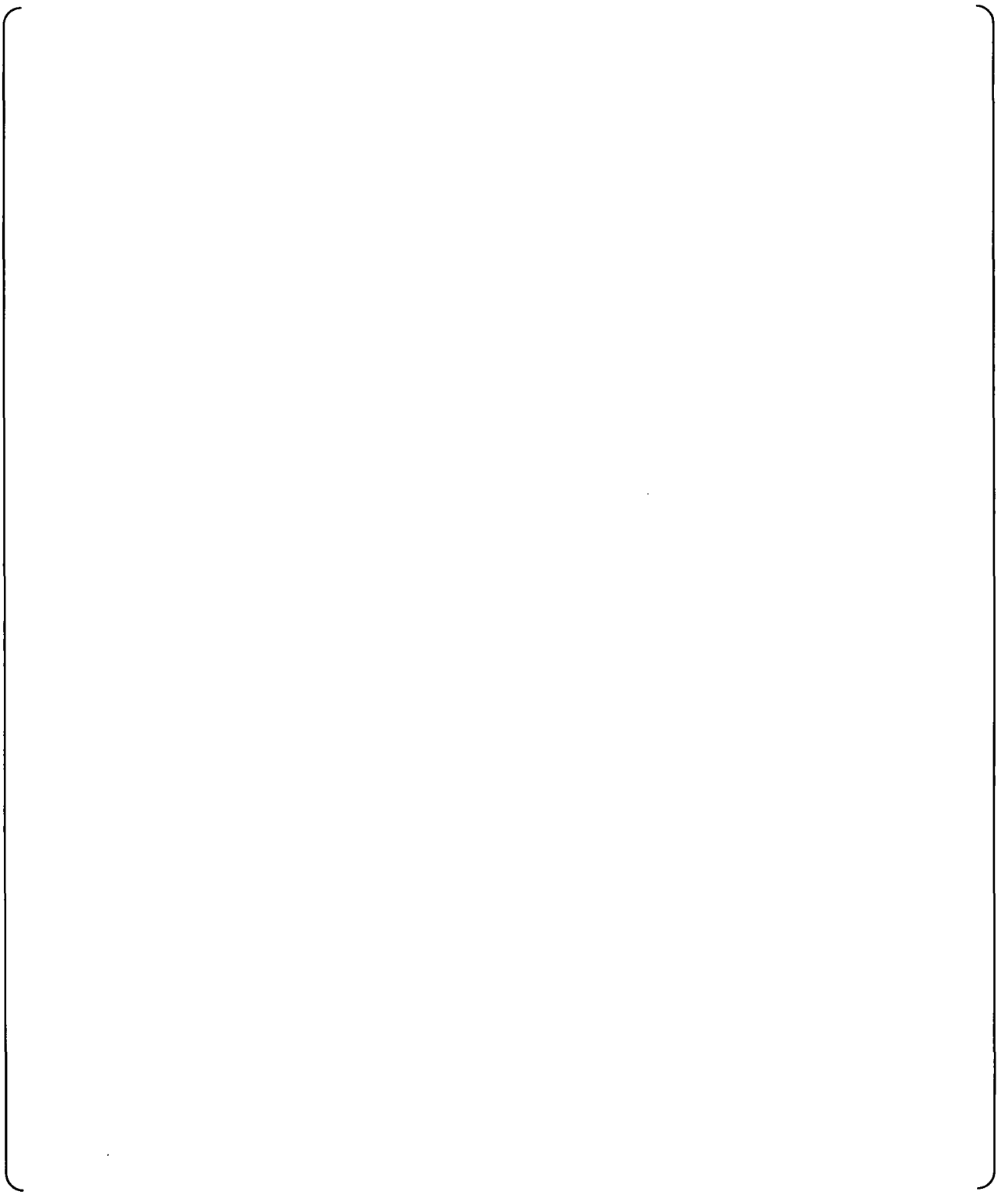

a,c

Figure 4.1-6 Comparison of fuel rod peak cladding temperatures in Beaver Valley Unit 1 2.6 inch SBLOCA with different large bubble radius limits.

References

4.1-1. Wallis, G.B., One-Dimensional Two-Phase Flow, 1969.

4.1-2. Ishii, M., and Hibiki, T., Thermo-Fluid Dynamics of Two-Phase Flow, 2ed, Springer, 2011.

4.1-3. Liles, et al., "TRAC-PF1/MOD1 Correlations and Models", NUREG/CR-5069, 1988.

4.1-4. Dimenna, R.A., et al., "RELAP5/MOD2 Models and Correlations," NUREG/CR-5194, 1988.

4.1-5. NUREG/CR-5535, Rev.1, Vol.4, "RELAP5/MOD3.3 Code Manual, Models and Correlations," 2001.

4.1-6. Salko, R., and Avramova, M.N., CTF Theory Manual, The Pennsylvania State University, 2012.

4.1-7. NAI 8907-06 Rev. 17, "GOTHIC Containment Analysis Package Technical Manual," EPRI, 2009.

4.1-8. LA-UR-00-910, TRAC-M/FORTRAN 90 (Version 3.0) Theory Manual, Los Alamos National Laboratory, 2000.

4.1-9. Richter, H.J., et al., Effect of Scale on Two-Phase Counter-Current Flow Flooding, NUREG/CR-0312, 1979.

4.1-10. Zuber, N., and Findlay, J.A., "Average Volumetric Concentration in Two-Phase Flow Systems," Journal of Heat Transfer, pp.453-468, 1965.

4.1-11. LTR-NRC-13-37, Submittal of Westinghouse Responses to "WCAP-16996-P, 'Realistic LOCA Evaluation Methodology Applied to the Full Spectrum of Break Sizes (FULL SPECTRUM LOCA Methodology)' Request for Additional Information" (Proprietary/Non-Proprietary), Project 700, TAC No. ME5244 dated June 5, 2013.

4.1-12. LTR-NRC-13-73, Submittal of Westinghouse Responses to "WCAP-16996-P, 'Realistic LOCA Evaluation Methodology Applied to the Full Spectrum of Break Sizes (FULL SPECTRUM LOCA Methodology)' Request for Additional Information – RAIs 46 – 58, 75 and 77" (Proprietary/Non-Proprietary), Project 700, TAC No. ME5244, dated October 28, 2013.

4.2 RAI 60

Question #60 Pressurized Water Reactor Core Two-Phase Mixture Level and Sensitivity to Axial Nodalization

WCAP-16996-P/WCAP-16996-NP, Volumes I, II, and III, Revision 0, Subsection 13.3, "WCOBRA/TRAC-TF2 Determination of the Mixture Level," explains that "WCOBRA/TRAC-TF2 does not include a specific model or pointer to identify the exact location of the mixture level. Rather, mixture level tracking is accomplished through detailed nodalization." It continues to say that " ... the ability of WCOBRA/TRAC-TF2 to track a mixture level is dependent upon the axial noding. In the core, the typical height of a hydraulic cell is 10 to 12 inches." With regard to the WCOBRA/TRAC-TF2 axial core noding strategy, Subsection 26.1.2, "Modeling Consistency," of WCAP-16996-P/WCAP-16996-NP, Volumes I, II, and III, Revision 0, explains that "the axial noding in a PWR core and in tests with simulated cores is established by the overall heated length and the location of spacer grids." According to noding details provided in Table 26.1-1 , "Core Section Axial Cell Lengths," the PWR core models for V. C. Summer (CGE) and Beaver Valley Unit 1 (DLW), considered in Volume III, employed 14 axial cells with a minimum cell length of 7.78 in and 7.46 in, correspondingly, and a maximum cell length of 12.84 in. It is stated in Subsection 26.1.2 of WCAP-16996-P/WCAP-16996-NP, Volumes I, II and III, Revision 0, that "the average cell heights for all of the test models and the plant models fall within a narrow range."

NRC Regulatory Guide (RG) 1.157, Revision 0, "Best-Estimate Calculations of Emergency Core Cooling System Performance," requires that "sensitivity studies and evaluations of the uncertainty introduced by noding should be performed."

(1) Please describe assessment studies that have been performed to examine sensitivity effects related to core axial nodalization on the mixture level predictions by WCOBRA/TRAC-TF2 under conditions of interest for SBLOCA analyses. Results from such studies should include quantification of nodalization effects on core mixture level predictions and the resulting impact on peak clad temperature predictions in WCOBRA/TRAC-TF2 analyses of test facilities and plant SBLOCA transients.

(2) It is recognized that with cell heights of 10-12 inches, a very small quantity of liquid in the cell containing the two-phase level will cause the entire cell to saturate, thus greatly reducing the PCT as the mixture level is not tracked nor used to determine the axial elevation of the uncovered region in the core. Please explain the impact of cell height on PCT considering a cell containing the two-phase mixture surface when the mixture level is any small finite distance above the bottom interface of this cell. Given such possible circumstances and taking into account the fact that the two-phase mixture level is not tracked, it appears that finer axial nodalization involving many more cells is needed to properly capture the location of the two-phase mixture surface and the degree of superheat that is associated with the cell containing the mixture level once core uncovery begins.

Response:

The response to this RAI is provided in Section 2 of this letter.

4.3 RAI 61

Question #61 Oak Ridge National Laboratory Thermal Hydraulic Test Facility Mixture Level Predictions and Axial Nodalization Sensitivity

WCAP-16996-P/WCAP-16996-NP, Volumes I, II, and III, Revision 0, Subsection 13.4.2, "ORNL-THTF Small Break Tests," presents WCOBRA/TRAC-TF2 prediction results for ORNL THTF tests. The analyzed tests include six bundle uncovery tests (3.09.10I, 3.09.10J, 3.09.10K, 3.09.10L, 3.09.10M, 3.09.10N) and six level swell tests (3.09.10AA, 3.09.10BB, 3.09.10CC, 3.09.10DD, 3.09.10EE, 3.09.10FF) described in NUREG/CR-2456 (March 1982).

Figure 1.3.4.2-3, "WCOBRA/TRAC-TF2 Model of the ORNL-THTF," shows the noding of the WCOBRA/TRAC-TF2 model of ORNL THTF. [

]^{a,c}

Subsection 13.4.2.5, "WCOBRA/TRAC-TF2 Model of the ORNL-THTF," also explains that "This section is divided into twelve axial nodes, in a manner consistent with the PWR core noding (Subsection 26.1.2, WCAP-16996-P/WCAP-16996-NP, Volumes I, II, and III, Revision 0, Volume III)." According to Table 26.1-1, "Core Section Axial Cell Lengths," all cells have practically an identical axial length of 12 inches.

(1) Figures 13.4.2-4 through 13.4.2-15 show the results of WCOBRA/TRAC-TF2 void predictions for all 12 analyzed ORNL THTF bundle uncovery and level swell tests. Please explain how the predicted void profiles shown in these figures relate to Channel 2 and Channel 3 results in the described WCOBRA/TRAC-TF2 THTF model.

(2) Please provide results from a noding sensitivity study performed with WCOBRA/TRAC-TF2 when using "nominal" two-phase flow correlations (no bias or sampling) with the number of cells modeling the heated bundle length set to 24 and 48. The axial length of each cell in Section 2 of the ORNL THTF model shown in Figure 13.4.2-3 would amount to 6 and 3 inches, respectively. Include axial void fraction distribution, two-phase mixture level, and collapsed liquid level predictions as well as vapor and wall temperature profiles for the uncovered-bundle heat transfer tests. Compare the sensitivity results against those obtained with a cell height of 12 inches and presented in Figures 13.4.2-4 through 13.4.2-15 as well as against measured test data. In all comparisons, please use results that are representative for the entire test bundle flow area.

(3) In analyzing WCOBRA/TRAC-TF2 capabilities in predicting level swell, Section 13, "Core Void Distribution and Mixture Level Swell," makes use of a mixture level swell parameter, S. This parameter is defined by Equation (13-1) through the two-phase mixture level, $Z_{2\Phi}$, the elevation where the liquid reaches the saturation point, Z_{SAT}, and the collapsed liquid level,

Z_{CLL}, as follows:

$S=[(Z_{2\Phi} - Z_{SAT}) - (Z_{CLL}-Z_{SAT})]/(Z_{CLL}-Z_{SAT})$.

Please explain the way in which quantities $Z_{2\Phi}$ and Z_{SAT} are determined from code results and assess their uncertainties considering nodalization effects. Assess and provide the uncertainty of S that results from uncertainties associated with $Z_{2\Phi}$ and Z_{SAT}.

(4) Please provide code results for the two-phase mixture levels in the THTF test bundle that are determined with the assumption that the void fraction in the computational cell containing the two-phase mixture level is equal to the void fraction in the neighboring cell located flow upstream. Compare the computed two-phase mixture levels against the measured data. Include data uncertainty bars in the comparison figures.

Response:

The response to this RAI is provided in Section 2 of this letter.

4.4 RAI 62

Question #62: Oak Ridge National Laboratory Thermal Hydraulic Test Facility WCOBRA/TRAC-TF2 Detailed Prediction Results

WCAP-16996-P/WCAP-16996-NP, Volumes I, II, and III, Revision 0, Subsection 13.4.2, "ORNL-THTF Small Break Tests," presents WCOBRA/TRAC-TF2 prediction results for ORNL THTF tests that included six bundle uncovery tests (3.09.10I, 3.09.10J, 3.09.10K, 3.09.10L, 3.09.10M, 3.09.10N) and six level swell tests (3.09.10AA, 3.09.10BB, 3.09.10CC, 3.09.10DD, 3.09.10EE, 3.09.10FF).

To illustrate the performance of WCOBRA/TRAC-TF2 two-phase flow models, including flow regime maps, employed by the vessel component to predict the thermal hydraulic response of the reactor core region, please provide code prediction results for two THTF bundle uncovery tests: 3.09.10J performed at 610 psia and 3.09.10M performed at 1,010 psia, and two level swell tests: 3.09.10AA at 590 psia and 3.09.10DD at 1,170 psia. For these tests, please provide code prediction results identified below and obtained with WCOBRA/TRAC-TF2 using "nominal" two-phase flow correlations (no bias or sampling) and the existing THTF model shown in Figure 13.4.2-3. Please include the following parameters: (1) predicted flow regime with flow regime indicator number, (2) pressure, (3) fluid phase temperatures, (4) wall temperature, (5) void fraction and its attributed components (e.g., SB, large bubbles, slugs, continuous field), (6) diameter and number of bubbles in each category (small, large), (7) liquid fraction and its attributed components (e.g., entrained drops, film, slugs, continuous field), (8) diameter and number of droplets, (9) phase mass flow rates for each field, and (10) phase velocities for each field and relative velocities as used in any related constitutive equation, e.g., Equation (4-15).

Please present the results in a table format for each of the twelve cells or associated interfaces, as appropriate, with the cells listed in the first column and each of the above parameters provided in a separate column. Please provide results that are representative for the entire test bundle cross sectional flow area based on results for individual channels.

Response:

The requested information was reviewed during an NRC audit of the WCOBRA/TRAC-TF2 calculations in July 2013 per LTR-NRC-13-70 (Reference 4.4-1).

Reference(s)

4.4-1. LTR-NRC-13-70, "Summary of July 2013 NRC Code Workshop and August 2013 NRC Audit of the FULL SPECTRUM LOCA (FSLOCA) Evaluation Model (Proprietary/Non-Proprietary)," October 10, 2013.

4.5 RAI 63

Question #63: Interfacial Drag Correlations in WCOBRA/TRAC-TF2

WCAP-16996-P/WCAP-16996-NP, Volumes I, II, and III, Revision 0, Subsection 5.4, "Vessel Component Interfacial Shear Models," describes the relationships used in WCOBRA/TRAC-TF2 to quantify interfacial friction forces between flow fields in various two-phase flow regimes by means of interfacial drag coefficients. The interfacial drag forces appear in the vessel component momentum conservation equations described in WCAP-16996-P/WCAP-16996-NP, Volumes I, II, and III, Revision 0, Section 3. The interfacial drag coefficients are calculated in subroutine INTFR to yield the average interfacial drag force per unit length when multiplied by the new time velocity difference between the fluid phases. Thus, Equation (5-42) defines the average interfacial drag force, F_D, exerted on the continuous liquid phase by vapor per unit length along the X axis, $F_D / \Delta X = \tau'_{iX,vl}$, as a product of the flow regime dependent interfacial drag coefficient, $K_{iX,v}$, and the axial relative velocity between the vapor and the continuous liquid, $\underline{U}_{vl}$:

$$F_D / \Delta X = \tau'_{iX,vl} = K_{iX,vl}\, \underline{U}_{vl}.$$

Thus defined dimensional drag coefficient, $K_{iX,vl}$. is calculated using a dimensionless drag coefficient, C_D, commonly used in the literature. Equation (5-45) provides the relationship between $K_{iX,vl}$ and C_{Db} for a bubbly flow as:

$$K_{iX,vl} = C_{Db}\, \rho_l\, \underline{U}_{vl}\, A_{P,b} / 2\Delta X ,$$

where $A_{P,b}$ is the total projected area of all bubbles in the volume. From the above equations, the drag force, F_D, is obtained from the dimensionless drag coefficient, C_{Db}, and relative velocity, $\underline{U}_{vl}$:

$$F_D = C_{Db}\, \rho_l\, \underline{U}_{vl} \left| \underline{U}_{vl} \right| A_{P,b} / 2.$$

Subsections 5.4.1 through 5.4.4 present the WCOBRA/TRAC-TF2 approach to interfacial drag calculation for vessel component "Cold Wall" two-phase flow regimes. Table 1 summarizes this modeling approach.

Table 1: WCOBRA/TRAC-TF2 Approach to Interfacial Drag for Vessel Component "Cold Wall" Two-Phase Flow Regimes

Flow Regime	Void Fraction α (%)	Major Constitutive Correlations	Note
Small Bubble	$0 < \alpha \leq 20$	$C_{Db} = 24/Re_b\,(1+0.1Re_b^{0.75})$	Equation (5-50)
		$C_{Db} = (2/9)^{1/2}\, N\mu\, Re'_b\,(1-\alpha_v)^2$	Equation (5-53)
		$C_{Db} = (8/3)\,(1-\alpha_v)^2$	Equation (5-57)
		$C_{Db} = 0.45\,(1-\alpha_v)^2$	Equation (5-58)

Small-to-Large Bubble	$20 < \alpha \leq 50$	$C'_{Db} = C_{Db}(1-\alpha_v)^2$ Interpolation between small bubble drag at 20% void and large bubble drag at 50% void.	Equation (5-71)
Churn-Turbulent	$50 < \alpha \leq \alpha_{crit}$	Interpolation between large bubble drag at 50% void and film/drop interfacial drag.	Equation (5-78)
Film/Drop	$\alpha_{crit} < \alpha \leq 100$	$f_{i,W} = 0.005[1+75(1-\alpha_v)]$ [ ]^{a,c}	Equation (5-92)

In a SB regime, the interfacial drag between the continuous liquid and the vapor is calculated from Equations (5-67a). For a SLB regime, the interfacial drag between the continuous liquid and vapor is calculated by interpolation between the SB drag at 20 percent void and the Large Bubble (LB) drag at 50 percent void in accordance with Equations (5-74a) and (5-74b). Similarly, for a CT flow, the drag is assumed to be a linear combination between the LB drag and the FD drag according to Equation (5-78). In a FD regime with a stable liquid film, the interfacial friction factor is calculated using Equation (5-92). In the case of an unstable wall film, [

]^{a,c}

(1) WCAP-16996-P/WCAP-16996-NP, Volumes I, II, and III, Revision 0, does not provide a complete description of individual interfacial drag correlations as implemented in the vessel component interfacial shear models. Thus, WCAP-16996-P/WCAP-16996-NP, Volumes I, II, and III, Revision 0, does not define applicability ranges for individual interfacial drag correlations nor does it provide supporting data and analysis that demonstrate the technical bases for individual models. Important description characteristics include, among others, applicability ranges for participating parameters, possible extrapolation beyond ranges for which correlations were developed or assessed and associated limitations, availability and quality of supporting test data and validation analyses, relevant source references as appropriate. Please provide a table that describes the interfacial drag correlations implemented in the two-phase flow regimes of the vessel component "Cold Wall" flow map. For each individual constitutive correlation, please describe the following items: (1) expressions for the dimensionless drag coefficient for an individual flow element (bubble, droplet, slug, film) in a form allowable to calculate drag force using element's characteristics such as projected cross-sectional or interfacial area and an appropriate relative velocity, (2) source references as appropriate, (3) applicability ranges for defining parameters, (4) extrapolation outside of applicability ranges as applicable and associated limitations, (5) qualified available test data, and (6) references to validation analyses.

Please include description for each item (1) to (6) above in a separate column with each constitutive correlation described in a separate raw. Closure relations that are based on interpolation between distinct constitutive correlations should be provided at the end of the table following the description of all other constitutive correlations. Please define all participating quantities including participating dimensionless numbers, thermodynamic fluid

properties, and experimentally determined parameters. State and explain code implementation assumptions including phenomenological considerations related to treatment of characteristic sizes (e.g., bubble diameter or film thickness), ensemble numbers (e.g., number of drops or bubbles), distributions and categories (e.g., size distribution, large versus small bubbles). Please identify any quantities that are nodalization or input dependant or have other implementation conditions and restrictions.

(2) Please provide information for the interfacial drag constitutive correlations implemented in the two-phase flow regimes of the vessel component "Hot Wall" flow map as requested in item (1) above for the "Cold Wall" flow map.

(3) Please provide information for the interfacial drag constitutive correlations implemented in the drag models considered in Subsection 5.7, "One-Dimensional Component Interfacial Drag Models," for the one-dimensional component flow map as requested in item (1) above for the vessel component "Cold Wall" flow map.

(4) Please provide the information related to items (1) to (3) above using a consistent nomenclature set with units for included dimensional parameters.

Response:

Table 1 in RAI Question #63 should be corrected as follows:

Table 1: WCOBRA/TRAC-TF2 Approach to Interfacial Drag for Vessel Component "Cold Wall" Two-Phase Flow Regimes

Flow Regime	Void Fraction α (%)	Major Constitutive Correlations	Note
Small Bubble	$0 < \alpha \leq 20$	$C_{Db} = 24/Re_b\ (1+0.1Re_b^{0.75})$ $C_{Db} = (2/9)^{1/2}\ N_\mu\ Re'_b\ (1-\alpha_v)^2$ $C_{Db} = (8/3)\ (1-\alpha_v)^2$	Equation (5-50) Equation (5-53) Equation (5-57)
Small-to-Large Bubble	$20 < \alpha \leq 50$	$C'_{Db} = C_{Db}\ (1-\alpha_v)^2 = 24/Re_b\ (1+0.1Re_b^{0.75})\cdot\ (1-\alpha_v)^2$ $C_{Db} = 0.45\ (1-\alpha_v)^2$ Interpolation between small bubble drag and large bubble drag at local void fraction, using the interpolation factor defined as $F_{SB} = \alpha_{SB}\ (1-\alpha_v)/(1-\alpha_{SB})/\ \alpha_v$	Equation (5-71) Equation (5-58) Equation (5-76)
Churn-Turbulent	$50 < \alpha \leq \alpha_{crit}$	Interpolation between small to large bubble drag and film/drop interfacial drag at local void fraction, using the factor defined as $F_{CT} = (\alpha_v - \alpha_{LB})/\ (\alpha_{crit} - \alpha_{LB})$	Equation (5-78) Equation (5-79)
Film/Drop	$\alpha_{crit} < \alpha \leq 100$	$f_{i,w} = 0.005[1+75(1-\alpha_v)]$ [ ]^{a,c}	Equation (5-92)

The other information is not provided in tabular format as it is available in the topical report as supplemented by the RAI responses.

4.6 RAI 64

Question #64: Interfacial Area in Inverted Slug Flow

WCAP-16996-P/WCAP-16996-NP, Volumes I, II, and III, Revision 0, Subsection 5.4.6, "Inverted Liquid Slug Regime," explains that for the liquid slug regime "the interfacial area is calculated assuming that the liquid slugs are spherical, and have a diameter [ ]^{a,c} of the channel diameter, as described in WCAP-16996-P/WCAP-16996-NP, Volumes I, II and III, Revision 0, Section 4.3.3. The interfacial area is specified in Equation (5-104) as:

$A_{i,IVS} = 4A_x\alpha_l / D_h$.

Assuming that the above expression provides the interfacial slug area per unit length along the X axis, the volumetric concentration for the slug interfacial area is obtained from Equation (5-104):

$A'''_{i,IVS} = A_{i,IVS} / Ax = 4\alpha_l / D_h$.

WCAP-16996-P/WCAP-16996-NP, Volumes I, II, and III, Revision 0, Subsection 4.3.3, "Inverted Liquid Slug Flow Regime," estimates the interfacial area for the liquid slugs making the same assumption that continuous liquid slugs are spherical. An expression for the volumetric interfacial area concentration is provided in Equation (4-58):

$A'''_{i,S} = 6\alpha_l / D_S$.

Using the assumption that "the slugs have a diameter [ ]^{a,c}" the volumetric concentration for the slug interfacial area is provided in Equation (4-59):

[ ]^{a,c}

The above assumed slug diameter of [ ]^{a,c} is practically identical to a slug diameter of "[ ]^{a,c} of the channel diameter" used in WCAP-16996-P/WCAP-16996-NP, Volumes I, II, and III, Revision 0, Subsection 5.4.6.

From the above expressions for the volumetric concentration for the slug interfacial area, the ratio of the volumetric concentration for the slug interfacial area provided in WCAP-16996-P/WCAP-16996-NP, Volumes I, II, and III, Revision 0, Subsection 4.3.3, Equation (4-58) to the same quantity given in WCAP-16996-P/WCAP-16996-NP, Volumes I, II, and III, Revision 0, Subsection 5.4.6, Equation (5-104) is determined to be:

[ ]^{a,c}

Please explain why the slug interfacial area volumetric concentrations for the Inverted Liquid Slug flow regime, as defined in WCAP-16996-P/WCAP-16996-NP, Volumes I, II, and III, Revision 0, Subsection 4.3.3, "Inverted Liquid Slug Flow Regime," and Subsection 5.4.6, "Inverted Liquid Slug Regime," differ by [ ]^{a,c} Please take into consideration that it

appears, as discussed above, that practically identical assumptions have been introduced and used for determining the slug interfacial area volumetric concentrations in both subsections.

Response:

The WCOBRA/TRAC-TF2 vapor/liquid film drag coefficient for Inverted Liquid Slug regime is defined as [Equation (5-103), Reference 4.6-1]

[ ]^{a,c} RAI.64-1

in which the interfacial friction coefficient $f_{i,IVS}$ is [ ]^{a,c} times the Wallis (Reference 4.6-2) equation given as Equation (5-92) of the Topical as follows:

[ ]^{a,c} RAI.64-2

Implicitly, WCOBRA/TRAC-TF2 means to model the interfacial drag force for the Inverted Annular Slug regime with [ ]^{a,c} times the Wallis equation is more than just defining the interfacial drag coefficient as shown in Equation RAI.64-2. The Wallis interfacial drag force is defined as Equation RAI.64-3 below as a function of interfacial drag coefficient, velocity head (based on relative velocity) and interfacial area, which is the general form of the interfacial drag force shown in most of the technical publications.

$$\tau_i = f_i \times \frac{\rho_v U_r^{\,2}}{2} \times A_i \qquad \text{RAI.64-3}$$

In comparison with RAI.64-4, WCOBRA/TRAC-TF2 calculates the interfacial drag force (force per unit length) as:

[ ]^{a,c} RAI.64-4

As can be seen, there is a difference of a factor of 2 for the WCOBRA/TRAC-TF2 interfacial drag force equation, RAI.64-4, in comparison with the calculation of the drag force using the Wallis equation (Equation RAI.64-3). Therefore, in order to calculate the equivalent interfacial drag force using RAI.64-3 and RAI.64-4, the term $A_{i,IVS}$ in Equation RAI.64-4 should be calculated as half of the interfacial area, since $f_{i,IVS}$ is coded in WCOBRA/TRAC-TF2 as Equation RAI.64-2. The interfacial area for the Inverted Liquid Slug regime is defined in Equation (4-60) in Section 4.3.3 of the Topical, which can be converted to interfacial area per unit length and results in:

RAI.64-5

[ ]^{a,c}

The $A_{i,IVS}$ derived as RAI.64-5 is the same as Equation (5-104) in Section 5 of the Topical.

Please note that Equation RAI.64-1 corrects the typographic error of $K_{iX,IVS}$ in Equation (5-103) in the Topical, which will be incorporated in the revised Section 5.4 of the Topical included in Section 5 of this letter.

Reference(s)

4.6-1. WCAP-16996-P, "Realistic LOCA Evaluation Methodology Applied to the Full Spectrum of Break Sizes (FULL SPECTRUM LOCA Methodology)," November 2010.

4.6-2. Wallis, G.B., One-Dimensional Two-Phase Flow, 1969.

4.7 RAI 65

Question #65: Interfacial Drag for Inverted Slug Flow

WCAP-16996-P/WCAP-16996-NP, Volumes I, II and III, Revision 0, Subsection 5.4.6, "Inverted Liquid Slug Regime," defines the interfacial drag coefficient for this "Hot Wall" flow regime in Equation (5-103):

$K_{iX,IVS} = f_{i,IVS}\, \rho_v\, |\underline{U}_{vl}|\, A_{i,IVS}$.

WCAP-16996-P/WCAP-16996-NP, Volumes I, II, and III, Revision 0, Subsection 5.4.6 explains that the interfacial friction factor "is calculated assuming an unstable liquid film surface exists on the large liquid ligaments or drops." To account for such flow conditions, the friction factor is assumed to be a factor [ ]^{a,c} compared to the friction factor for stable liquid films defined in Equation (5-92) for the FD flow regime. Thus, Equation (5-102) provides the interfacial friction factor for Inverted Slug flow as:

[ ]^{a,c}

The interfacial slug area per unit length of the flow is defined in Equation (5-104):

$A_{i,IVS} = 4A_X\alpha_l / D_h$.

Further, Equation (5-105) calculates the interfacial drag coefficient, $K_{iX,vl,IVS}$, as the maximum value from two different expressions as follows:

[ ]^{a,c}

(1) Please provide the technical basis for calculating the interfacial friction factor for unstable liquid films for Inverted Slug flow. In particular, please explain the basis for the assumed factor of [ ]^{a,c} between the Inverted Slug liquid film friction coefficient, $f_{iX,IVS}$, given by Equation (5-102), and the annular film friction coefficient, $f_{i,W}$, defined by Equation (5-92).

(2) Equation (5-105) that defines the interfacial friction factor in Inverted Slug flow $K_{iX,vl,IVS}$, as the maximum value from two expressions. As given, the first expression is provided by Equation (5-104), which defines the interfacial slug area as discussed above. At the same time, the second expression:

[ ]^{a,c}

does not include a relative velocity $|\underline{U}_{vl}|$, which is used in defining the interfacial drag coefficient, according to Equations (5-81), (5-103) and others. Please explain this apparent inconsistency. If necessary, please make corrections and provide justifications.

(3) The interfacial drag coefficient is denoted in Equation (5-103) of WCAP-16996-P/WCAP-16996-NP, Volumes I, II, and III, Revision 0, Subsection 5.4.6 as $K_{iX,IVS}$ and, in Equation (5-105), as $K_{iX,vl,IVS}$. Please explain if both notations refer to the same parameter and, if

so, why the nomenclature is not consistent.

Response:

(1) The factor of [ ]^{a,c} between the Inverted Slug liquid film friction coefficient given by Equation (5-102) of Reference 4.7-1 does not have theoretical basis, it is instead ad hoc in the simple drag model of inverted annular/liquid slug hot wall flow regimes. The hot wall flow regimes occur in the refill and reflood periods at the core entrance region in LBLOCA transients. At beginning of the reflood, liquid enters into the core to cool the heated rod where inverted annular/liquid slug regimes occur downstream of the progressing rod quench front until the liquid in the inner region is all entrained in the vapor stream as droplets and the flow regime goes into Dispersed Droplet regime.

The interfacial drag model of the WCOBRA/TRAC-TF2 hot wall flow regimes is shown to be capable of adequately predicting the thermal hydraulics response of the reflood validation tests, as seen in three series of FLECHT reflood tests, as documented in Sections 15.6.1, 15.6.2, 15.6.3 and 19.5 of the Topical, and Cylindrical Core Test Facility (CCTF) test (Section 19.6 of the Topical).

The hot wall interfacial drag model directly influences the prediction of the void distribution in the core during the reflood phase, during which inverted annular/ liquid slug and dispersed drop regimes occur sequentially downstream of the progressing quench front with each regime lasting varied duration of time depending on the flooding rate, liquid subcooling, pressure and rod power. Except for the forced reflood test with the extremely high flooding rate, the core pressure drop is mostly attributed to the hydrostatic head of the vessel fluid and a good indicator of the integrated void distribution in the core. The WCOBRA/TRAC-TF2 simulations of the FLECHT reflood test are presented in Sections 15.6.1, 15.6.2 and 15.6.3 of the Topical where the comparison of the pressure drop measurement of the lower core, upper core and total core between the test measurement and code prediction shows satisfactory performance of the WCOBRA/TRAC-TF2 hot wall drag model in predicting the core void fraction. The same conclusion is also supported by comparing the differential pressure from the lower plenum to the upper plenum in the WCOBRA/TRAC-TF2 simulation of the CCTF reflood test (Figure 19.6-26, Section 19.6 of the Topical).

The drag model also impacts the entrainment during reflood which impacts the quench front progression and rod heat up. Specific to reflood entrainment, the WCOBRA/TRAC-TF2 drag model, altogether with its entrainment model and heat transfer model is demonstrated to perform adequately in predicting the FLECHT test carryover fraction as documented in Section 19.5 of the Topical.

(2) There is no physical basis for the limit shown in Equation (5-105) of the Topical. It serves as an upper bound to the relative velocity, which is expected to be much larger than the calculated relative velocity in the Inverted Liquid Slug regime and only used rarely in WCOBRA/TRAC-TF2. This limit is part of the simple interfacial drag models used in WCOBRA/TRAC-TF2 for inverted liquid slug regime, and the overall hot wall drag model comprising inverted annular/liquid slug, dispersed droplet flow regimes is validated only as a whole using the FLECTH reflood tests as discussed in item (1) above, without specific validation on individual regimes and each part of the model. Please refer to Item (1) above for the discussion of the validation of the WCOBRA/TRAC-TF2 Inverted Liquid Slug regime.

(3) Instances of typographic errors were identified in Equations (5-103) and (5-105) in Section 5 of Reference 4.7-1, which should be respectively corrected as follows:

[ ]^{a,c} (5-1)

[ ]^{a,c} (5-2)

Reference(s)

4.7-1. WCAP-16996-P, "Realistic LOCA Evaluation Methodology Applied to the Full Spectrum of Break Sizes (FULL SPECTRUM LOCA Methodology)," November 2010.

4.8 RAI 66

Question #66: Annular Film Flow Interfacial Drag

In a FD flow regime, the interfacial drag "between the vapor and continuous liquid for the wetted wall film flow regime" is calculated from Equation (5-81) in WCAP-16996-P/WCAP-16996-NP, Volumes I, II, and III, Revision 0, Subsection 5.4.4, "Film/Drop Flow Regime: Model Basis":

[ ]^{a,c}

The subsection clarifies that "when the vapor content in the flow exceeds a critical void fraction, and the wall is below the wetted wall temperature criteria, the film is assumed to become stable and liquid can no longer bridge the channel."

WCAP-16996-P/WCAP-16996-NP, Volumes I, II, and III, Revision 0, Subsection 5.4.4, "Film/Drop Flow Regime: Model as Coded," defines the interfacial drag also in Equation (5-94) as follows:

[ ]^{a,c}

The interfacial drag coefficient in the Falling Film regime of the "Hot Wall" flow map, $K_{iX,lv,FF}$, provided in Equation (5-114) in Subsection 5.4.8, "Falling Film Flow Regime," of WCAP-16996-P/WCAP-16996-NP, Volumes I, II, and III, Revision 0, is defined in a way consistent with Equation (5-94) above.

[

]^{a,c}

[ ]^{a,c}

[

]^{a,c}

[ ]^{a,c}

(1) As Equation (5-81) and Equation (5-94) apparently define the same interfacial drag quantity, please clarify if the parameters appearing on the right-hand side of these two equations and standing for the interfacial friction factor, relative velocity and interfacial area are defined in the same manner and mean the same physical quantity. If this is the case, please explain why different nomenclature is used in both equations. Please examine the nomenclature and revise as needed so that it is appropriately consistent throughout Volume I of the WCAP-16996-P/WCAP-16996-NP, Volumes I, II, and III, Revision 0 TR.

(2) If Equation (5-81) and Equation (5-94) define the same interfacial drag quantity, please

explain why the interfacial drag from Equation (5-81) and that from Equation (5-94) differ by a factor of 2:

$[K_{iX,vl,FD}$ from Equation (5-94)] / $[K_{iX,vl,FD}$ from Equation (5-81)] = 2.

(3) Please provide the ranges of applicability for the interfacial friction factors as given by Equation (5-92) and attributed to stable films in annular flow and by Equation (5-86) and attributed to unstable films in co-current and countercurrent film flow. Please define the applicability range for each participating parameter. Describe the test conditions for the data that were used to develop these two correlations. Please compare these applicability ranges to typical flow conditions of interest for PWR LOCA analysis.

(4) Please provide the technical basis for calculating the interfacial friction factor for unstable liquid films using Equation (5-90) as described in Subsection 5.4.4, "Film/Drop Flow Regime: Model as Coded."

(5) According to WCAP-16996-P/WCAP-16996-NP, Volumes I, II, and III, Revision 0, Subsection 5.4.4, "Film/Drop Flow Regime: Model as Coded," the interfacial friction factor for unstable films is defined as [ ]^{a,c} At the same time, WCAP-16996-P/WCAP-16996-NP, Volumes I, II, and III, Revision 0, Subsection 5.4.6, "Inverted Liquid Slug Regime," defines the interfacial friction factor in the case of an unstable liquid film surface as [ ]^{a,c} times the annular flow friction factor defined in Equation (5-92) for stable liquid films in the FD flow regime. Please explain this discrepancy and compare the relevant technical bases used to demonstrate the validity of WCOBRA/TRAC-TF2 interfacial drag models for unstable liquid films as implemented in the FD flow of the "Cold Wall" flow regime map and in the Inverted Slug flow of the "Hot Wall" flow map.

(6) Please describe availability and quality of test data, describing two-phase film flow, and any supporting analyses performed to demonstrate the applicability of WCOBRA/TRAC-TF2 interfacial drag models for FD flow prediction. Identify references for such validation analyses, if available, including source references for applied film flow test data. Present comparisons between model predictions for the friction factor and test data under typical conditions of relevance to PWR LOCA analyses.

Response:

(1) Equations (5-81) and (5-94) in Section 5 of Reference 4.8-1 define the interfacial drag coefficients differing by a factor of [ ]^{a,c}, albeit calculating the identical drag force. Equation (5-81) uses a more general form of interfacial drag coefficient as it typically shows in the technical publications, while Equation (5-94) defines an interfacial drag coefficient more in line with the interfacial drag coefficient variable for Film/Drop flow regime in the WCOBRA/TRAC-TF2 source code.

The drag coefficient $f_{iX,FD}$ in Equation (5-94) of Reference 4.8-1 is coded in WCOBRA/TRAC-TF2 as:

[ ]^{a,c} RAI.66-1

which is equivalent to [ ]^{a,c} times the coefficient developed by Wallis, shown as Equation (5-92) of Reference 4.8-1, taking into account the factor of [ ]^{a,c} in Equations (5-81) and (5-94) therein.

(2) See explanation in (1) above.

(3) The WC/T-TF2 interfacial drag coefficients for stable and unstable films are justified in Reference 4.8-2, in which the documented discussion justified the extension of the applicable ranges of the original models for WCOBRA/TRAC's intended applications, comparing the model predictions to the Westinghouse test data from the test geometries typical of some PWR components.

(4) In Section 5 of the Topical, Equation (5-90) is used in lieu of Equation (5-91) to calculate the unstable film interfacial drag coefficient in WCOBRA/TRAC-TF2 due to the reasonable agreement of the two equations (<15%) over a Reynolds number range of 5,000 to 100,000, as explained in the Topical in the paragraph below Equation (5-91).

(5) The interfacial friction factor for the unstable film in the Film/Drop flow regime is limited to be at least [ ]^{a,c} times the Wallis correlation, which predicts reasonable pressure drop and void fraction in the simulation study documented in Reference 4.8-2 for Film/Drop flow regime.

In the Inverted Liquid Slug regime, WCOBRA/TRAC-TF2 defines the interfacial drag factor of unstable liquid film surface to be equivalent to [ ]^{a,c} times the Wallis correlation (see Section 4.7 of this letter for discussion). However, the appearance of similarity of the interfacial drag factors defined for the Film/Drop and Inverted Liquid Slug regimes to be based on Wallis equation and to account for the unstable liquid-vapor interface using an empirical factor is an unrelated coincidence. The Film/Drop regime occurs in high void fraction region ($\alpha > \alpha_{crit}$) while the inverted liquid slug regime typically exists before the void fraction gets too high, with 'flipped' phase distribution on the two sides of the vapor-liquid interface in the flow channel.

The Wallis correlation defines the interfacial friction coefficient to be a linear function of liquid fraction, as shown in Equation (5-92) of the Topical, to correlate the data of the impact of the liquid film thickness on the interfacial friction factor (Reference 4.8-3) in annular flow. The phase topology and interface geometry of the Film/Drop flow regime is similar to the annular flow regime for which the Wallis model was developed using low pressure air water data; however, an empirical multiplier to the Wallis model is adopted

in WCOBRA/TRAC-TF2 to model Film/Drop regime interfacial drag to account for the extended application range of the original Wallis model, as well as the different flow characteristics from the ideal annular flow of 'wavy' interface, for example the entrained liquid droplets.

The interfacial factors defined for Inverted Liquid Slug regime in WCOBRA/TRAC-TF2 using [ ]^{a,c} times the Wallis correlation is an empirical ad hoc model intended to be applicable only in the range of conditions under which the model is validated against the test data. The validation of the WCOBRA/TRAC-TF2 Inverted Annular/Liquid Slug regime is discussed in subsection 4.7 of this letter.

(6) The WCOBRA/TRAC-TF2 Film/Drop model is specifically justified by the study documented in Reference 4.8-2 [See item (3) above]. In addition, as one of the flow regimes encountered in all of the ORNL small break boil-off and level-swell test cases, WCOBRA/TRAC-TF2 predicts reasonably well the void fraction profiles of these tests in this regime which can be mostly attributed to the adequate Film/Drop interfacial model.

Reference(s)

4.8-1. WCAP-16996-P, "Realistic LOCA Evaluation Methodology Applied to the Full Spectrum of Break Sizes (FULL SPECTRUM LOCA Methodology)," November 2010.

4.8-2. Resolution of Requests for Additional Information for WCAP-12945-P, Volume 1 RAI No.68. (Included following this response)

4.8-3. Wallis, G.B., One-Dimensional Two-Phase Flow, 1969.

Reference 4.8-2

a,c

a,c

[ ] a,c

a,c

[ ] a,c

[ ] a,c

a,c

Figure 68-1. Variation of Interfacial Friction Factor with N Dimensional Film Thickness for Various Pipe Diameters

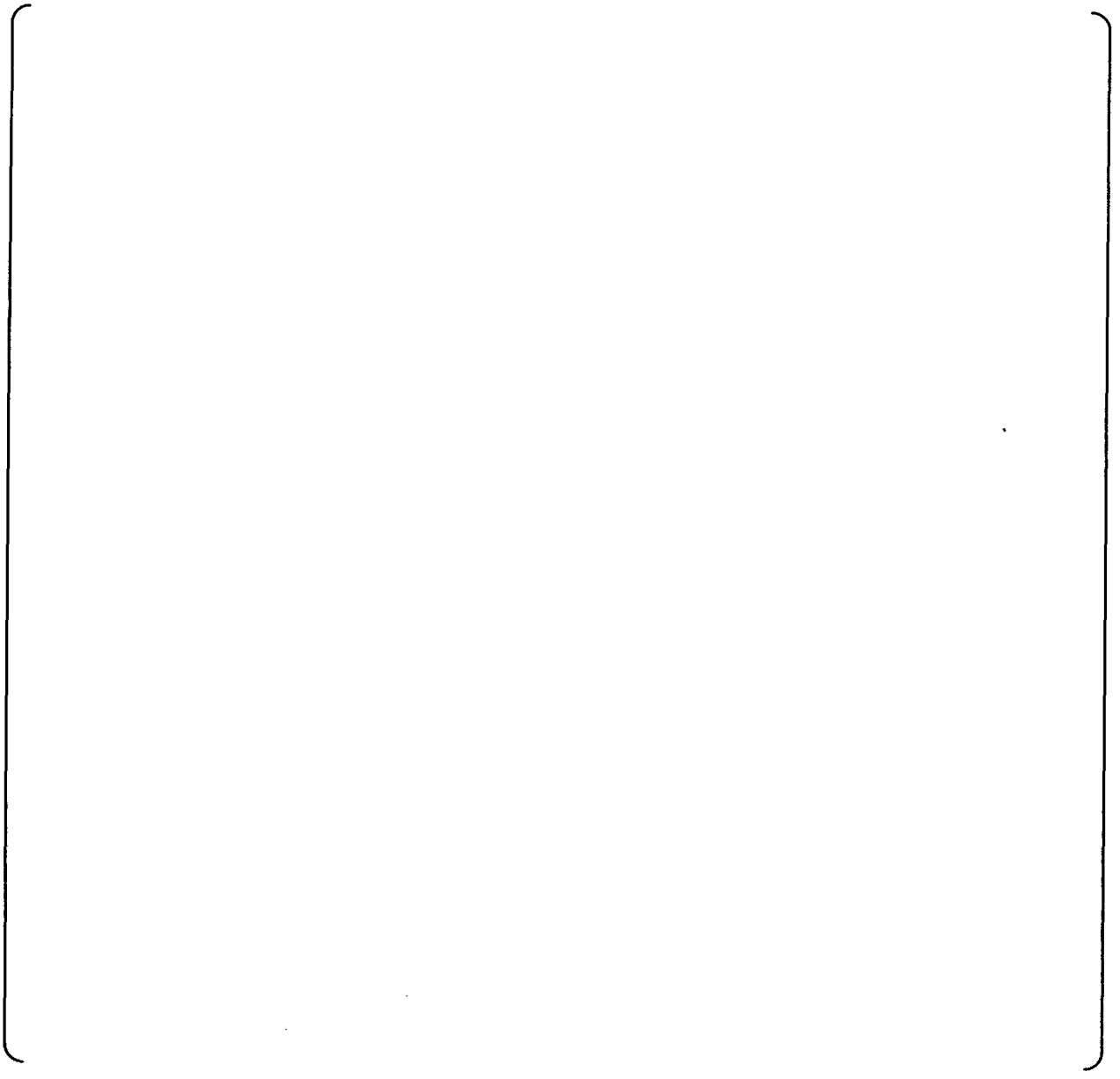

a,c

Figure 68-2. Comparison of Five Times Wallis f_i (----) with correlation from reference 1.

Figure 68-3. Crossection View of MDR and RCC Guide for APWR

a,c

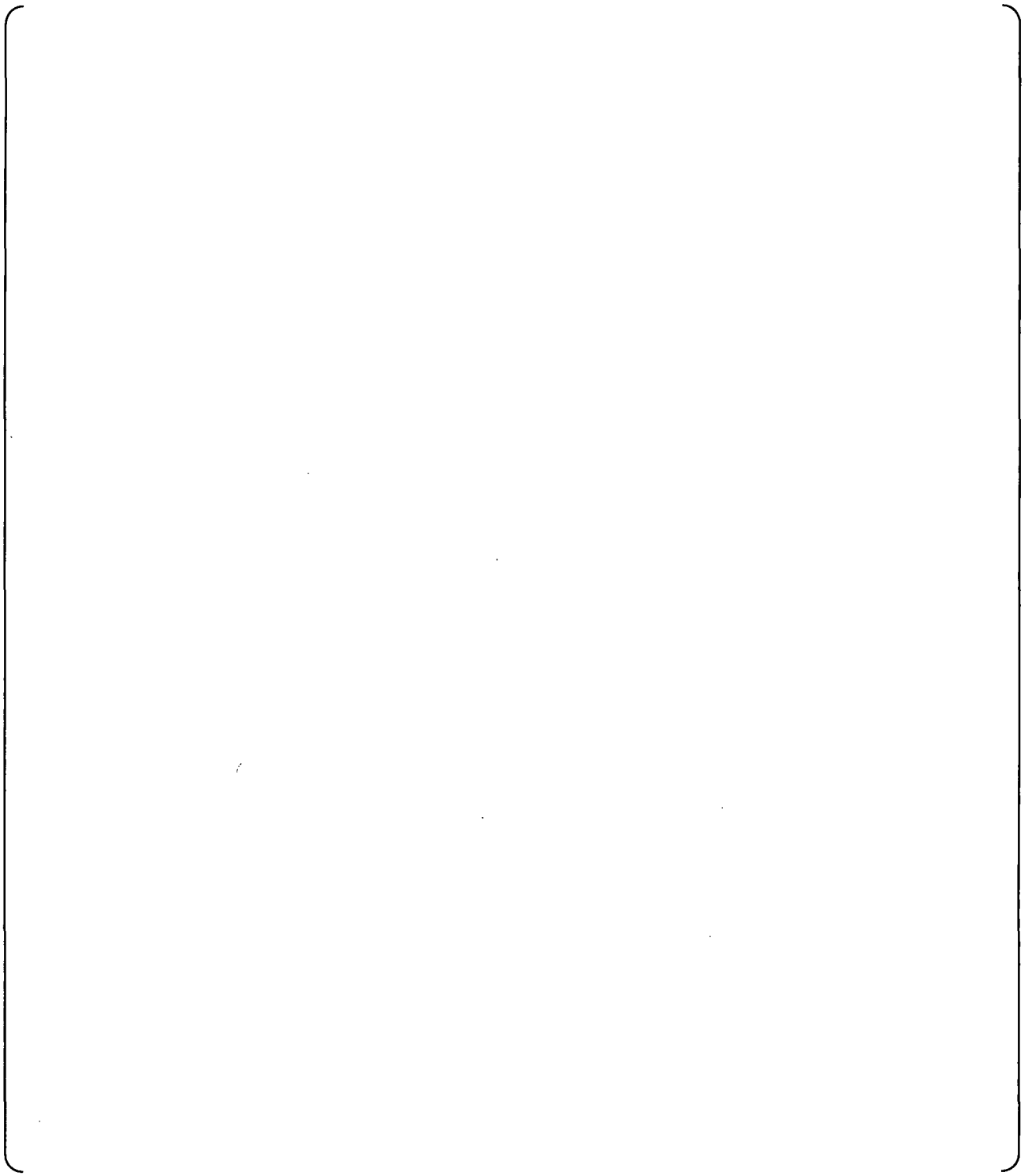

Figure 68-4. Axial View of WDR Guide

[ ] a,c

243

Figure 68-5. Crossection Views of Typical Operating Plant Guide Tube.

Top Figure: Normal Plate geometry.
Bottom Figure: Plate geometry at bottom of Guide Tube

[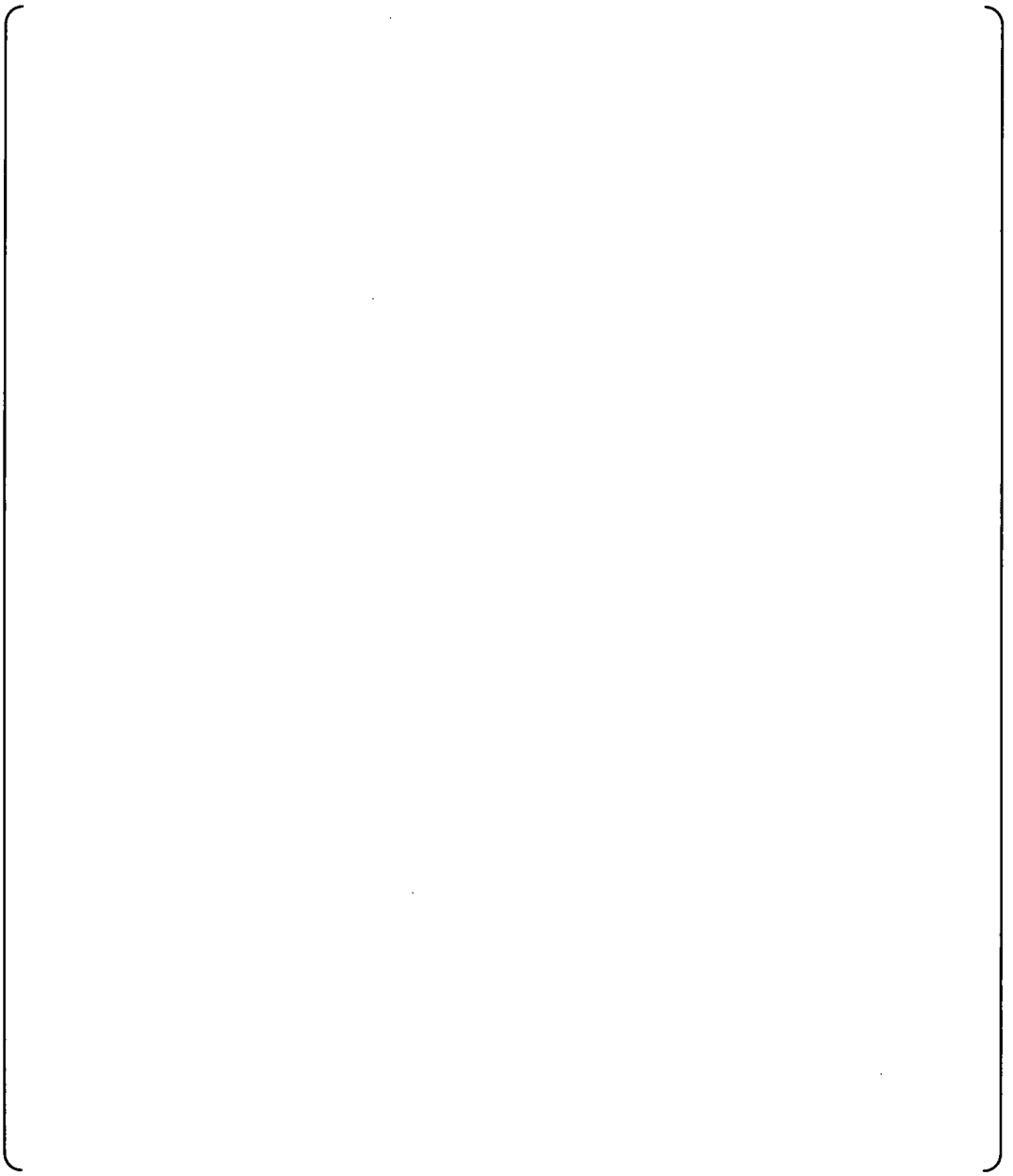] a,c

Figure 68-6. Flow Regimes in WDR and RCC Downflow Tests

[a,c]

Figure 68-7. Predicted vs Measured Static Pressure Gradient in the MDR Guide During Two Phase Downflow.

[ ] a,c

Figure 68-8. Predicted vs Measured Static Pressure Difference for Various Flow Qualities in the WDR Guide.

[ ] a,c

Figure 68-9. Predicted vs Measured Static Pressure Difference for Various Flow Qualities in the RCC Guide.

[ ] a,c

Figure 66-10. Predicted vs Measured Void Fraction Distribution for Downflow in the WDR Guide.

[ ] a,c

Figure 68-11. Predicted vs Measured Void Fraction Distribution for Downflow in the RCC Guide.

[ ] a,c

Figure 68-12. Flooding Curve for WDR Guide

[ ] a,c

Figure 68-13. Flooding Curve for RCC Guide

[ ] a,c

68. *Westinghouse stated Eqn. 4-92 was taken from Reference 8. Review of Wallis indicated Eqn. 4-92 was for thin films in pipes; therefore, justify the applicability of this equation to the vessel geometry where it is applied in WCOBRA/TRAC.*

Additional comments:

4. *Westinghouse's response to question 68 discussed the effect of scale on the use of Eqn. 4-92 in PWR calculations and started to address the effects of the differences in geometry between the tests used to develop Eqn. 4-92 (thin films in pipes) and the intended use of the equation in WCOBRA/TRAC (vessel geometry). However, to help close question 68, clarify if the Wallis model was used in the WCOBRA/TRAC results compared to data in your latest response. If not, are there other assessments that could be performed to justify the extension of the Wallis model to the vessel geometry? If yes, provide appropriate comparisons for review. If no, provide other information to justify the extension.*

Additional information:

[ ] a,c

69. Provide a reference or derivation for Eqn. 4-93. Also, provide the basis for the minimum value of 0.8 applied to Eqn. 4-93.

[ ] a,c

4.9 RAI 67

Question #67: Bubbly Flow Interfacial Drag "Ramping" to "Hot Wall" Inverted Annular Drag

WCAP-16996-P/WCAP-16996-NP, Volumes I, II, and III, Revision 0, Subsection 5.4.1, "Small Bubble Flow Regime Interfacial Drag," explains that in a SB regime of the "Cold Wall" flow map, the interfacial drag is calculated by interpolation between the SB value and the value for an Inverted Liquid Slug regime of the "Hot Wall" flow map "if there is significant vapor generation at the wall." To account for the presence of "significant vapor generation at the wall," the interfacial drag coefficient, $\overline{K}_{iX,vl,SB}$, is computed from Equation (5-67b) by interpolating or "ramping" between the drag coefficient for SB flow, $K_{iX,vl,SB}$, given by Equation (5-67a), and the drag coefficient for Inverted Annular regime of the "Hot Wall" flow map, $K_{iX,vl,HW}$, defined by Equation (5-105):

[ ]^{a,c}

In the above equation, the interpolated drag coefficient is multiplied by the ratio of the limited relative velocity, U_Γ, found in Equation (5-66), to the absolute value of the axial relative phase velocity, $|\underline{U}_{vl}|$. The dimensionless interpolation factor, F_Γ, is calculated from Equation (5-68) using the terminal relative velocity, U_{rb} , between a bubble with a Webber number of 10 and the liquid as determined by Equations (5-59) and (5-60):

[ ]^{a,c}

The axial vapor velocity accounting for vapor generation in a computational cell, U_Γ, is calculated from Equation (5-69) as follows:

[ ]^{a,c}

In the above equation, α_v is the vapor void fraction with an upper limit of 0.2 for SB flow, ρ_v is the vapor density, A_x is the is the cell momentum flow area in the axial direction, and Γ_v is the interfacial vapor generation rate for the cell calculated in accordance with Equation (6-101). Q_{wl} is the rate of heat transfer between the wall and the combined liquid fields (continuous liquid and entrained liquid) and Q_b is the rate of heat transfer at the wall that results in vapor generation from subcooled boiling. Both hest transfer rates correspond to the entire node surface area present in a computational cell.

(1) To take account for "significant vapor generation at the wall," WCOBRA/TRAC-TF2 computes the interfacial drag coefficient for the SB regime, $\overline{K}_{iX,vl,SB}$, through interpolation between a bubbly flow drag coefficient calculated without the assumption of vapor film existence at the wall, $K_{iX,vl,SB}$, and a drag coefficient for "Hot Wall" Inverted Annular flow, $K_{iX,vl,HW}$. The dimensionless interpolation factor, F_Γ, accounts for wall heat transfer and associated vapor generation through a velocity parameter U_Γ. The rate of vapor generation at the wall surface in the cell is divided by the void fraction, α_v, and axial momentum flow area, A_x, to compute an equivalent axial vapor velocity, which is used to determine U_Γ. As U_Γ and F_Γ are based on the vapor generation rate at wall surfaces associated with a certain

cell size, these parameters are nodalization dependant. Thus, for a cell in the core region with a defined axial area, A_x, the interfacial vapor generation rate, Γ_v, the wall heat transfer rates, Q_{wl} and Q_b, are dependent on the axial cell length, ΔX:

$\Gamma_v \sim \Delta X$, $Q_{wl} \sim \Delta X$, $Q_b \sim \Delta X$.

Accordingly, F_Γ and $\overline{K}_{iX,vl,SB}$ will depend on ΔX: $U_\Gamma \sim \Delta X$ and $\overline{K}_{iX,vl,SB} \sim \Delta X$. Please demonstrate that the implementation of nodalization dependant parameters in the WCOBRA/TRAC-TF2 interfacial drag model for SB flow is appropriate considering the intended purposes of obtaining best estimate code predictions. Provide results from relevant sensitivity studies examining the effect of noding.

(2) Please provide the technical basis that demonstrates the applicability of the interpolation correlation in Equation (5-67b) and used for "ramping" the SB flow drag coefficient in the presence of "significant vapor generation at the wall," $\overline{K}_{iX,vl,SB}$, and define the applicability conditions for this correlation:

[ ]^{a,c}

Define the validity ranges for the parameters used to calculate it from the above equation. Please clarify if such "ramping" technique is also applied to surfaces associated with passive heat structures.

(3) Please provide the technical basis that demonstrates the applicability of the correlation for computing the dimensionless interpolation factor, F_Γ, defined by Equation (5-68):

[ ]^{a,c}

Define the acceptable range for F_Γ and the validity ranges for the parameters used to calculate it from the above equation.

(4) The axial vapor velocity accounting for vapor generation in a computational cell, U_Γ, is calculated from Equation (5-69) using the minimum of two quantities. Accordingly, under saturated liquid boiling conditions when vapor is being generated only at the wall surface, the lack of interfacial vapor generation rate in a cell will produce a zero outcome for U_Γ regardless of the wall vapor generation. Please explain the appropriateness of the relationship defined by Equation (5-69) and used to calculate U_Γ and demonstrate its applicability.

Response:

(1) The calculation of U_Γ for hot wall ramping in bubbly flow regimes will be revised as follows based on the discussion in Section 3 of this letter.

[ ]^{a,c}

It is true that $Q_{w\ell}$ and Q_b are wall heat transfer rates and linearly depend on axial cell length ΔX, but their dependence is reduced due to the dependence of α_v on ΔX in the region of interest. Mostly, the hot wall ramping is only in effect at the entrance of the boiling channel where α_v starts to ramp up and U_Γ is thus calculated high (small α_v), as can be seen from the plots shown in Figures 3-1.1 through 3-1.12 in Section 3 of this letter.

In WCOBRA/TRAC-TF2 applications, consistency of the node sizes between the intended applications in PWR plant and validation test simulations has always been maintained to the extent practical, so that the applicable range of the models validated through the validation tests can be extended to the PWR plant simulations with minimum impact resulting from the node size. In all WCOBRA/TRAC-TF2 validation test and the demonstration PWR plant simulations, the node size spans in the range from 0.5~1.0 ft as seen in Table 26.1-1 of the Topical.

The core axial nodalization sensitivity studies conducted for the selected ORNL-THTF small break tests and Beaver Valley plant as documented in Section 2 in this response indicate the hot wall ramping model works properly for typical range of axial node size in the intended WCOBRA/TRAC-TF2 applications.

(2) See Section 3 of this letter.

(3) The interpolation end points as defined in Equation (5-68) of the Topical is ad hoc and demonstrated to provide reasonable prediction agreement with the validation tests of the overall code wall flow regime interfacial drag models. (See Section 3 of this letter)

(4) The U_Γ will be redefined for the hot wall ramping model as explained in Section 3 of this letter.

4.10 RAI 68

Question #68: Approach to Interfacial Drag "Ramping" Between "Cold Wall" and "Hot Wall" Regimes

WCAP-16996-P/WCAP-16996-NP, Volumes I, II, and III, Revision 0, Subsection 5.4.1, "Small Bubble Flow Regime Interfacial Drag," states that in a SB regime of the "Cold Wall" flow map, the interfacial drag is calculated by interpolation between the SB value and the value for an Inverted Liquid Slug regime of the "Hot Wall" flow map "if there is significant vapor generation at the wall." It is explained that the "Hot Wall" drag coefficient used for the purpose of SB flow drag "ramping" is calculated from Equation (5-105). Equation (5-67b) defines how the interfacial drag is "ramped:"

[ ]^{a,c}

Subsection 5.4.2, "Small-to-Large Bubble Flow Regime Interfacial Drag," clarifies that "for conditions in which there is a large vapor generation rate at the wall, the bubble drag coefficient is ramped to the interfacial drag used in the hot wall flow regime." It is explained that the "Hot Wall" drag coefficient used for the purpose of SLB flow drag "ramping" is calculated from Equation (5-106). The SLB drag "ramping" is performed according to Equation (5-73):

[ ]^{a,c}

According to Subsection 5.4.3, "Churn-Turbulent Flow Regime Interfacial Drag," interfacial drag ramping is applied for the CT flow regime as well.

It is explained that "The same ramp as in Section 5.4.2 of WCAP-16996-P/WCAP-16996-NP, Volumes I, II, and III, Revision 0, is applied to consider the vapor generation rate at the wall-by-wall heat transfer."

Table 1 below summarizes the approach to interfacial drag "ramping" used in various flow regimes modeling by WCOBRA/TRAC-TF2.

Table 1: Approach to Interfacial Drag Ramping Between "Cold Wall" and "Hot Wall" Flow Regimes in WCOBRA/TRAC-TF2 Vessel Component

"Cold Wall" Flow Regime	Drag Ramping Criterion	"Hot Wall" Regime Cited in Ramping	Referenced "Hot Wall" Drag Coefficient
Small Bubble	"Significant vapor generation at the wall"	Inverted Liquid Slug	Equation (5-105). Related drag factor: [ ]^{a,c} (Equations (5-92) and (5-102))
	"A large vapor generation rate at	Dispersed	Equation (5-106). Related drag factor:

Small-to-Large Bubble	the wall"	Droplet	$K_{iX,ve,DD} = 0.375\ C_{Db}\alpha_v\rho_v\lvert\underline{U}_{ve}\rvert/r_b$ [ ]^{a,c} (Equations (5-106) and (5-108))
Churn-Turbulent	"The vapor generation rate at the wall-by-wall heat transfer"	Dispersed Droplet	Equation (5-106). Related drag factor: $K_{iX,ve,DD} = 0.375\ C_{Db}\alpha_v\rho_v\lvert\underline{U}_{ve}\rvert/r_b$ [ ]^{a,c} (Equations (5-106) and (5-108))

(1) Interfacial drag "ramping" between "Cold Wall" and "Hot Wall" drag coefficients is used to account for wall vapor generation in modeling SB, SLB, and CT two-phase flow regimes when recognized by the "Cold Wall" flow map. In the case of Small Bubble flow, film drag for "Hot Wall" Inverted Liquid Slug flow, as suggested by Equation (5-105), is used to "ramp" the bubbly flow drag as described in WCAP-16996-P/WCAP-16996-NP, Volumes I, II, and III, Revision 0, Subsection 5.4.1 .

In contrast to this approach and as explained in Subsections 5.4.2 and Subsection 5.4.3, interfacial drag for both SLB and CT flow regimes is "ramped" using droplet drag for entrained liquid droplets in "Hot Wall" Dispersed Droplet flow defined by Equation (5-106) and calculated using [ ]^{a,c} which is representative for a solid sphere in the Newton regime at high Reynolds numbers.

Please clarify this modeling disparity. If Subsection 5.4.2 erroneously refers on page 5-20 to Equation (5-105) instead of Equation (5-106), please provide a proper modeling description. Otherwise, please justify the difference in the modeling approaches.

(2) Please explain the technical rationale behind interfacial drag ramping for "Cold Wall" SB, SLB, and CT flow regimes using interfacial drag defined for "Hot Wall" flow regimes. Present supporting phenomenological considerations and refer to specific experimental observations and data. Please provide and explain the criterion used for detection of "significant vapor generation at the wall" in SB flow and that applied for identification of "a large vapor generation rate at the wall" in SLB flow. In the case of CT flow, please define and explain the criterion used to identify the need "to consider the vapor generation rate at the wall-by-wall heat transfer" and clarify the meaning of the expression "vapor generation rate at the wall-by-wall heat transfer" on page 5-21 in WCAP-16996-P/WCAP-16996-NP, Volumes I, II and III, Revision 0, Subsection 5.4.3.

(3) Please explain if the criteria for recognition of "significant vapor generation at the wall," as considered in item (2) above, were used to classify existing two-phase flow data sets into separate groups that can be used to validate "Cold Wall" interfacial drag models with no drag ramping, such that are appropriate for "Hot Wall" interfacial drag model validation, and data sets that are applicable for validation of "Cold Wall" interfacial drag models with drag

ramping. Please provide references to such validation analyses, if available, and summarize analysis results that demonstrate the applicability of the applied interfacial drag "ramping" approach in WCOBRA/TRAC-TF2 for each individual flow regime. Please present comparisons of code predictions obtained with interfacial drag "ramping" being present and absent against void fraction data measurements. In particular, consider an appropriate data set for which interfacial drag "ramping" is supposed to be applied and present code comparisons obtained with and without drag "ramping" versus measured data.

Response:

(1) A review of Reference 4.10-1 and WCOBRA/TRAC-TF2 code found that there is a typo in the paragraph below Equation (5-73) in the Topical (Reference 4.10-1), which should be corrected as:

[

]^{a,c}.

Through the above correction, it clarifies that the 'hot wall ramping' for the small bubble and small to large bubble flow regimes is ramped to the same hot wall interfacial drag of the inverted liquid slug regime.

(2) See Section 3 of this letter for 'Hot Wall Ramp' discussion.

(3) See Section 3 of this letter for 'Hot Wall Ramp' discussion.

Reference(s)

4.10-1. WCAP-16996-P, "Realistic LOCA Evaluation Methodology Applied to the Full Spectrum of Break Sizes (FULL SPECTRUM LOCA Methodology)," November 2010.

4.11 RAI 69

Question #69: Calculation Results for Bubbly Flow Interfacial Drag

WCAP-16996-P/WCAP-16996-NP, Volumes I, II, and III, Revision 0, Subsection 5.4.1, "Small Bubble Flow Regime Interfacial Drag," refers to Figure 5-3(a), "Effect of Ramps on Interfacial Friction Factor: (a) SB Regime," as an illustration of the effect of ramps and limits, described in this subsection, on the interfacial drag for the SB flow regime. The figure plots a quantity denoted K_i referred to as "interfacial drag factor" versus relative velocity U_v-U_l. It is explained that the drag factor is plotted in Figure 5-3(a) for "typical fluid conditions." As seen from the graph, the two-phase flow conditions correspond to a SB flow regime with a vapor void fraction of α_v=0.1 and a pressure of 40 psia (0.276 MPa). The plot depicts four curves for the interfacial drag factor calculated at different cell vapor generation rates that correspond to values of 0, 1, 1.1, and 1.2 for the ratio between the axial velocity of vapor generation in a computational cell and the terminal relative velocity, U_Γ/U_{rb}.\

Figure 5-3(a), "Effect of Ramps on Interfacial Friction Factor: (a) SB Regime," does not provide units for both plotted quantities: the interfacial drag factor, K_i, and the relative velocity, U_v-U_l. The figure also does not include geometric characteristics that describe channel geometry, heated surfaces and cell nodalization parameters nor does it define inlet and boundary conditions related to mass flow rates and surface heat flux. As such, the results presented in the figure are not amenable to assessment.

(1) Please provide, in a table format, prediction results presented in Figure 5-3(a) to document the following information: (i) parameter, (ii) unit, (iii) correlation used to calculate the parameter, (iv) range of applicability, (v) values and units for input parameters, and (vi) calculated result. Include each of the indentified items in a separate column and use a separate raw to present individual parameters. Analyze and include results for three U_Γ/U_{rb} ratio values of 0, 1, and 1.2. Please provide the results at relative velocities equal, in units used for the horizontal axis in Figure 5-3(a), to 0 (or an appropriately defined low value), 0.5, the value at which the gradient of the curves, shown in Figure 5-3(a) for U_Γ/U_{rb} of 0, 1, and 1.1, changes a sign from positive to negative (value appears very close to unity), and 10. Please include the results for $K_{iX,vl,SB}$, $K_{iX,vl,HW}$, and $\overline{K}_{iX,vl,SB}$, as computed from Equations (5-67a), (5-105), and (5-67b). The numerical results provided should be self-contained and allow for independent verification of the values. For this purpose, all applied inlet and boundary conditions need to be given along with other assumed parameters such as bubble diameter or terminal relative velocity. Please include used fluid properties as well.

(2) Using the obtained results for $\overline{K}_{iX,vl,SB}$ from Equation (5-67b), please calculate and provide the values for the corresponding dimensionless drag coefficient, $\overline{C}_{Db}$, that is commonly used in the relevant literature to calculate drag force for a single dispersed element through its projected cross-sectional area and continuous phase kinetic head corresponding to the relative velocity. To obtain $\overline{C}_{Db}$, please use the general form of the interfacial drag coefficient for bubbly flow as given by Equations (5-45) and (5-67a):

[ ]^{a,c}

In addition, please calculate the dimensionless drag coefficient, C_{Db}, which corresponds to

the drag coefficient, $K_{iX,vl,SB}$, determined from Equation (5-67a) prior to "ramping" in order to account for "significant vapor generation at the wall:"

[ ]^{a,c}

Include the results for $\bar{C}_{Db}$, C_{Db}, and $f_{iX,IVS}$ in the tables prepared according to item (1) above.

(3) Please provide figures that plot the results for the following parameters as functions of the relative velocity, U_v-U_l, including the units for the displayed quantities: (1) "ramped" dimensionless drag coefficient, $\bar{C}_{Db}$, (2) uncorrected for wall vapor generation dimensionless drag coefficient, C_{Db}, (3) interfacial friction factor for "Hot Wall" Inverted Liquid Slug flow, $f_{iX,IVS}$, as applied in bubbly flow drag "ramping," (4) $K_{iX,vl,SB}$ drag coefficient, (5) $K_{iX,vl,HW}$ drag coefficient, and (6) $\bar{K}_{iX,vl,SB}$ drag coefficient.

(4) Please provide results for the WCOBRA/TRAC-TF2 interfacial drag model for the vessel component SLB flow regime by providing prediction results as requested in items (1) through (3) above for SB flow. Apply the same conditions as those used to produce Figure 5-3(b), "Effect of Ramps on Interfacial Friction Factor: (b) Large Bubble Regime."

(5) Please provide results for the WCOBRA/TRAC-TF2 interfacial drag model for the vessel component CT flow regime by providing prediction results as requested in items (1) through (3) above for SB flow. Apply the same conditions as those used to produce Figures 5-3(a) and 5-3(b) except for using a void fraction of 0.6 instead of 0.1 and 0.4, respectively.

Response:

(1) Interfacial drag factor for small bubble flow regime

The calculation in this subsection explains how Figure 5-3(a) in Section 5 of the Topical was generated.

- Input parameters:

Pressure: [ ]^{a,c}

Void fraction (α):

Liquid velocity (U_l): [ ]^{a,c}

Flow Area (A_{mom}):

Hydraulic Diameter (D_h):

- Properties (Saturation at given pressure):

[ ] a,c

- Calculation correlations:

Each curve in Figure 5-3(a) is calculated for a given U_r/U_{rb}, with each point of the curve for a given vapor-liquid relative velocity.

The relative velocity is limited as described in Section 5.4.1 of the Topical [Equations (5-62) through (5-66)], and calculated as:

[ ] a,c

where

[ ] a,c

The small bubble drag factor calculation is done in equations as follows, consistent with Sections 5.4.1 and 4.2.2 of the Topical.

[a,c]

[ ]a,c

The 'if' statement in the CD_{SB} calculation above is used to cap the CD_{SB} value at $CD_{SB,2}$ if $CD_{SB,tmp}$, the maximum of the $CD_{SB,0}$ and $CD_{SB,1}$, is over the limit of $CD_{SB,2}$.

The hot wall drag factor calculation is done through the equations as follows, consistent with Section 5.4.6 of the Topical.

For Inverted Liquid Slug Regime, the drag factor is calculated as:

[ ]a,c

The 'Ramp' in the equation below is identical to F_Γ as defined in Equation (5-68) of the Topical,

[ ]a,c

Based on this definition of 'Ramp', as well as the fact that liquid velocity is assumed to be zero in the calculation, it is evident that the four curves in Figure 5-3(a) of the Topical corresponding to the U_Γ equals to 0, $1.0U_{rb}$, $1.1U_{rb}$ and $1.2U_{rb}$ can be obtained by setting the 'Ramp' values to be 0.0, 0.5, 0.75 and 1.0.

Table RAI69-1 shows the results of the calculated drag coefficients as well as other selected parameters for each of the data points for the curve of 'U_Γ=0' in Figure RAI69-1, which is a duplication of Figure 5-3(a) of the Topical. The units of the ordinate parameters are included in Figure RAI69-1.

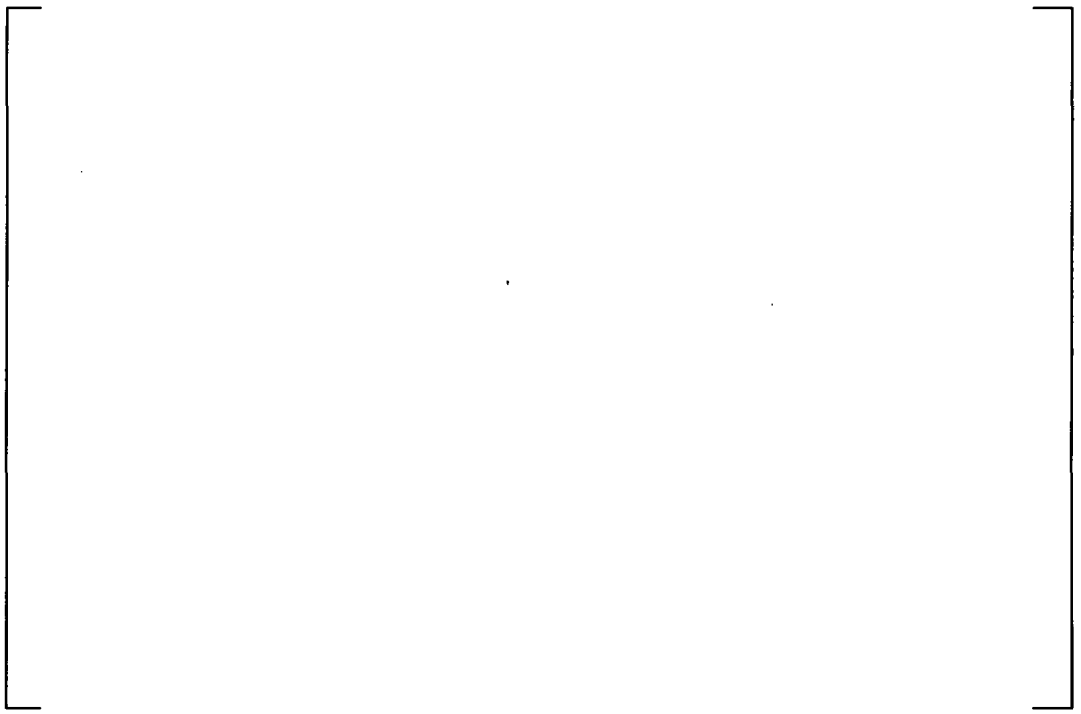

a,c

Figure RAI69-1 Small Bubble Regime Interfacial Drag Factor with Hot Wall Ramping Effects

Please note that [ ]^{a,c} term shown in Equation (5-67b) of the Topical is incorporated in the above equation in the $K_{IX,vl,SB}$, thus the equation for K_{SB} above is the same as Equation (5-67b) of the Topical.

Please also note that there is a typographical error in Equation (5-67b) of the Topical, which should be corrected as pointed out in Section 3 of this letter.

(2) Interfacial drag factor for small to large bubble flow regime

This subsection explains how Figure 5-3(b) in Section 5 of the Topical was generated first, then a corrected calculation consistent with the WCOBRA/TRAC-TF2 coding of the large bubble interfacial drag factor is provided together with the revised Figure 5-3(b).

The input parameter and property values are the same as those listed in subsection (1) for Figure 5-3(a) except that the void fraction is assumed to be 0.4 instead of 0.1 in the input parameter.

WCOBRA/TRAC-TF2 calculates the interfacial drag factor for the small to large bubble regime ([ ]^{a,c}) interpolating the interfacial drag factor for the small bubbles and large bubbles, [ ]^{a,c}. The detailed model is explained in Sections 5.4.2 and 4.2.3 of the Topical.

To calculate the interfacial factor at [ ]^{a,c} for small to large bubble regime, the steps described in (1) are first followed to obtain the small bubble drag factor at [ ]^{a,c}, which are followed by calculating the drag factor using the large bubble drag correlations as described as follows.

[a,c

Large bubble radius is calculated consistently with Equation (4-24) of the Topical and its limits [Equation (4-23) in the Topical]. A cell axial length of [

]^{a,c}.

[a,c

[ ] a,c

Please note that the equation for $K_{IX,vl,LB}$ above uses [

]a,c.

[ ] a,c

The results of these two ways of defining $K_{IX,vl,LB}$ is shown in Figures RAI69-2 and RAI69-3. It can be seen that Figure RAI69-2 duplicates Figure 5-3(b) in the Topical. The drag factor shown in Figure RAI69-3 is consistent with the code implementation in WCOBRA/TRAC-TF2. The calculation results of selected parameters are listed in Tables RAI69-2 and RAI69-3 corresponding to Figures RAI69-2 and RAI69-3, respectively.

The interfacial drag factor for small to large bubble regime is obtained by [

]a,c.

[ ] a,c

a,c

Figure RAI69-2 Small to Large Bubble Regime Interfacial Drag Factor with Hot Wall Ramping Effects (Using [ ]^{a,c})

a,c

Figure RAI69-3 Small to Large Bubble Regime Interfacial Drag Factor with Hot Wall Ramping Effects (Using [ ]^{a,c})

From the parameter values provided in Tables RAI69-1, RAI69-2 and RAI69-3, it is straightforward to obtain the dimensionless interfacial drag coefficients for bubbly flow regimes of small and small to large bubbles, as are commonly used in relevant literature to calculate drag forces, either prior to "ramping" or after "ramping" to [

]^{a,c}

As a final note, churn turbulent regime is modeled simplistically in WCOBRA/TRAC-TF2 as [

]^{a,c} flow drag model provides reasonable simulation results in these validation tests in the regime of the churn turbulent flow.

Table RAI69-1 Interfacial Drag Factor of Small Bubble Flow Regime (Case $U_\Gamma = 0.0$)

a,c

Table RAI69-2 Interfacial Drag Factor of Small to Large Bubble Flow Regime using limited relative velocity (Case $U_r = 0.0$)

a,c

Table RAI69-3 Interfacial Drag Factor of Small to Large Bubble Flow Regime Using Local Relative Velocity (Case $U_r = 0.0$)

a,c

4.12 RAIs 70 and 71

Question #70: Film Flow Drag Assessment Using Thermal Hydraulic Test Facility Test Data

WCAP-16996-P/WCAP-16996-NP, Volumes I, II, and III, Revision 0, Subsection 29.1.5, "Interfacial Drag in the Core Region," presents the treatment of film flow interfacial drag in WCOBRA/TRAC-TF2 uncertainty assessments. It is explained that "The FDRAG multiplier is the sole contributor for void fractions α_v greater than α_{cril} ~0.8." In addition, "in the interpolation region between the small and small-to-large bubbly flow regime ($\alpha_v < 0.5$) and the annular film flow regime ($\alpha_v > \alpha_{cril}$ ~0.8) both YDRAG and FDRAG have an effect." According to WCAP-16996-P/WCAP-16996-NP, Volumes I, II, and III, Revision 0, Subsection 29.1.5, the film drag multiplier, FDRAG, is applied directly to the interfacial drag as calculated for the FD flow regime using Equation (5-81) in Subsection 5.4.4, "Film/Drop Flow Regime: Model Basis":

[ ]^{a,c}

WCAP-16996-P/WCAP-16996-NP, Volumes I, II, and III, Revision 0, Subsection 13.4.2, "ORNL-THTF Small Break Tests," explains that "the parameter FDRAG has been introduced to facilitate WCOBRA/TRAC-TF2 ranging of film interfacial drag, which tends to impact the drag most significantly in the transition and annular flow regimes. It is specified on an individual cell basis." The subsection also describes the approach to determining FDRAG in plant calculations. It involved sensitivity calculations performed with WCOBRA/TRAC-TF2 for 12 ORNL THTF tests. The FDRAG sensitivity studies included 6 bundle uncovery and 6 level swell tests as summarized in Table 1.

Table 1: ORNL THTF Tests Used in FDRAG WCOBRA/TRAC-TF2 Sensitivity Analysis

Test Facility	Test Bundle	Test Runs	Number and Type of Test Runs		FDRAG and Number of Test Runs Analyzed	
			Bundle Uncovery	Level Swell	[ ]^{a,c}	[ ]^{a,c}
ORNL THTF	8x8	12	6	6	12	12

The WCOBRA/TRAC-TF2 void fraction predictions with [ ]^{a,c} are compared against ORNL THTF bundle void fraction measurements in Figures 13.4.2-4 through 13.4.2-15. From the results predicted in these figures, it was concluded [

]^{a,c}

[ ]^{a,c} It is also explained that [

]^{a,c}

(1) Figures 13.4.2-4 through 13.4.2-15 contains 9 measured void fraction data points for each of the analyzed THTF test runs. Please identify the void fraction data points measured in these THTF tests, for which WCOBRA/TRAC-TF2 predicts an annular flow configuration with a stable liquid film at the wall based on the interfacial drag model and document the data in a table. For each point, provide the measured void fraction value, void fraction measurement uncertainty (shown in Figures 13.4.2-4 through 13.4.2-1), corresponding liquid, vapor and entrained liquid mass flow rates, liquid film thickness, criteria used to identify the data points, such as α_{crit} and entrained liquid fraction, α_e, along with their numerical values, predicted nominal interfacial drag coefficient, f_i. Include corresponding void fraction predictions for [ ]^{a,c}) Please document each data point in a separate row and present the above identified quantities in separate columns. Please provide a plot comparing predicted void fractions (with [ ]^{a,c}) versus measured data showing void fraction measurement accuracy. Please explain why the identified data points were considered representative of a stable film configuration. Please apply the nominal YDRAG value (YDRAG=1) in code predictions. In a separate table, please compare the flow conditions characterizing each measured data point against the applicability range for the interfacial drag correlations used in the code void fraction predictions.

(2) Please identify the measured void fraction data points in the analyzed THTF test runs, for which the unstable liquid film model was used in predicting the interfacial drag coefficient. For these data points, please provide the information as requested in item (1) above for annular flow with a stable liquid film at the wall. Please apply the nominal YDRAG value (YDRAG=1) in code predictions and provide a separate table, which compares the flow conditions characterizing each measured data point against the applicability range for the interfacial drag correlations used in the code void fraction predictions.

(3) Please identify the measured void fraction data points in the analyzed THTF test runs, for which the flow is predicted to exist in a CT flow regime ($0.50 < \alpha \leq \alpha_{crit}$). For these data points, please provide the information requested in item (1) above for annular flow. Please apply the nominal YDRAG value (YDRAG=1) in code predictions and provide a separate table, which compares the flow conditions characterizing each measured data point against the applicability range for the interfacial drag correlations used in the code void fraction predictions.

(4) Please clarify what was the value for the YDRAG multiplier that was used in the code predictions shown in Figures 13.4.2-4 through 13.4.2-15.

(5) Considering items (1) through (4) above, please explain why the ORNL THTF test data, analyzed in WCAP-16996-P/WCAP-16996-NP, Volumes I, II, and III, Revision 0, Subsection

13.4.2, "ORNL-THTF Small Break Tests," represent a suitable and sufficient technical basis to demonstrate the applicability and treatment of film flow interfacial drag in WCOBRA/TRAC-TF2 PWR LOCA analyses. Please provide validation results for the WCOBRA/TRAC-TF2 film drag model based on appropriately selected data describing annular film flow under conditions typical for PWR LOCA analyses.

Question #71: Film Drag Impact on Bubbly Flow Void Predictions for Thermal Hydraulic Test Facility Tests

WCAP-16996-P/WCAP-16996-NP, Volumes I, II, and III, Revision 0, Subsection 29.1.5, "Interfacial Drag in the Core Region," states that 'The YDRAG multiplier is the sole contributor for void fractions α_v less than 0.5." Explaining the development of a proposed PDF for the film drag multiplier FDRAG, the subsection refers to WCOBRA/TRAC-TF2 ORNL THTF void fraction predictions obtained with [ ]^{a,c} and compared against ORNL THTF test bundle void fraction measurements as described in WCAP-16996-P/WCAP-16996-NP, Volumes I, II, and III, Revision 0, Subsection 13.4.2, "ORNL-THTF Small Break Tests," and illustrated in Figures 13.4.2-4 through 13.4.2-15. In particular, Figure 13.4.2-12 shows the comparison between WCOBRA/TRAC-TF2 code predictions and void fraction measurements for THTF Test 3.09.10CC. In this test, both the measured void fractions and the code prediction results are less than 0.5. As seen from Figure 13.4.2-12, changing the FDRAG multiplier [ ]^{a,c} had a significant impact on the predicted void fraction results under flow conditions corresponding to SB and SLB flow regimes used in the WCOBRA/TRAC-TF2 vessel component "Cold Wall" flow map. Such an effect, although to a smaller degree, is also seen in Figure 13.4.2-11 for Test 3.09.10BB, in Figure 13.4.2-5 for Test 3.09.10J, in Figure 13.4.2-7 for Test 3.09.10L, and in Figure 13.4.2-13 for Test 3.09.10DD.

(1) Please explain why changing the interfacial drag multiplier for film flow, FDRAG, causes such a pronounced effect on WCOBRA/TRAC-TF2 void fraction predictions for the identified ORNL THTF tests at elevations below the two-phase mixture level where measured void fractions are less than 0.5. Relate the explanation to the statement in WCAP-16996-P/WCAP-16996-NP, Volumes I, II, and III, Revision 0, Subsection 29.1.5, "Interfacial Drag in the Core Region," that "The YDRAG multiplier is the sole contributor for void fractions α_v less than 0.5."

(2) WCAP-16996-P/WCAP-16996-NP, Volumes I, II, and III, Revision 0, Subsection 5.4.1, "Small Bubble Flow Regime Interfacial Drag," explains that in a SB regime of the "Cold Wall" flow map, the interfacial drag is calculated by interpolation between the SB value and the value for an Inverted Liquid Slug regime of the "Hot Wall" flow map "if there is significant vapor generation at the wall." Similarly, WCAP-16996-P/WCAP-16996-NP, Volumes I, II, and III, Revision 0, Subsection 5.4.2, "Small-to-Large Bubble Flow Regime Interfacial Drag," clarifies that "for conditions in which there is a large vapor generation rate at the wall, the bubble drag coefficient is ramped to the interfacial drag used in the hot wall flow regime." Please clarify if interfacial drag "ramping" caused the observed effect on WCOBRA/TRAC-

TF2 void fraction predictions as exhibited by varying the film flow interfacial drag multiplier, FDRAG, in the code simulation for THTF Test 3.09.10CC for flow conditions with void fractions less than 0.5 that correspond to SB and SLB flow regimes.

(3) Please explain what is unique for THTF tests, such as 3.09.10CC, for which FDRAG variation had a pronounced impact on the void fraction predictions at low voids according to Figure 13.4.2-12, in comparison to other analyzed THTF tests as seen in Figure 13.4.2-6 for Test 3.09.10K, in Figure 13.4.2-8 for Test 3.09.10M, in Figure 13.4.2-9 for Test 3.09.10N, in Figure 13.4.2-10 for Test 3.09.10AA, in Figure 13.4.2-11 for Test 3.09.10BB, in Figure 13.4.2-14 for Test 3.09.10EE, and in Figure 13.4.2-15 for Test 3.09.10FF.

(4) If interfacial drag "ramping" caused the exhibited effect on WCOBRAITRAC-TF2 void fraction predictions for the identified THTF tests, please present the technical basis that validates the implemented approach to interfacial drag "ramping" in WCOBRA/TRAC-TF2 for applications aimed at obtaining realistic thermal-hydraulic predictions of PWR core level swell under typical SBLOCA conditions.

Response:

[

]^{a,c} A brief explanation of the sensitivity was provided in LTR-NRC-13-70 (Reference 4.12-2). A more detailed explanation follows.

The ORNL test simulations are initially in a transient condition. The transient condition exists until the quasi steady-state is reached, at which point the results of the simulation are extracted. The initialization of the simulations is such that the void in the top cells of the core is initially [

]^{a,c} would impact the results during the initial transient

behavior. For the particular simulation of ORNL Test CC presented in the topical, the different transient behavior resulted in a different void fraction profile once the quasi steady-state condition was reached. The initialization of this simulation was then changed such that the initial void fraction in the top cells of the core was set lower. This resulted in the expected non-sensitivity of the results to [ ]^{a,c}, as presented in Figure 2-12.

As such, it is concluded that there is no sensitivity of the ORNL Test CC results to ranging [ ]^{a,c} Figure 13.4.2-12 in WCAP-16996-P should be replaced with an updated figure based on this response.

The introduction of [

]^{a,c} It was observed that application of [ ]^{a,c} in the core provided a better prediction of the data in the upper regions of the bundle from the ORNL test series. As such, a decision was made to utilize [ ]^{a,c} in the core region. Not only does this cause a better prediction of the data, but since [

]^{a,c} which is considered conservative relative to the calculation of peak cladding temperature and oxidation for a SBLOCA transient. Since [ ]^{a,c} is only applied in a conservative direction and only in the core, no additional validation is considered necessary. Note that all the IET validation was performed with [ ]^{a,c}

It is also relevant to note that the YDRAG multiplier is ranged within the uncertainty analysis, while the FDRAG multiplier is held constant. Under SBLOCA boil-off core uncovery conditions, where there is a clear interface between the two-phase mixture and single-phase vapor, it is not expected that the FDRAG multiplier would have a significant impact. This was already shown in the FDRAG sensitivity studies for ORNL Tests K, N, and FF. Rather, it was observed that the YDRAG multiplier tends to control the two-phase level (Figures 13.4.2-18, 13.4.2-21, and 13.4.2-27 of WCAP-16996-P, Reference 4.12-1).

[ ]^{a,c} was utilized in the sensitivity studies presented in Figures 13.4.2-4 through 13.4.2-15 of WCAP-16996-P.

Reference(s)

4.12-1. WCAP-16996-P, "Realistic LOCA Evaluation Methodology Applied to the Full Spectrum of Break Sizes (FULL SPECTRUM LOCA Methodology)," November 2010.

4.12-2. LTR-NRC-13-70, "Summary of July 2013 NRC Code Workshop and August 2013 NRC Audit of the FULL SPECTRUM LOCA (FSLOCA) Evaluation Model (Proprietary/Non-Proprietary)," October 10, 2013.

5. Revised Section 5.4 of the Topical

Section 5.4 of the Topical is updated as follows to clarify the definition of the vessel component interfacial drag factors. A limited number of small, grammatical corrections are also included.

5.4 VESSEL COMPONENT INTERFACIAL SHEAR MODELS

Flow regime maps used in the vessel component of WCOBRA/TRAC-TF2 are described in Section 4. The vessel momentum equations described in Section 3 require the interfacial drag coefficient in units which, when multiplied by the new time velocity difference between the phases, will yield force per unit length for that phase. During the numerical solution, these coefficients are divided by the appropriate phasic densities, when the phasic mass flow rate is solved for. In subroutine INTFR, the interfacial drag coefficients are defined based on phasic velocity, as shown below. The average interfacial drag force per unit length between the vapor and continuous liquid is defined as:

$$\tau'_{iX,v\ell} = K_{iX,v\ell}\,\underline{U}_{v\ell} \tag{5-42}$$

where:

$\tau'_{iX,v\ell}$	=	the force per unit length on the liquid by the vapor
$K_{iX,v\ell}$	=	the flow regime dependent interfacial drag coefficient
$\underline{U}_{v\ell}$	=	the axial relative velocity between the vapor and the continuous liquid

A similar expression exists for the drag force between the vapor and entrained liquid. This expression is given as:

$$\tau'_{iX,ve} = K_{iX,ve}\,\underline{U}_{ve} \tag{5-43}$$

where:

$\tau'_{iX,ve}$	=	the force per unit length on the entrained liquid phase by the vapor
$K_{iX,ve}$	=	the flow regime dependent interfacial drag coefficient
$\underline{U}_{ve}$	=	the axial relative velocity between the vapor and the entrained phase

When accounting for the relative velocity between the phases in some calculations, for example the Reynolds number in Equation 5-51, the relative velocity value generally assumed is the [

]^{a,c}:

$$\left[\qquad\qquad\right]^{a,c} \tag{5-44}$$

where $\underline{W}_{v\ell,max}$ is the maximum lateral relative velocity and $\underline{U}_{v\ell}$ is the axial relative velocity for the cell. However, in some cases, this value is modified as described in the Model as Coded sections. When the value has been modified, it is expressed as U_r.

5.4.1 Small Bubble Flow Regime Interfacial Drag

Model Basis

For the bubbly regime, the general form of the interfacial drag coefficient is:

$$K_{iX,v\ell} = C_{Db}\frac{\rho_\ell |\underline{U}_{v\ell}|}{2} A_{p,b}/\Delta X \quad (5\text{-}45)$$

where $A_{p,b}$ is the total projected area of the bubbles in the volume. For spherical bubbles, this results in:

$$A_{p,b} = N_b \pi r_b^2 \quad (5\text{-}46)$$

where N_b is the number of bubbles in the cell, and r_b is the bubble radius. This can be shown to be equivalent to:

[ ] a,c (5-47)

where $A_{i,b}$ is the bubble interfacial area, described in Section 4. Two alternate forms of the interfacial drag coefficient are obtained:

[ ] a,c (5-48a)

(5-48b)

Similarly, for lateral flow,

[ ] a,c (5-49a)

(5-49b)

Expressions for the bubble drag coefficient (C_{Db}) are discussed by Ishii (1977) and Ishii and Chawla (1979). The drag coefficients are Reynolds number dependent and closely related to the drag coefficients for single bubbles and drops in an infinite medium. The drag coefficient for a single bubble in an infinite liquid medium is shown in Figure 5-2. The bubble is considered to behave as a solid sphere in the viscous

regime. At a higher Reynolds number, the bubble is characterized by a distorted shape and irregular motion. In this distorted particle regime the drag coefficient decreases with the Reynolds number. As the Reynolds number further increases, the bubble becomes spherical-cap shaped and the drag coefficient becomes constant.

As discussed by Ishii (1979), in the viscous regime the drag coefficient of a single particle in a multi-particle system may be assumed to have the same functional form as that of a single particle in an infinite medium, provided that the Reynolds number is computed using the appropriate mixture viscosity. Therefore, in the viscous regime the drag coefficient on a bubble is given by:

$$C_{Db} = \frac{24}{Re_b}(1.0 + 0.1 Re_b^{0.75}) \tag{5-50}$$

where:

$$Re_b = \frac{2 r_b \rho_\ell \underline{U}_{v\ell}^{*}}{\mu_{m_b}} \tag{5-51}$$

and

$$\mu_{m_b} = \mu_\ell (1 - \alpha_v)^{-2.5 \frac{(\mu_v + 0.4\mu_\ell)}{(\mu_v + \mu_\ell)}} \tag{5-52}$$

In the distorted particle regime, it is again assumed that the drag coefficient for a particle in a multi-particle system is the same as that of a single particle in an infinite medium with the Reynolds number based on a mixture viscosity. In addition, it is assumed that churn-turbulent flow always exists in the distorted particle regime. Under these conditions, a particle tends to move in the wake caused by other particles. Therefore, the velocity used in the drag coefficient and Reynolds number should be the drift velocity, $\underline{U}_{vj} = (1 - \alpha_v)\,\underline{U}_{v\ell}$. The drag coefficient in the distorted particle regime is then,

$$C_{Db} = \frac{\sqrt{2}}{3} N_\mu \, Re_b' (1 - \alpha_v)^2 \tag{5-53}$$

where:

$$N_\mu = \frac{\mu_\ell}{\left[\rho_\ell \sigma \sqrt{\frac{\sigma}{g(\rho_\ell - \rho_v)}}\right]^{1/2}} \tag{5-54}$$

$$Re_b' = \frac{2 r_b \rho_\ell (1 - \alpha_v) |\underline{U}_{v\ell}|}{\mu_m} \tag{5-55}$$

and

$$\mu_m = \frac{\mu_\ell}{(1-\alpha_v)} \tag{5-56}$$

The $(1-\alpha_v)^2$ in the expression for the drag coefficient results from using the drift velocity to compute the drag force.

Churn-turbulent flow is also assumed for the cap bubble regime where:

$$C_{Db} = \frac{8}{3}(1-\alpha_v)^2 \tag{5-57}$$

For the large-bubble flow regime, Equation 5-50 is assumed to apply down to the limit of Newton's regime where the drag coefficient for a single solid sphere becomes constant at a value of 0.45. Within Newton's regime the large bubbles are assumed to move with respect to the average volumetric flux and, therefore,

$$C_{Db} = 0.45(1-\alpha_v)^2 \tag{5-58}$$

The mixture viscosity is used in Re'_b in Equation 5-55 because a particle moving in a multi-particle system experiences a greater resistance than a single particle in an infinite medium. As it moves it must deform not only the fluid, but the neighboring particles as well. The effect is seen by the particle as an increased viscosity.

The terminal relative velocity between the bubble and liquid is also calculated from a bubble rise model given by Ishii (1977) as:

$$U_{rb} = 1.414\left[\sigma g g_c(\rho_\ell - \rho_v)/\rho_\ell^2\right]^{0.25}/(1-\alpha_v) \tag{5-59}$$

The bubble size is assumed to depend on a Weber number criterion:

$$r_b = 0.5\, We_b\, \sigma g_c/(\rho_\ell \underline{U}_{v\ell}^2) \tag{5-60}$$

where:

$We_b = 10$

[

]^{a,c}

[ ] a,c (5-61)

If large heat releases exist at a solid boundary within the cell, then vapor is assumed to concentrate as a film at the wall. The interfacial shear between the vapor film and the bulk liquid is then determined by assuming a transition inverted slug regime described in Section 5.4.6.

Model as Coded

The WCOBRA/TRAC-TF2 coding logic uses the above correlations with consistency checks to establish limits on parameters such as relative velocities and bubble size before the interfacial drag is calculated. The relative velocity is compared using different methods and the minimum value is used in the bubble Weber number and drag coefficient. The reason for this is that in the small bubble regime the interfacial area is large and would lead to excessively large forces if a large relative velocity were used.

The relative velocity to be used in Equation 5-45 is initially set at the local vector sum value ($U_r = \underline{U}_{v\ell}$), given in Equation 5-44. It is then limited as follows.

The first limit is calculated by [

]^{a,c}:

[ ]^{a,c} (5-62)

[

]^{a,c}

[ ]^{a,c} (5-63)

and the drift velocity is determined by:

[ ]^{a,c} (5-64)

The second limit is calculated by [ ]^{a,c}:

[ ]^{a,c} (5-65)

[

]^{a,c}

The value of $\underline{U}_{v\ell}$ used in Equation 5-44 is then:

[ ]^{a,c} (5-66)

[

]^{a,c}

[

]a,c

Next, the bubble drag coefficient is calculated, using Equations 5-50, 5-53, 5-57, and 5-58. [

]a,c

The interfacial drag between the continuous liquid and the vapor in the small bubble regime is calculated as:

[ ] a,c (5-67a)

where the interfacial area $A_{i,SB}$ is given in Equation 4-17. If there is significant vapor generation at the wall, the interfacial drag is ramped between the small bubble value calculated from Equation 5-67a and the inverted slug value as:

[ ] a,c (5-67b)

The hot wall drag coefficient, $K_{iX,v\ell,HW}$ is calculated from Equation 5-105.

The value of F_Γ is given as:

[ ] a,c (5-68)

where U_{rb} is calculated from Equation 5-59 and:

[ ] a,c (5-69)

where A_x is the cell momentum area in the axial direction and Γ_v (Equation 6-101) is the cell vapor generation rate and $Q_{w\ell}$ and Q_b are the heat flow from wall to liquid and the subcooled boiling heat flow, respectively (Section 7.2). To illustrate the effect of the ramps and limits described above, Equation 5-67b was evaluated as a function of $\underline{U}_{v\ell}$ for typical fluid conditions, and plotted in Figure 5-3a. It can be seen that, at high heat flux and high relative velocities, the interfacial drag factor approaches a value more typical of separated, rather than bubbly, flow.

For lateral flow through gaps, the procedure is similar, with the following differences: the relative velocity is limited to a maximum value of [ ]a,c. The more complicated channel model is not used because, in general, gaps tend to have a large flow area, and the flow velocities are relatively small.

[

]a,c

The lateral flow interfacial drag uses the same expression for bubble drag coefficient except that the vector sum relative velocity is used in the Reynolds number as described earlier. The bubble drag coefficient for lateral flow uses the same logic as the axial or vertical flow. The interfacial area is calculated in the same fashion for the lateral flow as the axial flow, except the velocity is the lateral relative velocity for the gap flow. The lateral flow interfacial drag is given as:

[ ]a,c (5-70)

[ ]a,c

Scaling Considerations

The formulation used in the small bubble regime is scale independent, since it is based on an individual bubble in the flow stream. Therefore, no scale dependence or bias would be introduced into the calculation by this model. Since the small bubble regime would be only a small region in the reactor core, before the flow regime would transition to other regimes, the noding selection used could influence the size of this regime and how it is weighted with other regimes. However the model is assessed against prototypical rod bundle data in Volume 2 of this report.

Conclusions

The small bubble regime models are based on the work of Ishii and Chawla (1979), which represents the current state of knowledge in this area. The same coding logic is used to represent the axial bubble behavior as well as the gap or lateral bubble effects.

5.4.2 Small-to-Large Bubble Flow Regime Interfacial Drag

Model Basis

The approach used for the large bubble regime is similar to that for the small bubble regime. The small bubbles are primarily in the viscous regime where $1.0 \leq Re_b \leq 1000$ whereas the larger bubbles may be in Newton's Regime where $Re_b \geq 1000$. In the Newton Regime the large bubbles are assumed to move with the average volumetric flux in the flow.

[

]a,c

As discussed by Ishii (1977) the presence of other particles affects the resulting drag for a multi-particle system. This effect is corrected by using the appropriate mixture viscosity for multi-particle systems. As a single bubble moves in a multi-particle system, it deforms not only the neighboring fluid, but the other

particles as well. The individual particle or bubble is, in turn, distorted by its neighbors as it moves through the fluid. This effect is seen as an increased fluid viscosity. The bubble Reynolds number is defined as Equation 5-51 with the mixture viscosity correction given as Equation 5-52.

[

]^{a,c} In the Newton regime, the large bubbles are assumed to move relative to the average volumetric flux such that:

$$C'_{Db} = C_{Db}(1-\alpha_v)^2 \tag{5-71}$$

where the $(1-\alpha_v)^2$ term results from using the drift velocity to calculate the drag force, and C_{Db} is the maximum drag from Equation 5-50 or a value of [ ]^{a,c}.

The same basis is used for the transverse drag relationships in this regime. [

]^{a,c}

Model as Coded

The interfacial drag between the continuous liquid and vapor in the small-to-large bubble regime is calculated as:

$$\left[\qquad\qquad\right]^{a,c} \tag{5-72}$$

where $A_{i,LB}$ is given by Equation 4-34. The calculation for the large bubble regime follows the same general procedure as the small bubble model, where $|\underline{U}_{v\ell}|$ is modified by the limits described by Equation 5-66.

For conditions in which there is a large vapor generation rate at the wall, the [

]^{a,c}:

$$\left[\qquad\qquad\right]^{a,c} \tag{5-73}$$

[

]^{a,c}

The interfacial drag coefficient between the continuous liquid and vapor for the small to large bubble regime is then calculated by [

]^{a,c}

[ ] a,c (5-74a)

or:

[ ] a,c (5-74b)

[ ]a,c

[ ] a,c (5-75)

which can be shown to be the as-coded expression:

[ ] a,c (5-76)

The term α_{SB} represents the upper bound of the small bubble regime, assumed to be [ ]a,c.

The bubble drag relationship for the lateral flow through the gaps for the small-to-large bubble and large bubble regime are the same as the axial flow coding logic. As mentioned earlier, the lateral relative velocity along with the gap bubble radius is used to calculate the bubble Reynolds number for the bubble drag coefficient. The small-to-large bubble range is the same for the lateral flow as the axial flows given in Equation 5-72.

The effect of the models, ramps, and limits on the axial interfacial drag factor for this flow regime is shown in Figure 5-3b, and indicates similar trends as the small bubble regime.

Scaling Considerations

As described in Section 5.4.1, the noding selection could influence this flow regime and how it is weighted with other regimes. The verification of this model with noding similar to PWR noding is considered in the code assessment presented in Volume 2.

Conclusions

The bubble drag coefficient and interfacial drag relationships are consistent between lateral flow and axial flow in the WCOBRA/TRAC-TF2 model. The drag relationships are based on the extensive work by Ishii and Chawla (1979). A number of prototypical rod bundle experiments with different rod array sizes are considered in Volume 2 to assess the interfacial drag model in the small to large bubble flow regime.

5.4.3 Churn-Turbulent Flow Regime Interfacial Drag

Model Basis

The churn-turbulent regime is assumed to be a combination of the large bubble regime and the film/drop regime. The model basis for the film/drop regime is described in Section 5.4.4.

Model as Coded

The interfacial drag is calculated from the selected drag coefficient and the relative velocity as previously described in Section 5.4.2:

[ ]a,c (5-77)

where the interfacial area $A_{i,LB}$ is given by Equation 4-34. The same ramp as in Section 5.4.2 is applied to consider the vapor generation rate at the wall-by-wall heat transfer.

The interfacial drag relationships for the film/drop component are described in Section 5.4.4.

For the churn-turbulent regime, a [ ]a,c:

[ ]a,c (5-78)

where:

[ ]a,c (5-79)

where α_{LB} = [ ]a,c, and α_{crit} is given as:

[ ]a,c (5-80)

The same logic is used in the lateral direction to combine large bubble and film/drop components.

Scaling Considerations

This model for interfacial drag has some scale dependence. Ishii (1977) attempted to compensate for the interaction effects of one bubble or groups of bubbles on each other through adjustments of the effective viscosity.

Conclusions

Although the model has some scale dependence, the coding logic will limit the bubble sizes based on the true physical dimensions for the problems.

5.4.4 Film/Drop Flow Regime

Model Basis

This section describes the interfacial drag models between the vapor and continuous liquid for the wetted wall film flow regime. The interfacial drag between the vapor and entrained liquid for this regime is the same as that for the hot wall dispersed droplet flow regime, and is discussed in Section 5.4.7. As shown in Section 4, when the vapor content in the flow exceeds a critical void fraction, and the wall is below the wetted wall temperature criteria, the film is assumed to become stable and liquid can no longer bridge the channel.

In the film regime, the general form of the interfacial drag coefficient is, for axial flow,

[ ] a,c (5-81)

where $A_{iX,film}$ is the interfacial area in the volume. For a thin liquid film, the interfacial area is:

[ ] a,c (5-82)

For lateral flow, the expression for interfacial area is:

[ ] a,c (5-83)

where the gap is viewed as a series of N_g vertical slots of height ΔX.

With the above equations, alternate versions of Equation 5-81 are defined:

[ ] a,c (5-84)

(5-85)

The friction factor ($f_{i,FD}$) for film flow is dependent on whether the film is stable or unstable. It has been observed experimentally that the onset of film instability causes a sudden increase in system pressure drop. This is a result of increased roughness of the liquid film caused by large, unstable waves. The film friction factor for stable film flow in tubes has been studied by Wallis (1969), and Henstock and Hanratty (1976) have correlated a large amount of co-current and countercurrent film flow data for unstable films.

Henstock and Hanratty's correlation is of the form,

$$f_{i,HH} = f_s\left\{1+1400F\left[1-\exp\left(-\frac{1}{G}\cdot\frac{(1+1400F)^{3/2}}{13.2F}\right)\right]\right\} \quad (5\text{-}86)$$

where:

$$G = \frac{\rho_\ell \, g \, D_h}{\rho_v \, U_v^2 \, f_s} \tag{5-87}$$

and

$$F = \frac{m^+}{Re_v^{0.9}} \frac{\mu_\ell}{\mu_v} \sqrt{\frac{\rho_v}{\rho_\ell}} \tag{5-88}$$

with:

$$m^+ = [\,(0.707\, Re_\ell^{0.5})^{\,2.5} + (0.0379\, Re_\ell^{0.9})^{\,2.5}\,]^{\,0.40} \tag{5-89}$$

and

[ ]a,c (5-90)

[ ]a,c The single-phase friction factor is different from that given in the Henstock and Hanratty (1976) paper which was:

$$f_s = 0.046\, Re_v^{-.20} \tag{5-91}$$

[

]a,c

For stable films, the annular flow interfacial correlation developed by Wallis (1969) is used:

$$f_{i,W} = 0.005[1 + 75(1 - \alpha_v)] \tag{5-92}$$

[

]a,c

As discussed in Section 4, the transition to churn-turbulent (large bubble) regime begins at a void fraction of [ ]a,c percent and continues until a stable film is achieved. The void fraction at which a stable liquid film will exist depends on the flow channel size and the vapor velocity. The critical void fraction is determined from a force balance between the disruptive force of the pressure gradient over the crest of waves on the film and the restraining force of surface tension. The resulting expression for the critical vapor fraction is:

[ ]a,c (5-93)

The critical void fraction is limited to a minimum value of [ ]a,c, the value below which waves can be expected to bridge across the flow channel and cause a transition to churn-turbulent flow.

The interfacial drag logic for the lateral flow is simplified relative to the vertical flow since the film flow between the gaps is assumed to be stable and the Wallis interfacial friction factor given in Equation 5-92 is used. [

]a,c

Model as Coded

[

]a,c The interfacial drag is calculated as,

[ ]a,c (5-94)

where the interfacial area $A_{i,film}$ is given by Equation 4-51 and $f_{iX,FD}$ is given by Equation (5-92).

For lateral flow through the gaps, the interfacial friction factor is calculated using:

[ ]a,c (5-95)

where the factor of 2 in Equation 5-85 has been taken into account, and giving a lateral drag coefficient of:

[ ]a,c (5-96)

Scaling Considerations

The Wallis friction factor for film, Equation 5-92 has been examined for horizontal and vertical flow from pipe sizes ranging from 1-inch to 3-inch diameter as shown in Figure 5-4. The Hanstock and Hanratty film friction model has also been compared to vertical film flow data on diameter of 0.503 inches to 2.5 inches over a range of different fluid velocities and pressures. The comparison of their correlation to data is shown in Figure 5-5. This comparison shows that the correlation provides a good fit to the data over a range of scales.

Conclusions

The film wall drag models have been compared for both horizontal and vertical flows over a range of geometries and hydraulic diameters. WCOBRA/TRAC-TF2 has been used with these models to calculate the two-phase pressure drops in an annular film flow regime.

5.4.5 Inverted Annular Flow Regime

Model Basis

An inverted annular flow regime is assumed if the continuous liquid phase is subcooled and the surrounding surface is hot and dry. This regime consists of a liquid core surrounded by a vapor film.

For inverted annular flow, the interfacial friction factor is [ ]^{a,c}:

$$\left[\quad\right]^{a,c} \tag{5-97}$$

Model as Coded

WCOBRA/TRAC-TF2 calculates the continuous liquid enthalpy and compares it to the saturated liquid enthalpy in the cell. If the liquid is subcooled and the wall is in the hot wall regime, the flow regime is inverted annular. If the liquid enthalpy is saturated or superheated, the code assumes the inverted liquid slug regime.

The interfacial drag for the axial momentum equation then is set to:

$$K_{iX,v\ell,IVA} = f_{iX,IVA}\frac{\rho_v|\underline{U}_{v\ell}|}{2}A_{i,film}/\Delta X \tag{5-98}$$

where the interfacial area $A_{i,film}$ is given by Equation 4-54 and equal to $\frac{4\sqrt{\alpha_\ell}A_X\Delta X}{D_h}$.

The interfacial drag and friction models are simplified for the lateral flow in the inverted annular and inverted annular slug regimes. [ ]^{a,c}

[ ]^{a,c} A drag coefficient in the lateral direction of:

[ ]^{a,c} (5-99)

is used, and the radius of the chunk of liquid is:

[ ]^{a,c} (5-100)

The interfacial drag coefficient becomes:

[ ]^{a,c} (5-100)

where $|\underline{W}_{v\ell}|$ is the lateral relative velocity between the continuous liquid and the vapor.

Scaling Considerations

Inverted annular flow can most commonly occur during a rapid reflood process when subcooled liquid is forced into the core either at the beginning of reflood, or when the nitrogen pressurizes the downcomer. When this situation occurs, the subcooled continuous liquid is forced into the bundle at a much higher velocity than the quench front velocity on the rods, and a thin vapor film exists on the rods' surface, separating it from the liquid core. Inverted annular flow was observed in the FLECHT and FLECHT-SEASET rod bundle experiments (Sections 14 and 15). These experiments are full-length tests using prototypical rod dimensions and spacing such that the geometric effects for this flow regime are preserved, and there are no scaling effects. The experimental conditions were varied over wide ranges to ensure that the PWR plant conditions were covered.

Conclusions

The inverted annular interfacial drag model used in WCOBRA/TRAC-TF2 is derived from the annular film flow model used for high void fraction wetted wall flows. The inverted annular interfacial drag model is assessed with full-scale prototypical rod bundle experiments for different rod arrays.

5.4.6 Inverted Liquid Slug Regime

Model Basis

As the liquid flow in the inverted annular flow regime is heated by wall heat transfer, the liquid core is accelerated by the increased vapor content of the flow. When the liquid reaches the saturation temperature, it no longer can condense the vapor and the liquid begins breaking into ligaments or chunks

into a dispersed droplet flow as it progresses up along the heated channel. The interfacial friction is calculated assuming an unstable liquid film surface exists on the large liquid ligaments or drops as:

[ ]a,c (5-102)

This equation is [ ]a,c times the Wallis (1969) equation for stable liquid films discussed earlier, given as Equation 5-92.

The interfacial area is calculated assuming that the liquid slugs are spherical, and have a diameter [ ]a,c of the channel diameter, as described in Section 4.3.3.

Model as Coded

The axial flow interfacial drag coefficient is calculated as:

$$K_{iX,IVS} = f_{i,IVS} \frac{\rho_v |\underline{U}_{v\ell}|}{2} A_{i,IVS} / \Delta X \tag{5-103}$$

where the friction factor is calculated from Equation 5-102 and the interfacial area $A_{i,IVS}$ for the liquid slug regime is from Equation 4-60 as:

$$A_{i,IVS} = \frac{8.04\alpha_\ell}{D_h} A_X \Delta X \approx \frac{8\alpha_\ell}{D_h} A_X \Delta X \tag{5-104}$$

where α_ℓ is the minimum of the liquid void fraction in the mesh cell $\alpha_\ell(i,j)$ and the average liquid void is given by Equation 4-13.

Note that the ΔX term is absent from both equations, so the resulting expression is equivalent to that in Equation 5-81.

This is further modified by:

[ ]a,c (5-105)

The lower limit is necessary to allow for [

]a,c.

The lateral flow interfacial drag for the inverted slug regime is calculated in the same fashion as the inverted annular regime, as described in the previous section.

Scaling Considerations

As mentioned earlier in this subsection, the inverted annular flow regime is an evolution of the inverted annular flow regime as heat is transferred by the wall to the fluid. The inverted slug regime is a transition from the inverted annular flow regime, where the liquid column breaks up into ligaments or large liquid slugs, and into the dispersed droplets.

The interfacial drag in the inverted liquid slug regime will be somewhat sensitive to the number of heated surfaces per unit volume since the vapor layers along the heated rods will be growing. The liquid will not be continuous, but will still be trapped between the heated surfaces. Reflood experiments used to validate the WCOBRA/TRAC-TF2 code have full-height and full-scale subchannel dimensions prototypical of PWR fuel bundles. The inverted annular flow regime is expected to exist in those experiments so scaling effects if present will be evaluated as part of the code assessment.

Conclusions

The inverted slug regime is a transition hot wall regime where the liquid is breaking up into a dispersed droplet flow regime.

5.4.7 Dispersed Droplet Flow Regime

Model Basis

As discussed in Section 3, WCOBRA/TRAC-TF2 has a separate entrained liquid field. The droplet drag model is based on the work by Ishii (1977) using the analogy of a single drop in an infinite vapor medium to a single bubble in an infinite liquid field. The droplet drag models discussed in this section are used for both the hot wall and cold wall flow regimes. The interfacial friction coefficient used is:

$$K_{iX,ve,DD} = C_{Dd} \frac{\rho_v |\underline{U}_{ve}|}{2} A_{p,d} / \Delta X$$

$$= C_{Dd} \frac{\rho_v |\underline{U}_{ve}|}{2} \frac{A_{i,drop}}{4} / \Delta X \qquad (5\text{-}106)$$

where:

C_{Dd} = the droplet drag coefficient,

$|\underline{U}_{ve}|$ = the vector sum relative velocity between the vapor and the entrained droplet, and is given as

$$\underline{U}_{ve} = \sqrt{\max(\underline{W}_{ve})^2 + \underline{U}_{ve}^2} \qquad (5\text{-}107)$$

$A_{p,d}$ = total projected area of the droplets, $\frac{3\alpha_e}{4r_d} A_X \Delta X$

$A_{i,drop}$ = interfacial area of the droplets, $\frac{3\alpha_e}{r_d} A_X \Delta X$

and

r_d = the droplet radius,

α_e = the entrained liquid fraction in the flow, and

It can be see that $A_{p,d} = \frac{A_{i,drop}}{4}$.

It is assumed that the drops are in the Newton Regime where the droplet Reynolds number is large. The droplet drag coefficient that is used in this is assumed to be:

[ ]a,c (5-108)

Bird, Stewart, and Lightfoot (1960) recommend a value of 0.44 for the droplet drag in the Newton Regime while Ishii and Chawla (1979) recommend a value of 0.45.

The droplet sizes used in WCOBRA/TRAC-TF2 are discussed in Section 4. The drop size is calculated as:

[ ]a,c (5-109)

Model As Coded

The current droplet diameter is first established via Equation 5-109.

The droplet interfacial drag is then calculated as:

$$K_{iX,ve,DD} = \left(C_{Dd} \frac{\rho_v |\underline{U}_{ve}|}{2} \frac{A_{i,drop}}{4} \right) / \Delta X \quad (5\text{-}110)$$

where:

$$A_{i,drop} = A''_{i,d} A_X \Delta X \tag{5-111}$$

The droplet drag relationships for a cold wall are identical, except that there is no check on the drop size relative to the hydraulic diameters. If the drops were as large as the hydraulic diameter, they would intersect the liquid films on the wall and the channel would be filled with liquid. This would result in a different flow regime.

The lateral flow droplet calculation uses the average droplet radius calculated in each of the adjacent cells from Equation 5-109. The droplet drag coefficient for lateral flow is a constant value, C_{Dd} = [ ]^{a,c}, and the lateral droplet drag coefficient is calculated as:

$$K_{iZ,ve,DD} = C_{Dd} \frac{\rho_v |\underline{W}_{ve}|}{2} \frac{3\alpha_e}{4r_d} L_g \Delta X \tag{5-112}$$

Scaling Considerations

The droplet sizes have as their basis drop sizes measured in the FLECHT-SEASET program (Lee, N. et al., 1982). The interfacial drag is based on assuming spherical droplets to be in the Newton Regime (droplet Reynolds number is large). Since the rod bundle experiments have been performed on full-scale bundle simulations, the droplet interfacial drag models are applicable to the PWR.

Conclusions

There is consistency in how the droplet flow is modeled both axially and laterally. The same relationships for droplet drag are used for each drag coefficient formulation. Droplet size is derived from observations in prototypical rod bundle (FLECHT-SEASET) during reflood conditions, therefore the droplet interfacial drag models are applicable to the PWR.

5.4.8 Falling Film Flow Regime

Model Basis

As fuel rods quench from the top, a liquid film is formed on the rods behind the quench and sputtering front. Liquid is de-entrained from the upward flowing dispersed droplet flow to provide liquid source for the film on the rods. The interfacial drag relationships on the film behind the top quench front are the same as those for annular film flow except that the interfacial friction uses the Wallis (1969) friction factor given in Equation 5-92. [

]^{a,c} Therefore, the interfacial friction coefficient for falling films is:

$$f_{iX,FF} = 0.005(1 + 75\alpha_\ell) \tag{5-113}$$

In the falling film regime, the gap or transverse flow film interfacial drag is calculated in the same fashion as the annular film flow drag discussed earlier in Section 5.4.4. The lateral flow of drops which are sputtered from the top down quench front would be handled in the same fashion as the droplet flow discussed in Section 5.4.7.

Model as Coded

The interfacial drag coefficient is given as:

[ ]^{a,c} (5-114)

where $f_{iX,FF}$ is from Equation 5-113 and $A_{i,film}$ is calculated from Equation 4-64.

The interfacial drag is always calculated if a cold wall is present in the cell. If the cell void fraction is greater than [ ]^{a,c}, then the flow regime is a falling film regime with upward flowing entrained droplets. If the void fraction is below [ ]^{a,c} and the liquid flow is from the top, then the interfacial drag is ramped between the top deluge regime and the falling film regime. The top deluge interfacial drag coefficients will be discussed in Section 5.4.9.

Scaling Considerations and Conclusions

No major scaling issue was identified. The falling film flow regime was designed to simply approximate the behavior of the top quench front. The model is exercised as part of the assessment against prototypical rod bundle tests presented in Sections 14 and 15.

5.4.9 Top Deluge Flow Regime

Model Basis

When the walls are hot and a large amount of liquid flows downward into a computational cell, the flow regime is called the top deluge. This flow regime is similar to the liquid slug regime for upflow as discussed in Section 5.4.6. The top deluge regime is assumed present at void fractions less than [ ]^{a,c}. Physically, the top deluge regime could occur with large liquid injection rates in a PWR upper plenum due to upper plenum injection or upper head injection. The top deluge regime would also occur during blowdown when the core flow reverses and large amounts of liquid either drain out of the upper head or plenum and are forced into a hot core. PWR with combined injection, hot leg, and cold leg accumulators, where the hot leg accumulators inject large liquid flows in the upper plenum, could also experience the top deluge flow regime.

Model As Coded

The droplet drag coefficient is calculated as the maximum of:

$$C_{Dd} = \frac{24}{Re_v}\left[1.0 + 0.1 Re_v^{.75}\right] \tag{5-115}$$

where Re_v is the vapor Reynolds number in the cell based on local vapor properties; and:

$$\left[\qquad\qquad\right]^{a,c} \tag{5-116}$$

The interfacial drag coefficient for top deluge regime is calculated as:

$$K_{iX,v\ell,TD} = C_{Dd}\frac{\rho_v |\underline{U}_{v\ell}| A_{i,film}}{2}\frac{}{4} / \Delta X \tag{5-117}$$

where the interfacial area is given by Equation 4-66.

The low vapor fraction for this regime implies that the liquid is filling most of the channel. Note that the velocity used in Equation 5-117 is the relative velocity between the continuous liquid and the vapor, rather than the entrained liquid to vapor, since the liquid slugs are modeled by the continuous liquid field. Again, the model represents large liquid slugs or chunks which would nearly fill the channel and would capture any small droplets in the channel.

[

]^{a,c}

Scaling Considerations and Conclusions

The top deluge model is similar to the liquid slug model for upflow. The basic correlations that are used are scale dependent because they depend on the channel hydraulic diameter. However, models have been assessed against prototypical rod bundle tests as discussed in Sections 14 and 15.